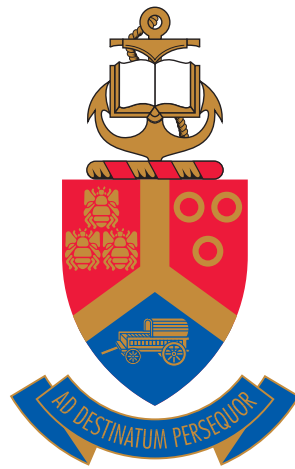


# Characterisation and uncertainty of measurement analysis of a detector spectral power responsivity measurement system



by

**Irma Rabe**

Submitted in partial fulfilment of the requirements for the degree

*Master of Science*

in the Department of Physics

in the Faculty of Natural and Agricultural Sciences

University of Pretoria

Pretoria


October 2022

Supervisor: Prof. WE Meyer

Co-supervisor: Mr RH Sieberhagen

## Declaration of originality

1. I, Irma Rabe, understand what plagiarism is and am aware of the University of Pretoria's policy in this regard.
2. I declare that this dissertation, which I hereby submit for the degree *Master of Science* at the University of Pretoria, is my own original work and has not previously been submitted by me for a degree at this or any other tertiary institution. Where other people's work has been used (either from a printed source, Internet or any other source), this has been properly acknowledged and referenced in accordance with departmental requirements.
3. I have not used work previously produced by another student or any other person to hand in as my own.
4. I have not allowed, and will not allow, anyone to copy my work with the intention of passing it off as his or her own work.

Signature:  .....

Irma Rabe

Student number: 28002522

Date: October 2022

## Acknowledgements

---

I would like to thank my co-supervisor, Mr RH Sieberhagen, for being an exceptional mentor since I started working at NMISA as a vacation student and especially for providing me with guidance and assistance throughout this project.

I am grateful for Prof. WE Meyer for agreeing to be my supervisor and for his helpful advice and guidance, and kind support during my dissertation.

I would like to thank my colleagues at NMISA for their assistance and support in this project. In particular, Dr C Sonntag for writing the control software of the monochromator and Mr PJW du Toit for his guidance and contribution to the wavelength calibration and uncertainty analyses. I would also like to thank the technical support staff at NMISA for the assistance provided during the project.

I am especially grateful to my manager, Dr L Burger, for offering advice and encouragement throughout my dissertation. Her continuous moral support and motivating guidance carried me through the times when I felt overwhelmed.

My warm and heartfelt thanks go to my family and friends for their endless encouragement, moral support and love. In particular, my parents, Johan and Ina Kruger, my sister Amelia Freysen, my sister Elana Treurnicht and her husband Petrus Treurnicht, my best friend, Maresia Bruwer, and her husband, Franz Bruwer.

Most importantly, I would like to express my deepest gratitude to my devoted husband, Randle Rabe. He endured this long process with me, always offering unconditional support and love even though he was studying towards his doctoral degree in Physics at the same time. I am grateful for his endless reassurance, working late nights and weekends with me, and encouraging me even when he was tired from his own studies. I am exceptionally fortunate to have such a loving husband with whom I could share this experience.

## Financial support

---

I would like to thank NMISA for providing me with the financial means and technical facilities to complete this project and for providing me with opportunities to grow professionally.

## Abstract

---

### **Characterisation and uncertainty of measurement analysis of a detector spectral power responsivity measurement system**

by

**Irma Rabe**

Supervisor: Prof. WE Meyer  
Co-supervisor: Mr RH Sieberhagen  
Degree: *Master of Science*  
Keywords: spectral power responsivity; calibration; PtSi photodiode; Si photodiode; pyroelectric; Si-trap detector; source; monochromator; wavelength; order sorting filters; diffraction gratings; uncertainty of measurement

The accurate measurement of spectral power responsivity of detectors is required in several applications, ranging from industries such as aerospace, defence and manufacturing to traceability for other optical measurements, such as the realisation of the SI unit, candela. At NMISA, the spectral power responsivity measurement capability is maintained on national measurement standards, published in the Government Gazette, to support such applications.

In this study, a new measurement system for spectral power responsivity of detectors was implemented and characterised. This measurement system consists of a scanning double monochromator and other components selected based on system requirements, including sources of optical radiation, order sorting filters, diffraction gratings, imaging optics and detectors.

The first step of characterisation was to perform the wavelength calibration of the monochromator. This was done for the wavelength regions of 200 nm to 400 nm and 600 nm to 1 100 nm and produced the wavelength calibration equations used in the spectral power responsivity calibrations performed. Uncertainty of measurement analyses were performed for these calibrations and the results were

used in the uncertainty of measurement determination for the spectral power responsivity calibrations.

The second step of characterisation was to perform spectral power responsivity calibrations of detectors. In the UV region, 260 nm to 400 nm, the spectral power responsivity of a PtSi photodiode detector was determined through calibration against a UV-enhanced Si photodiode detector, previously calibrated by the National Physical Laboratory of the United Kingdom for spectral power responsivity, using the substitution method. An uncertainty of measurement analysis was performed for this calibration as a function of wavelength. The measurement results obtained were successfully verified through comparison against a calibration performed by Physikalisch-Technische Bundesanstalt in Germany for the same PtSi photodiode detector for spectral power responsivity.

In the visible to near-IR region, 600 nm to 1 100 nm, the spectral power responsivity of a Si photodiode detector was determined. This was done through calibration for absolute power responsivity at 632,8 nm against a Si-trap detector using a stabilised HeNe laser source and extending this absolute calibration to the wavelength region of 600 nm to 1 100 nm, using a pyroelectric detector with known spectral absorptance, on the implemented measurement system. An uncertainty of measurement analysis was performed for this calibration.

The absolute tie point calibration of the Si photodiode detector at 632,8 nm was successfully verified through calibration against a second Si-trap detector as verification standard and through comparison against a previous calibration. The spectral power responsivity of a Si photodiode detector determined on the implemented measurement system was successfully verified through comparison with its previous calibration.

As a second verification, the Si photodiode detector was also calibrated for spec-

tral power responsivity against the UV-enhanced Si photodiode detector on the implemented measurement system in the 600 nm to 1 100 nm region and the uncertainty of measurement was determined as a function of wavelength. Using this uncertainty of measurement as a function of wavelength for comparison, the verification proved to be unsuccessful at some wavelengths between 650 nm and 720 nm and 1 060 nm to 1 100 nm. However, since the measurement results were within the stated uncertainty of the Si photodiode detector calibration against the pyroelectric detector and Si-trap detector between 600 nm and 1 050 nm, with the exception of 660 nm, the spectral power responsivity of the Si photodiode detector was considered successfully verified between 600 nm and 1 050 nm.

Following the implementation and characterisation of the new measurement system, the spectral power responsivity measurement capability at NMISA was assessed by SANAS for accreditation, which was obtained for the wavelength regions of 260 nm to 400 nm and 600 nm and 1 050 nm. Future research will include the establishment of the spectral power responsivity measurement capability in the wavelength regions of 200 nm to 260 nm and 400 nm to 600 nm.

# Contents

<b>List of figures</b>	<b>viii</b>
<b>List of tables</b>	<b>x</b>
<b>1 Introduction</b>	<b>1</b>
1.1 Background . . . . .	1
1.2 Research problem . . . . .	2
1.2.1 Aims . . . . .	3
1.2.2 Objectives . . . . .	3
1.3 Layout of the dissertation . . . . .	4
<b>2 Uncertainty of measurement</b>	<b>7</b>
2.1 Measurement . . . . .	7
2.2 Uncertainty of measurement . . . . .	8
2.3 Calibration . . . . .	8
2.4 Verification and validation . . . . .	9
2.5 Traceability . . . . .	10
2.6 International equivalence . . . . .	10
2.7 Accreditation . . . . .	11
2.8 Understanding uncertainty . . . . .	12
2.9 Evaluation of measurement results . . . . .	13
2.9.1 Uncertainty of measurement . . . . .	13
2.9.2 Normalised error . . . . .	15

<b>3</b>	<b>Optical detectors</b>	<b>16</b>
3.1	Detector standards . . . . .	16
3.2	Uncertainty contributors . . . . .	20
3.2.1	Drift in responsivity of the detector . . . . .	20
3.2.2	Spatial uniformity . . . . .	20
3.2.3	Linearity . . . . .	21
3.2.4	Temperature dependence . . . . .	21
3.2.5	Measurement equipment . . . . .	22
<b>4</b>	<b>Spectral power responsivity</b>	<b>23</b>
4.1	Measurement methods . . . . .	24
4.1.1	Substitution method . . . . .	24
4.1.2	Transferring spectral power responsivity using a wavelength-extending detector . . . . .	27
4.2	Realisation of responsivity scales at other NMIs . . . . .	28
<b>5</b>	<b>Sources of optical radiation</b>	<b>31</b>
5.1	Spectral distribution . . . . .	31
5.2	Uncertainty contributors . . . . .	34
5.2.1	Source stability . . . . .	34
5.2.2	Uniformity . . . . .	35
5.2.3	Polarisation . . . . .	36
<b>6</b>	<b>The monochromator system</b>	<b>37</b>
6.1	Basic operation of a monochromator . . . . .	37
6.2	Dispersive elements . . . . .	38
6.2.1	The grating equation . . . . .	40
6.2.2	Grating efficiency . . . . .	41
6.2.3	Dispersion . . . . .	42
6.3	Order-sorting filters . . . . .	44
6.4	Imaging optics . . . . .	45
6.5	Uncertainty contributors . . . . .	47



6.5.1	Inter-reflections between detector and exit slit of the monochromator . . . . .	47
6.5.2	Beam divergence and vignetting . . . . .	47
6.5.3	Passband, bandpass and bandwidth . . . . .	48
6.5.4	Resolution . . . . .	51
6.5.5	Stray light . . . . .	51
6.5.6	Wavelength accuracy . . . . .	53
<b>7</b>	<b>The wavelength calibration</b>	<b>54</b>
7.1	Wavelength standards . . . . .	54
7.2	Determining the wavelength calibration equation . . . . .	56
7.3	Method . . . . .	58
7.3.1	Wavelength region of 200 nm to 400 nm . . . . .	59
7.3.2	Wavelength region of 600 nm to 1 100 nm . . . . .	62
7.4	Results . . . . .	65
7.4.1	Wavelength region of 200 nm to 400 nm . . . . .	65
7.4.2	Wavelength region of 600 nm to 1 100 nm . . . . .	66
7.5	Uncertainty analysis . . . . .	67
7.5.1	Theoretical value of the spectral line in vacuum, $U_{sl}$ . . . . .	67
7.5.2	Uncertainty in modified Edlén equation calculation, $U_{Ed}$ . . . . .	67
7.5.3	Laboratory temperature effect, $U_T$ . . . . .	69
7.5.4	Laboratory humidity effect, $U_{RH}$ . . . . .	69
7.5.5	Laboratory air pressure effect, $U_{ap}$ . . . . .	70
7.5.6	Steep-side method offset, $U_{ssmo}$ . . . . .	71
7.5.7	Wavelength calibration equation offset, $U_o$ . . . . .	71
7.5.8	Wavelength reproducibility, $U_\lambda$ . . . . .	72
7.5.9	Mechanical resolution of monochromator, $U_{Mres}$ . . . . .	72
7.5.10	Resolution used in the calibration, $U_{Cres}$ . . . . .	73
7.5.11	Repeatability, $U_r$ . . . . .	73
<b>8</b>	<b>The spectral power responsivity calibrations</b>	<b>75</b>
8.1	Measurement system . . . . .	75
8.1.1	Sources of optical radiation . . . . .	75

8.1.2	Imaging optics . . . . .	77
8.1.3	Diffraction gratings and order-sorting filters . . . . .	79
8.1.4	Optical detectors and traceability chain . . . . .	79
8.2	Method . . . . .	81
8.2.1	Wavelength region of 200 nm to 400 nm . . . . .	82
8.2.2	Wavelength region of 600 nm to 1 100 nm . . . . .	84
8.3	Results . . . . .	88
8.3.1	Wavelength region of 200 nm to 400 nm . . . . .	88
8.3.2	Wavelength region of 600 nm to 1 100 nm . . . . .	91
8.4	Uncertainty analysis . . . . .	103
8.4.1	Spectral analysis of uncertainty . . . . .	103
8.4.2	Uncertainty analysis for calibration of the Si photodiode de- tector against the pyroelectric detector and Si-trap detector as standard in the wavelength region of 600 nm to 1 100 nm	119
<b>9</b>	<b>Discussion</b>	<b>126</b>
<b>10</b>	<b>Conclusions</b>	<b>131</b>
<b>11</b>	<b>Further research</b>	<b>134</b>
<b>A</b>	<b>Spectral power responsivity measurement system</b>	<b>A-1</b>
<b>B</b>	<b>Alignment of the monochromator</b>	<b>B-1</b>
<b>C</b>	<b>Software</b>	<b>C-1</b>
<b>D</b>	<b>Mounting of optical detectors</b>	<b>D-1</b>
<b>E</b>	<b>Experimental demonstration of slit functions</b>	<b>E-1</b>
<b>F</b>	<b>Use of the LDLS</b>	<b>F-1</b>
<b>G</b>	<b>Uncertainty of measurement for the wavelength calibration in the wavelength region of 200 nm to 400 nm</b>	<b>G-1</b>
<b>H</b>	<b>Uncertainty of measurement for the wavelength calibration in the</b>	

wavelength region of 600 nm to 1 100 nm	H-1
I Uncertainty of measurement for the calibration of the PtSi photodiode detector against the UV-enhanced Si photodiode detector in the wavelength region of 200 nm to 400 nm	I-1
J Uncertainty of measurement for the calibration of the Si photodiode detector against UV-enhanced Si photodiode detector in the wavelength region of 600 nm to 1 100 nm	J-1
K Uncertainty of measurement for the calibration of the Si photodiode detector against the pyroelectric detector and Si-trap detector in the wavelength region of 600 nm to 1 100 nm	K-1
References	R-1

# List of Figures

3.1	Typical relative spectral responsivity of a pyroelectric detector between 250 nm and 1 100 nm. . . . .	17
3.2	Absolute spectral power responsivity of a typical silicon photodiode, a platinum silicide photodiode and a UV-enhanced silicon photodiode detector. . . . .	19
4.1	Measurement geometry for power measurement . . . . .	23
5.1	Spectral distributions of a LDLS compared to a deuterium source. . . . .	32
5.2	Spectral distributions of Xenon arc and QTH sources. . . . .	33
6.1	The “W” configuration of the Czerny-Turner monochromator mounting used. . . . .	38
6.2	Illustration of a double monochromator in additive and subtractive dispersion mode . . . . .	39
6.3	A schematic representation of the derivation of the grating equation. . . . .	41
6.4	Grating efficiency curve for a grating with a groove density of 600g/mm blazed at 800 nm. . . . .	43
6.5	Transmittance of the order sorting filter GG395 . . . . .	45
6.6	Illustration of a lens collecting and collimating light from a source. . . . .	46
6.7	Illustration of beam divergence for a high vs low $F/\#$ . . . . .	48
6.8	Illustration of slit functions and bandwidths for equal and unequal slit widths . . . . .	50
7.1	Emission spectral lines in ambient air of the argon spectral line source used for the wavelength calibration in the visible to near-IR region. . . . .	55

7.2	Excerpt from Kostkowski [1997] indicating the steep-side method for wavelength calibration. . . . .	57
7.3	An example of the steep-side method and linear fits of data points around 10 % of maximum signal to determine the monochromator steps of the peak of a spectral line. . . . .	61
7.4	A linear fit for the wavelength calibration in the region 200 nm to 400 nm . . . . .	65
7.5	A linear fit for the wavelength calibration in the region 600 nm to 1 100 nm . . . . .	66
7.6	Visual representation of the wavelength and refractive index calculated for ambient conditions using the NIST Engineering Metrology Toolbox based on the modified Edlén equation. . . . .	68
8.1	A schematic representation of the traceability chain for spectral power responsivity in the wavelength region of 200 nm to 400 nm. . . . .	80
8.2	A schematic representation of the traceability chain for spectral power responsivity in the wavelength region of 600 nm to 1 100 nm. . . . .	81
8.3	Normalised output signal of the standard UV-enhanced Silicon photodiode detector indicating the low signal level below 260 nm. . . . .	89
8.4	Calculated spectral power responsivity and PTB determined spectral power responsivity for the PtSi photodiode detector in the wavelength region 260 nm to 400 nm. . . . .	90
8.5	Absolute spectral power responsivity of the Si photodiode detector determined using the pyroelectric detector and Si-trap detector as standard, from its previous calibration, and using the UV-enhanced Si photodiode detector as verification standard. . . . .	93
8.6	Verification of the calculated spectral power responsivity of the Si photodiode detector with its previous calibration. . . . .	96
8.7	Absolute spectral power responsivity of the Si photodiode detector as determined using the method described in Section 8.2.2 with its associated uncertainty of measurement, and using the UV-enhanced Si photodiode detector as a verification standard. . . . .	99
8.8	Absolute spectral power responsivity of the Si photodiode detector as determined using the method described in Section 8.2.2, and using the UV-enhanced Si photodiode detector as a verification standard with its associated uncertainty of measurement. . . . .	100

A.1	A schematic representation of the spectral power responsivity measurement system. . . . .	A-2
D.1	A picture of the detector mount indicating the translation axes and other components. . . . .	D-2
E.1	Graphical illustration of slit functions for equal and unequal slits when measuring the 823,38964 nm spectral line (in vacuum) of a xenon spectral line source . . . . .	E-2

# List of Tables

2.1	Uncertainty of measurement terminology . . . . .	14
8.1	The selection of sources, diffraction gratings based on their efficiency range discussed in Section 6.2.2, detectors and order-sorting filters for the operation wavelength ranges. . . . .	76
8.2	The absolute spectral power responsivity of the PtSi detector and comparison with the PTB calibration. . . . .	90
8.3	The absolute power responsivity of the Si photodiode detector obtained with DC and AC signals. . . . .	91
8.4	The absolute power responsivity of the Si photodiode detector obtained with the standard Si-trap detector and verification standard Si-trap detector. . . . .	92
8.5	The absolute power responsivity of the Si photodiode detector compared to its previous calibration. . . . .	93
8.6	The absolute spectral power responsivity of a Si photodiode detector compared with its previous calibration's measurement results. . . . .	95
8.7	Absolute spectral power responsivity of the Si photodiode detector as determined using the method described in Section 8.2.2 and using the UV-enhanced Si photodiode detector as a verification standard. . . . .	97
G.1	Uncertainty of measurement calculated for the wavelength calibration in the wavelength region of 200 nm to 400 nm. . . . .	G-2
H.1	Uncertainty of measurement calculated for the wavelength calibration in the wavelength region of 600 nm to 1 100 nm. . . . .	H-2

I.1	Standard uncertainty contributions, $u(x_i)$ , calculated for the PtSi photodiode detector calibration against the UV-enhanced Si photodiode detector in the wavelength region of 200 nm to 400 nm. . . . .	I-2
I.2	Continued: Standard uncertainty contributions, $u(x_i)$ , calculated for the PtSi photodiode detector calibration against the UV-enhanced Si photodiode detector in the wavelength region of 200 nm to 400 nm. . . . .	I-3
I.3	Continued: Standard uncertainty contributions, $u(x_i)$ , calculated for the PtSi photodiode detector calibration against the UV-enhanced Si photodiode detector in the wavelength region of 200 nm to 400 nm. . . . .	I-4
I.4	Combined standard uncertainty, $u_c(y)$ , and expanded uncertainty, $U$ , calculated for the PtSi photodiode detector calibration against the UV-enhanced Si photodiode detector in the wavelength region of 200 nm to 400 nm. . . . .	I-5
J.1	Standard uncertainty contributions, $u(x_i)$ , calculated for the Si photodiode detector calibration against the UV-enhanced Si photodiode detector in the wavelength region of 600 nm to 1 100 nm. . . . .	J-2
J.2	Continued: Standard uncertainty contributions, $u(x_i)$ , calculated for the Si photodiode detector calibration against the UV-enhanced Si photodiode detector in the wavelength region of 600 nm to 1 100 nm. . . . .	J-3
J.3	Continued: Standard uncertainty contributions, $u(x_i)$ , calculated for the Si photodiode detector calibration against the UV-enhanced Si photodiode detector in the wavelength region of 600 nm to 1 100 nm. . . . .	J-4
J.4	Continued: Standard uncertainty contributions, $u(x_i)$ , calculated for the Si photodiode detector calibration against the UV-enhanced Si photodiode detector in the wavelength region of 600 nm to 1 100 nm. . . . .	J-5
J.5	Combined standard uncertainty, $u_c(y)$ , and expanded uncertainty, $U$ , calculated for the Si photodiode detector calibration against the UV-enhanced Si photodiode detector in the wavelength region of 600 nm to 1 100 nm. . . . .	J-6
K.1	Uncertainty of measurement calculated for the Si photodiode detector calibration against the pyroelectric detector and Si-trap detector. . . . .	K-2



# Chapter 1

## Introduction

### 1.1 Background

Optical detectors are used to measure optical radiation or the part of the electromagnetic spectrum between ultraviolet (UV) and infrared (IR). The detectors produce a response, *i.e.* an electrical signal that is proportional to the power of the incident radiation, and is wavelength selective. This wavelength selective response is called spectral power responsivity of detectors.

Measurement of spectral power responsivity of detectors is required by industries such as aviation and aerospace, defence, manufacturing and agriculture. Characterisation of spectral power responsivity of detectors enables further optical measurements with applications in the mentioned industries, including photobiological safety, non-destructive testing, medical and health, water and sanitation, textiles and pharmaceuticals. These industries rely on accurate optical measurements.

Furthermore, accurate measurements require traceability to the SI (International System of Units). Such traceability is obtained through metrology institutes that establish the practical realisations of the definitions of the SI units. The established capability for spectral power responsivity of detectors is a key requirement

in the realisation of the SI base unit candela.

At the National Metrology Institute of South Africa (NMISA), the spectral power responsivity scale is maintained on a set of silicon trap detectors. The calibration of the silicon trap detectors is performed at a few discrete laser lines and extended, using a pyroelectric detector and a broadband source-monochromator system, to the UV, visible and near-IR regions. The broadband source-monochromator system was upgraded with a new monochromator. Therefore, the new measurement system had to be implemented and characterised to maintain the spectral power responsivity scale.

An essential part of the characterisation of the new measurement system, is an uncertainty analysis. Uncertainty of measurement provides a quantification of how close the measured spectral power responsivity is to the true spectral power responsivity of the detector. Factors of the measurement system that contribute to the uncertainty of measurement have to be investigated, quantified and minimised.

## **1.2 Research problem**

The need to maintain the measurement capability for spectral power responsivity of detectors at NMISA in support of local industries and maintenance of international equivalence motivated this study. The purpose was to establish this measurement capability in the UV to near-IR region on the new measurement system.

### **1.2.1 Aims**

The first aim of the study was to revise the setup and measurement system previously used for measuring the spectral power responsivity of detectors. The second aim was to characterise the new measurement system and calibrate a set of optical detectors for spectral power responsivity, and to perform a detailed uncertainty of measurement analysis.

### **1.2.2 Objectives**

The measurement setup and method for spectral power responsivity are well established and documented in technical papers and reports, and technical protocols used by laboratories across the world to determine international equivalence. In this study, such technical protocols, and technical reports provided by the International Commission on Illumination (CIE) were used as guides.

The typical setup for spectral power responsivity measurement requires spectrally selective sources of optical radiation, or a broadband source with a spectrally selective instrument, such as a monochromator, imaging optics to underfill the detector to measure the power of the incident optical radiation, and signal processing and measurement devices.

The first objective was to construct the new measurement system. This entailed selection of components based on wavelength regions. New components to be implemented were sources of optical radiation, filter selection, diffraction gratings, imaging optics and a new pyroelectric detector.

The second objective was to characterise the system through calibration. A wavelength calibration of the monochromator is required in each wavelength region of interest and is performed through comparison against spectral line

sources. This was followed by the calibration of optical detector standards for spectral power responsivity in different wavelength regions.

The final objective was to investigate any factors that contribute to the uncertainty of measurement in the new measurement system. This required a detailed analysis of measurement uncertainty.

### **1.3 Layout of the dissertation**

The relevance of optical detectors and the importance and application of their characterisation for spectral power responsivity is provided in Chapter 1. This chapter addresses the motivation for maintaining this measurement capability at NMISA and explains that this is done through the implementation and characterisation of a new, upgraded measurement system. The aims and objectives to achieve this are discussed.

In this study, the *International Vocabulary of Metrology* (VIM) [JCGM, 2012] will be used as a guide for terms and definitions. Technical methods prescribed in technical reports and international standards provided by CIE will be used as guides for methodologies and uncertainty contributions used and investigated in this study.

Chapter 2 provides background on uncertainty of measurement and explains some fundamental concepts and terms used in this study and metrology in general.

Chapter 3 describes the optical detectors used to characterise the new measurement system and uncertainty contributors to consider when performing the uncertainty of measurement analysis. Chapter 4 defines spectral power responsivity of detectors and the standard methodology for its measurement and calibration. This chapter also compares spectral power responsivity scales maintained

at other metrology laboratories.

An overview of sources of optical radiation is provided in Chapter 5 along with the related uncertainty contributors to consider. The new measurement system utilises such sources in conjunction with a scanning double monochromator, the main factors and components of which are discussed in Chapter 6. In this chapter, the basic operation of a monochromator is explained along with the core components of the new measurement system, such as imaging optics, diffraction gratings and order-sorting filters. Uncertainty contributors relevant to the monochromator system are also described.

One of the most important aspects of characterisation of the measurement system is the wavelength calibration of the monochromator, which is explained in Chapter 7. This chapter provides a detailed description of the method used to perform wavelength calibrations, as well as the results and uncertainty of measurement analysis for the two wavelength calibrations performed in preparation for the spectral power responsivity calibrations. The results of these uncertainty of measurement analyses are provided in Appendices G and H.

This links to Chapter 8, which provides the selection of components implemented for the measurement system of spectral power responsivity of detectors. Appendix A provides a schematic representation of this measurement setup. Discussed in this chapter is the characterisation of the measurement system through calibration of PtSi photodiode and Si photodiode detectors for spectral power responsivity in the wavelength regions of 200 nm to 400 nm and 600 nm to 1 100 nm, respectively. The chapter includes the method used, the results obtained and the uncertainty of measurement analysis performed considering the relevant uncertainty contributors, the latter of which is provided in Appendices I, J and K.

Some important aspects of the implementation of the measurement system, such as the alignment of the monochromator, the control software used, mounting of the optical detectors and experimental slit functions are described in Appendices B, C, D and E.

Chapter 10 provides the conclusions to the objectives set out in Chapter 1 and discusses further research to be considered as future work for improvement of the study performed.

The wavelength region of 400 nm to 600 nm was not covered in this study and is reserved for future work. Characterisation of this wavelength region would also require a wavelength calibration of the monochromator from 400 nm to 600 nm. After this, a spectral power responsivity calibration of the relevant detector would have to be performed using one of the methods described in Chapter 4. A complete uncertainty of measurement analysis would have to be performed to obtain the measurement results.

## Chapter 2

# Uncertainty of measurement

### 2.1 Measurement

Metrology, as defined by the VIM, is the science, theoretical and practical, of measurement and its application. Metrology involves the development of measurement methods and systems, realising measurement standards and disseminating them to users.

To practise metrology, it is important to understand what a measurement is. The VIM defines a measurement as "the process of experimentally obtaining one or more quantity values that can reasonably be attributed to a quantity", adding that a "measurement presupposes a description of the quantity commensurate with the intended use of a measurement result, a measurement procedure, and a calibrated measuring system operating according to the specified measurement procedure, including the measurement conditions" [JCGM, 2012:16]. In this study, the quantity is spectral power responsivity,  $s$ .

Standard measurement procedures or methods are sometimes made available by standardisation bodies, such as the International Standardization Organisation (ISO). The CIE is considered as representing the best authority on all matters relating to the science of among others, light, lighting and vision. The CIE is also

recognised by the International Commission for Weights and Measures (CIPM), ISO and the International Electrotechnical Commission (IEC) as an international standardisation body. The CIE provides technical notes, technical reports and international standards related to vision and colour, the physical measurement of light and radiation and more. These are all written by technical committees consisting of the leading experts in the relevant fields across the world.

## **2.2 Uncertainty of measurement**

Once the value of a quantity is obtained through measurement, its quality or estimate of how close it is to the true value should be determined. This is known as uncertainty, defined by the VIM as the characterisation of the dispersion of values attributed to a quantity. The uncertainty defines an interval of values in which the true value is considered to lie, with a stated probability. This interval is called the coverage interval and the probability is called the coverage probability or level of confidence.

A measurement result is expressed as the measured value of the quantity and the uncertainty associated with the value for a given probability, *e.g.*  $0,351 \text{ A W}^{-1} \pm 0,63 \%$  with a level of confidence of 95,45 %.

## **2.3 Calibration**

Calibration is the measurement through a comparison of an unknown quantity with associated uncertainty, to a known or reference quantity with provided uncertainty. For example, a test detector is calibrated for the unknown quantity spectral power responsivity against a reference or standard detector with a known spectral power responsivity (known quantity) and associated uncertainty.



Through this comparison, the uncertainty associated with the measured value of the unknown quantity is determined to yield the measurement result.

Calibration is a process that must be repeated on an ongoing basis at a time interval dependent on the frequency of use, susceptibility to drift and the level of importance of the measurement. The benefits of calibration are among others, having a reliable quantification of an instrument, avoiding inaccurate readings and ensuring consistency between measurements with different instruments.

## **2.4 Verification and validation**

Verification and validation are terms that are at times used interchangeably. For this study, the terms refer to verification of results and validation of the measurement method. The VIM defines verification as the provision of evidence that a measurement system meets a specified requirement. Such a requirement may be a manufacturer's specification, a performance property or a target measurement uncertainty. In many cases measurement uncertainty is used as evaluation criteria to determine whether a requirement is met.

A measurement method is validated when evidence is available that it is adequate for its intended use. A method may be validated by performing a measurement of the same quantity using another method and obtaining measurement results from both methods which are within a specified requirement, such as a measurement uncertainty. Validation may also be through verification. For example, if a detector is calibrated at two national metrology institutes (NMIs), using the same or different methods and different traceability routes, the successful comparison of the detector values is considered as a verification of the measurement results, and validation through verification.

## 2.5 Traceability

A measurement result can be disseminated through metrological traceability. Metrological traceability is when the measurement result is related to a reference through a documented unbroken chain of calibrations, with each calibration contributing to the measurement uncertainty. This chain of calibrations relating a measurement result to a reference is called a traceability chain.

Traceability provides confidence in the calibration through the relation to a higher accuracy reference. The top level of a traceability chain consists of the realisation of the SI units [BIPM, 2019] at NMIs, which are typically maintained in national measurement standards. National measurement standards are registered in the Government Gazette, e.g. Government Gazette no. 41982 [DTI, 2018] provides for the national measurement standards maintained by the National Metrology Institute of South Africa.

The next level of the traceability chain may be local calibration laboratories, which will in turn provide the calibration of a master item to a company, which will be able to calibrate other equipment against the master item, and so on. At each lower level of the traceability chain, the uncertainty increases.

## 2.6 International equivalence

The role of an NMI is to maintain the national measurement standards and disseminate traceability to industry. This requires the development of measurement standards and their comparison to other national measurement standards or international standards. Through this comparison, international equivalence is established. This process of comparison is governed by the International Committee for Weights and Measures – Mutual Recognition Arrangement (CIPM MRA).

NMIs participate in international key comparisons through the Consultative Committees of the CIPM, such as CCPR (Consultative Committee for Photometry and Radiometry). Two examples of such international key comparisons are CCPR-K2.c, spectral responsivity in the wavelength range of 200 nm to 400 nm, and CCPR-K2.b, spectral responsivity in the wavelength range of 300 nm to 1 000 nm. During these comparisons, several NMIs from countries across the world measure the same quantity and the results are then compared to obtain the reference value. The outcome of these international key comparisons is Calibration and Measurement Capabilities (CMCs) of the NMIs, which are listed in the Key Comparison Database (KCDB) on the website of the International Bureau of Weights and Measures (BIPM).

## **2.7 Accreditation**

One of the requirements for a laboratory to have its CMCs entered in the BIPM KCDB is having a total quality management system (TQMS) based on the international standard ISO/IEC 17025. The TQMS may be accredited by an accreditation body such as the South African National Accreditation System (SANAS) which is internationally recognised by the International Laboratory Accreditation Cooperation (ILAC).

Obtaining this accreditation requires being assessed against the internationally recognised standard ISO/IEC 17025 [ISO/IEC, 2017], or the locally adopted standard, for example, SANS (South African National Standard) 17025, *General requirements for the competence of testing and calibration laboratories* [SABS, 2018]. During this process, the laboratory demonstrates its competence and capability. Staff is witnessed and assessed by a local or international assessor who is considered an expert in the field for which accreditation is applied for.

Following this study, the quantity, spectral power responsivity,  $s$ , maintained by the Photometry and Radiometry laboratory of the NMI of South Africa after the design, implementation and characterisation of a new measurement system, was assessed by SANAS. The SANS 17025 requirements that had to be in place for this assessment were, among others, a validated measurement method, a recent calibration performed on the measurement system with verified measurement results, stated traceability and associated uncertainty of measurement analysis.

## 2.8 Understanding uncertainty

Measurement uncertainty is an extensive field of study. Many statistical concepts have to be understood before attempting an uncertainty calculation. These concepts are taught through in-depth courses on measurement uncertainty based on JCGM 100:2008, *Evaluation of measurement data — Guide to the expression of uncertainty in measurement* (GUM) [JCGM, 2008]. A brief overview of terms used in this study to determine the uncertainty of measurement is provided in Table 2.1, for further explanations, refer to the GUM.

During a calibration of an unknown quantity such as spectral power responsivity, there are many factors that influence the measurement result and therefore contribute to the uncertainty. These sources of uncertainty are called input quantities,  $X$ , or uncertainty contributors, and their estimates are combined to produce the uncertainty of measurement.

An uncertainty calculation starts with the estimated uncertainty,  $u_e(x)$ , of the value,  $x$ , of these input quantities or uncertainty contributors, each of which has a defined probability distribution with an associated coverage factor,  $k$ . From this, the standard uncertainty,  $u(x)$ , is calculated as the quotient of the estimate of the uncertainty contributor and the coverage factor.

A sensitivity coefficient,  $c$ , describes how sensitive the quantity (e.g. spectral power responsivity) is to a change in a given input quantity,  $X$ . The contribution to the combined standard uncertainty,  $u(y)$ , is therefore calculated as the product of the standard uncertainty of the input quantity and its sensitivity coefficient.

These contributions,  $u(y)$ , are combined through the law of propagation of uncertainty to obtain the combined standard uncertainty,  $u_c(y)$ :

$$u_c^2(y) = \sum_{i=1}^N c_i^2 u^2(x_i) + 2 \sum_{i=1}^{N-1} \sum_{j=i+1}^N c_i c_j u(x_i, x_j), \quad (2.1)$$

where the first term is used for independent uncertainty contributions and the second term is used for correlated uncertainty contributions.

Typically, the expanded uncertainty,  $U$ , is reported and determined by multiplying the combined standard uncertainty with the appropriate coverage factor.

At NMISA, the convention is to report the expanded uncertainty for a coverage factor of  $k = 2$  at a confidence level of 95,45 %. This uncertainty of measurement is rounded up and reported to at most two significant figures.

## 2.9 Evaluation of measurement results

### 2.9.1 Uncertainty of measurement

As mentioned previously in Section 2.4, the measurement uncertainty may be used to evaluate whether a requirement is met. When a verification of a measurement result is performed with, for example, another standard *i.e.* a verification standard with a known uncertainty, the measurement result may be considered verified if the deviation between the results obtained with the standard and the verification standard is within the known uncertainty of the verification standard.

Table 2.1 : Uncertainty of measurement terminology.

Term	Symbol	Examples
Numbering label	$i$	
Input quantity, source of uncertainty	$X_i$	Uncertainty in spectral power responsivity of reference detector
Estimate of $i^{th}$ input quantity	$x_i$	Values of reference spectral power responsivity
Estimated uncertainty of $i^{th}$ input quantity	$u_e(x_i)$	Uncertainty in spectral power responsivity of reference detector
Probability distribution, spread of the set of values		Normal distribution - where values are more likely to fall near the average than further away Rectangular distribution - even spread between the highest and the lowest values U-shaped - where values are more likely to fall near the limits than the centre of the spread
Coverage factor associated with the probability distribution	$k$	Normal distribution, $k = 1$ Rectangular distribution, $k = \sqrt{3}$ U-shaped, $k = \sqrt{2}$
Standard uncertainty of $i^{th}$ input quantity, estimated uncertainty divided by the coverage factor	$u(x_i) = u_e(x_i)/k$	Uncertainty in spectral power responsivity of reference detector divided by the coverage factor reported in its calibration certificate
Sensitivity coefficient for $i^{th}$ input quantity, sensitivity of the contribution to the combined uncertainty to a change in the $i^{th}$ input quantity	$c_i$	Degree of change in spectral power responsivity of a detector with a change in wavelength
Contribution to the combined standard uncertainty from the $i^{th}$ input quantity, standard uncertainty multiplied by the sensitivity coefficient	$u_i(y) =  c_i u(x_i)$	
Combined standard uncertainty, obtained by combining the individual contributions	$u_c(y)$	
Expanded uncertainty, product of a combined standard uncertainty and a coverage factor	$U$	NMISA reports the combined standard uncertainty multiplied by a coverage factor of $k = 2$ .

## 2.9.2 Normalised error

It is a requirement of a SANS 17025 accredited calibration laboratory to participate in proficiency testing or other comparison programmes. The international standard ISO/IEC 17043 [ISO/CASCO, 2010] provides guidance on the evaluation of measurement results obtained from proficiency testing. ISO/IEC 17043 describes a number of performance statistics used to compare measurement results, among others, the normalised error, or  $E_n$  score, given by

$$|E_n| = \frac{v_{lab} - v_{ref}}{\sqrt{U_{lab}^2 + U_{ref}^2}}, \quad (2.2)$$

where  $v_{lab}$  is the value determined by the laboratory,  $v_{ref}$  is the reference value,  $U_{lab}$  is the expanded uncertainty of the laboratory's value, and  $U_{ref}$  is the expanded uncertainty of the reference value.

The performance of a measurement result can be evaluated from the statistical determination of the  $E_n$  score in the following way:

- $|E_n| \leq 1,0$  indicates satisfactory performance
- $|E_n| > 1,0$  indicates unsatisfactory performance

This method of comparing measurement results is common for calibration laboratories and may also be applied to the measurement results to determine whether a verification was successful.

## Chapter 3

# Optical detectors

### 3.1 Detector standards

Spectral power responsivity calibrations require the use of detector standards traceable to SI units. Detector standards with the lowest uncertainty of measurement, called primary standards, are electrical substitution cryogenic radiometers (ESCR) and silicon trap (Si-trap) detectors. ESCRs compare incident optical power to electrical power using the electrical substitution method, where radiant heating power is substituted with electrical heating power. Operation at cryogenic temperatures improves the system's sensitivity and reduces measurement uncertainty.

The most common Si-trap detectors consist of three single-element silicon (Si) photodiodes arranged in a retro-reflecting configuration, where the incident beam is reflected five times along the optical path, which allows for increased sensitivity.

Si-trap detectors are commonly calibrated against ESCRs at specified wavelengths using intensity-stabilised laser sources. Such spectral responsivity calibrations may be extended to a wider wavelength range with spectrally flat or constant responsivity detectors, such as pyroelectric detectors or thermopiles, see Figure 3.1.



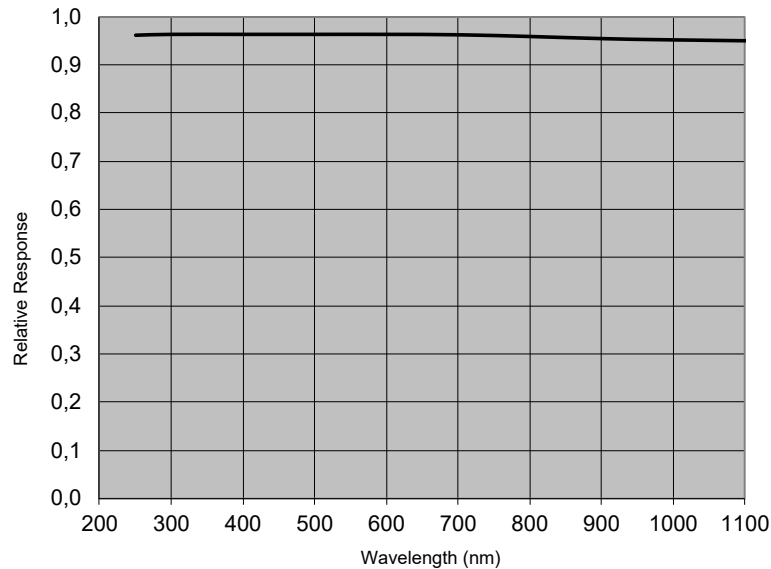


Figure 3.1: Typical relative spectral responsivity of a pyroelectric detector between 250 nm and 1 100 nm as provided by manufacturer specifications.

A pyroelectric detector consists of crystalline material with electric polarisation covered in a black absorbing coating which provides a spectrally neutral absorbance. When exposed to optical radiation the crystal heats and expands, causing a change in polarisation. This produces a build-up of charge at the opposing surfaces of the crystal, generating a current which in turn charges a capacitor. The capacitor produces a voltage, or a current when the voltage is held constant. Since the current is produced by a change in temperature, pyroelectric detectors only respond to modulated radiation which is achieved with the use of an optical chopper [Newport, 2021d]. For electrical measurement with pyroelectric detectors, lock-in amplifiers are used to lock onto the AC voltage output.

Thermopile sensors consist of a number of thermocouples which work on the principle of the Seebeck effect, where a temperature difference in the thermocouple generates a voltage. A thermocouple is constructed from two different metals which are connected in series. To absorb radiation, one junc-

tion is blackened. A voltage is generated when radiation is incident on the blackened junction, producing a temperature difference between this hot junction and the cold, non-irradiated junction. Since a single thermocouple produces a low voltage, many thermocouple junctions are connected in series to create a thermopile [Newport, 2021e].

Thermopiles can also be operated with an AC signal using an optical chopper. This is possible since thermopiles have a slow response time due to the heating and cooling process which typically takes a few seconds. This means that thermopiles can only measure a pulse every few seconds. However, since the voltage output is due to the heat flowing through the thermocouples after a pulse, the measured pulse may be short, despite the slow response time.

Detectors like thermopiles which can be operated with both DC signal and AC signal are used to determine duty cycles. The duty cycle is a property of the signal generated with an optical chopper and is the ratio of signal measured to no signal measured. The duty cycle of the signal generated by the optical chopper should be measured and considered in the determination of spectral responsivity. A way to determine the duty cycle is to calculate the ratio of the AC signal with the optical chopper switched on, to the DC signal with the optical chopper switched off.

Pyroelectric detectors are sensitive to thermal, electromagnetic and acoustic disturbances and require sufficient insulation, baffling and noise dampening. Since the optical chopper causes acoustic noise, placement far from the pyroelectric detector is preferred.

Other detector standards that may be calibrated against Si-trap detectors and used on a more regular basis are referred to as working standards. These detectors are typically single-element photodiodes. Photodiodes generate current

from incident photons. The material from which the photodiode is made determines the energy band to which the detector is sensitive. Incident photons which have energy greater than the energy band gap create electron-hole pairs in the semiconductor, generating a photocurrent [Gardner *et al.*, 2011].

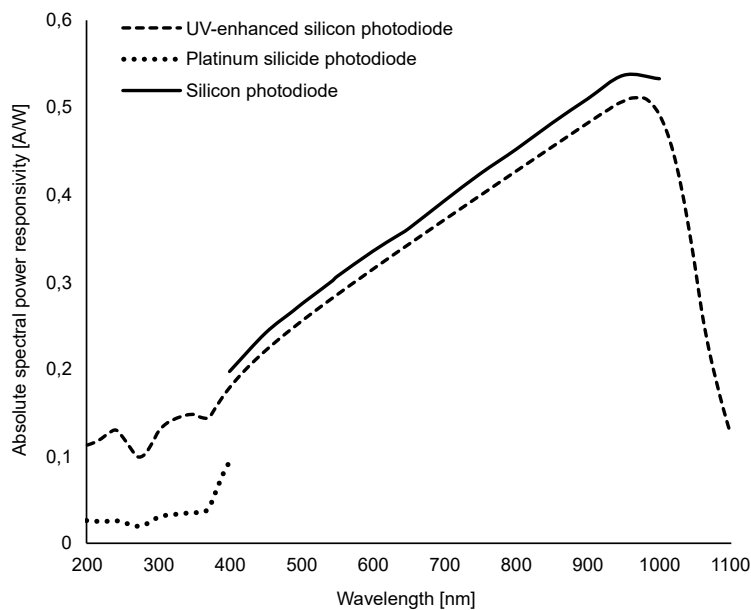


Figure 3.2: Absolute spectral power responsivity of a typical silicon photodiode, a platinum silicide photodiode and a UV-enhanced silicon photodiode detector.

Selection of these detectors depends on their responsivity characteristics. Si photodiode detectors have sensitivity in the UV to near IR region and are commonly used for analysis applications. The use of platinum silicide (PtSi) photodiodes is preferred in the UV region, since they are less susceptible to change due to UV radiation exposure than silicon photodiodes. See Figure 3.2 for the absolute spectral power responsivity of typical Si photodiode [Theron and Botha, 2003], PtSi photodiode [Werner and Vogel, 2018] and UV-enhanced Si photodiode [Winkler, 2018] detectors which have a spectral response varying from 200 nm to 1 100 nm.

## **3.2 Uncertainty contributors**

Detector-related factors that contribute to the uncertainty associated with the spectral power responsivity measurement of a detector are discussed below. These uncertainty contributors are determined for the spectral power responsivity calibrations performed in this study and are discussed in detail in Section 8.4.

### **3.2.1 Drift in responsivity of the detector**

The responsivity of a detector standard may change with time. This drift is wavelength dependent and can be predicted with models or determined from available calibration history. To minimise the contribution of drift to the measurement uncertainty, the detector standard should be re-calibrated within the required time interval.

The responsivity of Si photodiode detectors is known to change with exposure to UV radiation. PtSi photodiodes are stable at low UV radiation exposure, but their responsivity may also change when exposed to UV radiation for long periods of time or at high UV irradiance levels. To reduce changes in responsivity due to UV radiation exposure, these detectors are typically aged before use. This is done by exposing the detector to UV radiation for a period of time, thereby minimising any changes to responsivity due to UV radiation after initial exposure.

### **3.2.2 Spatial uniformity**

For spectral power responsivity measurements, the light beam underfills the detector. Therefore, the uniformity of the spatial responsivity of the detector needs to be considered. This may be done by measuring the responsivity at individual spots in a grid over the detector surface and quantifying the effect.

### **3.2.3 Linearity**

The effect where the responsivity of a detector changes with different levels of incident flux is called non-linearity. It is therefore important to calibrate a detector for responsivity at or near the power level of its intended use. The linearity of a detector may be characterised by measuring its responsivity at different power levels of incident flux and quantifying the effect. Some causes of non-linearity may be wavelength-dependent, so unless wavelength independence is known with certainty, responsivity at different power levels should be measured at more wavelengths in the region of interest.

At lower power levels, (below 500  $\mu\text{W}$ ) detectors such as Si photodiodes and PtSi photodiodes are linear and the contribution to uncertainty due to non-linearity is very low [Werner, 2014].

### **3.2.4 Temperature dependence**

The responsivity of detectors is dependent on temperature. To determine this effect, wavelength-dependent temperature coefficients are determined and used to correct the responsivity measured for a detector [Gardner *et al.*, 2011]. This temperature correction is required when the temperature during the calibration of a detector is different to that during use.

Temperature coefficients are quantifications of the sensitivity of detectors to changes in temperature. This sensitivity is determined by measuring the responsivity at specified temperatures over a range of temperatures and once determined may be used for similar types of detectors.

### **3.2.5 Measurement equipment**

Equipment, such as amplifiers and digital multimeters, used in a measurement system to measure the signals received by the detectors also contributes to the measurement uncertainty. Typically these uncertainty contributions can be obtained from the calibration certificates of such equipment.

In cases where the same equipment and ranges are used for the detector standard and the detector being measured, no corrections are necessary. However, if *e.g.* different amplification settings are used, relevant corrections should be made to the responsivity calculation, refer to Equation 4.6.

## Chapter 4

# Spectral power responsivity

The responsivity,  $s$ , of a detector is defined by CIE S 017:2020 ILV, the *International Lighting Vocabulary* [CIE, 2021], as the quotient of the detector output,  $Y$ , and the detector input,  $X$ ,

$$s = \frac{Y}{X}. \quad (4.1)$$

Typically, as is the case in this study, the detector input is incident optical power and the detector output is an electrical signal.

The spectral power responsivity is the quotient of detector output and detector input as a function of wavelength. To determine the spectral power responsivity of a detector, it must be underfilled with a monochromatic light beam, *i.e.*, the total optical power of the light beam must be incident on the detector, see Figure 4.1.

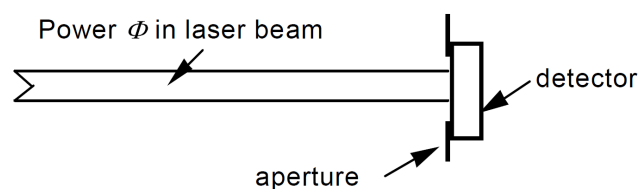


Figure 4.1: Measurement geometry for power measurement taken from technical report CIE 202:2011 [Gardner *et al.*, 2011].

Measurement of spectral power responsivity may be with a stabilised laser source when the standard detector is an ESCR or Si-trap detector, or with a broadband source in combination with narrow-band filters or a monochromator [Gardner *et al.*, 2011]. See Section 6.1 for a detailed description of the operation of a monochromator system.

Spectral power responsivity functions of detectors provide traceability to other photometric and radiometric calibrations and are therefore key in providing traceability for many calibration services.

A spectral power responsivity calibration transfers a spectral power responsivity function from a reference detector to a test detector. The reference detector is a standard detector traceable to the SI units, which are realised by NMIs and maintained on national measurement standards. The national measurement standards for spectral power responsivity are typically Si-trap detectors, which are traceable to the national measurement standards for optical power, typically electrical substitution cryogenic radiometers (ESCRs). ESCRs are traceable to the SI unit for electric current, ampere. The spectral power responsivity scale realised at an NMI can be transferred to working standard detectors.

## **4.1 Measurement methods**

### **4.1.1 Substitution method**

The transfer of a spectral power responsivity function can be done by direct comparison of the test detector against a standard detector using the substitution method [Gardner *et al.*, 2011]. To use this method, the test and standard detectors must have similar properties, such as sensitivity in the same wavelength region and linearity. The standard detector measures the incident monochromatic



radiant power,  $\Phi(\lambda)$ , and produces an output signal,  $V_S(\lambda)$ , given by

$$V_S(\lambda) = s_S(\lambda)\Phi(\lambda), \quad (4.2)$$

where  $s_S(\lambda)$  is the known spectral power responsivity of the standard detector.

The standard detector is then substituted with the test detector, which measures the same incident monochromatic radiant power and produces an output signal,  $V_T(\lambda)$  given by

$$V_T(\lambda) = s_T(\lambda)\Phi(\lambda), \quad (4.3)$$

where  $s_T(\lambda)$  is the unknown spectral power responsivity of the test detector that can be calculated from Equation 4.2 and Equation 4.3:

$$s_T(\lambda) = s_S(\lambda) \frac{V_T(\lambda)}{V_S(\lambda)}. \quad (4.4)$$

In a typical spectral power responsivity setup using a broadband source and monochromator, the output voltage signal includes the responsivity of the detector,  $s(\lambda)$ , the gain setting of the amplifier,  $G$ , the sensitivity setting of the lock-in amplifier if used,  $S$ , the incident quasi<sup>1</sup>-monochromatic radiant power,  $\Phi(\lambda)$ , contributions from the monochromator,  $M(\lambda)$ , such as the efficiency of the gratings and reflectance of the mirrors, and the input and output optics,  $O(\lambda)$ , and is given by

$$V(\lambda) = s(\lambda)GS\Phi(\lambda)M(\lambda)O(\lambda). \quad (4.5)$$

The gain setting of the amplifier,  $G$ , and sensitivity setting of the lock-in amplifier,  $S$ , are not wavelength dependent. However, they are adjusted, if necessary, according to the signal level measured as the monochromator scans through the

<sup>1</sup>The distinction between monochromatic and quasi-monochromatic radiant power is explained in Section 6.5.3.

wavelength region of interest.

When using the substitution method, the ratio of output signals of the test detector and the standard detector is given by

$$\frac{V_S(\lambda)}{V_T(\lambda)} = \frac{s_S(\lambda)G_S S_S \Phi_S(\lambda)M_S(\lambda)O_S(\lambda)}{s_T(\lambda)G_T S_T \Phi_T(\lambda)M_T(\lambda)O_T(\lambda)}. \quad (4.6)$$

Since the test detector and standard detector are substituted in the same measurement setup, some contributions in Equation 4.5 may cancel in the ratio. Even though these contributions cancel, their effects on spectral power responsivity should still be considered in the uncertainty of measurement determination. A few examples of this are discussed below.

For an ideal case, it is assumed that the source used remains constant during the comparison between the standard and test detectors. This is not the case in a real measurement, since the radiant power of the source may have fluctuations and may drift during the measurement. The contribution of the source stability must therefore be considered in the determination of the measurement uncertainty.

If the gain setting of the amplifier is the same for the standard and test detectors, it will cancel in the ratio, but the uncertainty in the gain setting provided for the amplifier must be considered in the uncertainty calculation of the calibration.

The contributions of the monochromator and the input and output optics will be the same for the standard and test detectors, however several effects related to the monochromator and optics influence the measurement result. For example, the wavelength calibration of the monochromator will be the same in certain wavelength regions, but its contribution to the standard and test detectors differ and must be determined for the measurement uncertainty calculation.

Other contributions that cancel but contribute to the measurement uncertainty are discussed in detail in Section 8.4.

Typically, the contributions from the source, the monochromator, the input and output optics and (if applicable) amplifier gain and sensitivity settings are the same, and cancel in the ratio. Equation 4.6 simplifies to

$$\frac{V_S(\lambda)}{V_T(\lambda)} = \frac{s_S(\lambda)}{s_T(\lambda)}, \quad (4.7)$$

and the spectral power responsivity of the test detector,  $s_T(\lambda)$ , is given by

$$s_T(\lambda) = s_S(\lambda) \frac{V_T(\lambda)}{V_S(\lambda)}. \quad (4.8)$$

#### **4.1.2 Transferring spectral power responsivity using a wavelength-extending detector**

A spectral power responsivity calibration may also be transferred from a reference detector that has been calibrated at one or more specific wavelengths. For example, a Si-trap standard detector may be calibrated for spectral power responsivity against an ESCR using one or more stabilised laser sources. A working standard detector may then be calibrated against the Si-trap detector standard at one or more of the same wavelengths used with ESCR with one or more stabilised laser sources using the substitution method. These calibration points are known as absolute tie points.

A spectrally flat detector, which has a constant responsivity over a large wavelength region, may be used as a transfer standard to extend the spectral power responsivity calibration of the working standard detector to a larger wavelength range, outside the wavelength range of the calibrated points. This

## *Spectral power responsivity      Realisation of responsivity scales at other NMIs*

---

can be done only if the spectrally flat detector's relative spectral power responsivity is known in a wavelength range larger than that of the working standard detector [Gardner *et al.*, 2011].

If a pyroelectric detector is used as such a wavelength-extending transfer standard, its surface coating may be measured to determine the spectral absorptance, which is proportional to the relative spectral responsivity. The working standard detector can be calibrated against the pyroelectric detector for relative spectral power responsivity using a broadband source and a monochromator setup, and the substitution method. This relative calibration can be converted to an absolute spectral power responsivity calibration using one or more absolute tie points.

## **4.2 Realisation of responsivity scales at other NMIs**

Some spectral power responsivity scales maintained at other NMIs are discussed as a comparison to the scale maintained at NMISA.

At NMISA, the spectral power responsivity scale in the UV region is maintained on a UV-enhanced Si photodiode detector, which is a national measurement standard. This scale is transferred to working standard detectors, such as single-element PtSi photodiodes, using the substitution method and a monochromator system.

In the visible to near-IR region, the spectral power responsivity scale is maintained on a set of Si-trap detectors, which are the national measurement standards and which have been calibrated against the ESCR at the National Physical Laboratory (NPL) of the United Kingdom at a few single wavelengths. A pyroelectric detector is used outside the range where the Si-trap detectors have been calibrated to transfer the scale to an extended wavelength region using a mono-

## *Spectral power responsivity      Realisation of responsivity scales at other NMIs*

---

chromator system. This spectral power responsivity scale provides the traceability for calibration of working standard detectors, such as single element Si photodiodes, using the substitution method and a monochromator system.

The National Institute of Standards and Technology (NIST) maintains the primary standard for optical power, the primary cryogenic radiometer, against which a secondary cryogenic radiometer is calibrated. The secondary cryogenic radiometer is used to calibrate transfer detectors using tuneable laser sources and the substitution method [Larason and Houston, 2008]. By using tuneable laser sources, the spectral power responsivity calibration is performed at numerous wavelengths in the UV to the near-IR range and interpolated at other wavelengths using a curve fit.

The transfer standards are a Si photodiode detector, Si-trap detectors, a germanium (Ge) photodiode detector and an indium gallium arsenide (InGaAs) photodiode detector. For the region of 1 650 nm to 1 800 nm, a pyroelectric detector is used to extend the spectral power responsivity calibration. The transfer standard detectors are used to calibrate a set of working standard detectors on a monochromator system.

The national metrology institute of Germany, Physikalisch-Technische Bundesanstalt (PTB), calibrates transfer detectors against a cryogenic radiometer using discrete laser line sources and a tuneable laser source [Werner *et al.*, 2000]. From this, the spectral power responsivity is interpolated between available laser lines. The transfer detectors are Si-trap and UV Si-trap detectors used to calibrate working standards such as Si photodiode detectors. As mentioned in the publication Werner *et al.* [2000], for the wavelength region of 238 nm to 1 015 nm, no monochromator-based system is used, instead, several laser lines are used and interpolation is performed between these wavelengths. This method eliminates the use of wavelength-extending detectors, which may reduce the measurement

## *Spectral power responsivity      Realisation of responsivity scales at other NMIs*

---

uncertainty.

At the Korea Research Institute of Standards and Science (KRISS), the primary standard for spectral power responsivity is a cryogenic radiometer, against which Si-trap detectors are calibrated using discrete laser line sources. The Si-trap detectors are used as working standards and disseminate the spectral power responsivity scale to other detectors using the substitution method. To extend the calibration beyond the wavelength range in which the Si-trap detectors were calibrated, a pyroelectric detector is used on a monochromator system as a transfer detector standard [Lee *et al.*, 2006].

At NPL, the spectral power responsivity scale is traceable to their primary standard, a cryogenic radiometer. The spectral power responsivity is transferred to Si-trap detectors at single laser lines and pyroelectric detectors are used outside the range covered by the Si-trap detectors. These transfer detectors are used to calibrate single-element photodiodes on a monochromator system which serve as working standards [Goebel and Stock, 2004b].

From this discussion, it can be concluded that NMISA uses similar methods to other NMIs to maintain the spectral power responsivity scale and therefore maintains international equivalence for the spectral power responsivity measurement capability.

## Chapter 5

# Sources of optical radiation

The *International Lighting Vocabulary* [CIE, 2021], defines optical radiation as electromagnetic radiation ranging from the wavelengths of X-rays to radio waves. Spectral power responsivity is typically determined from around 200 nm, UV wavelengths, through the visible wavelength range, approximately 380 nm to 780 nm, up to the IR wavelengths, approximately 1 800 nm.

### 5.1 Spectral distribution

Sources of optical radiation have distinct spectral distributions over a specific wavelength region which are referred to as continuum or spectral lines [Kostkowski, 1997]. Spectral line sources are typically used for the wavelength calibration of a monochromator or spectroradiometric system. See Section 7.1 that describes spectral line sources as wavelength standards. Continuum sources have spectral distributions that vary smoothly with wavelength and are used in conjunction with a monochromator to produce quasi-monochromatic radiation.

When choosing a source for a spectral power responsivity calibration, its spectral distribution should be considered. It should be a continuum source having a

spectral distribution without spectral lines in the wavelength region to be measured. A source with a high output power in the region of interest should be used, since high throughput of the monochromator system is an important aspect of a spectral power responsivity calibration.

Sources typically used in the UV wavelength region are deuterium lamps, xenon-arc lamps or laser-driven light sources (LDLSs). In an LDLS, optical power from a laser beam is used to sustain a high-intensity plasma. The plasma typically consists of xenon or another inert gas and is an optical-discharge plasma, whereas a xenon-arc lamp uses an electrical-discharge plasma [Zhu *et al.*, 2006]. Quartz Tungsten Halogen (QTH) lamps are used for the visible to the IR wavelength region.

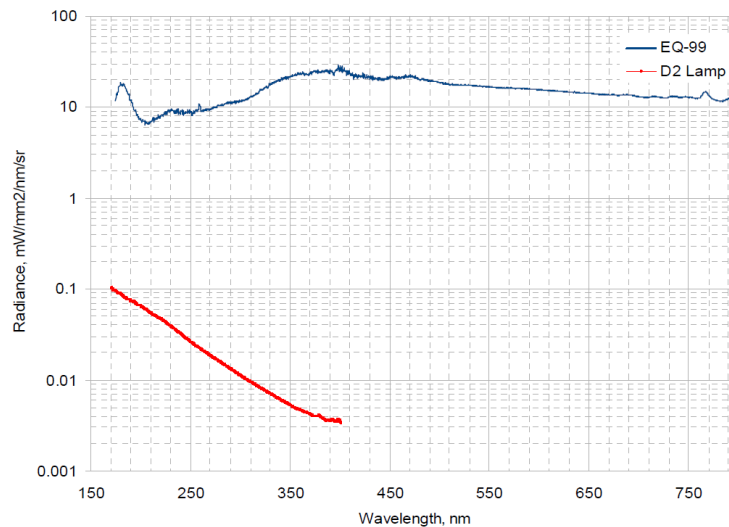
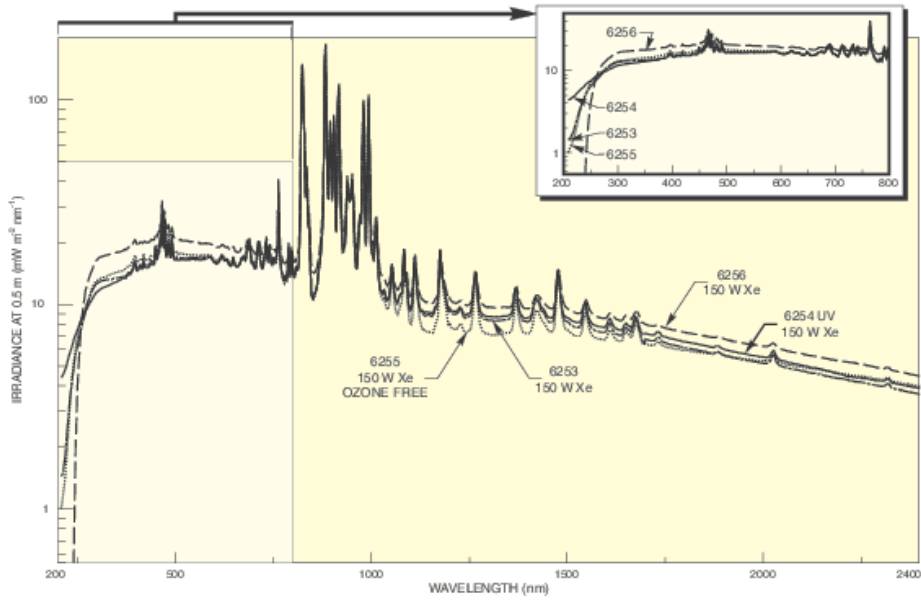


Figure 5.1: Spectral distributions of a LDLS compared to a deuterium source obtained from Energetiq [2011].

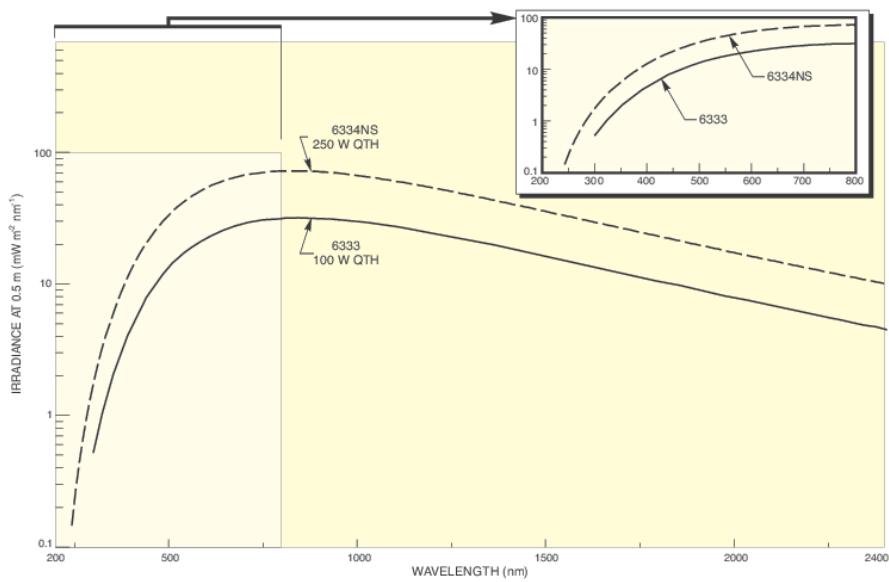
Figure 5.1 provides a comparison between a deuterium source and a LDLS (EQ-99), indicating the overall higher spectral distribution of the LDLS. A LDLS has a higher spectral radiance in the UV region than both deuterium and xenon-arc



sources.



(a) Xenon-arc source



(b) QTH source

Figure 5.2: Spectral distributions of xenon-arc and QTH sources obtained from Newport [2021b].

As seen in Figure 5.2(a), the continuum spectral distribution of a xenon-arc source also contains spectral lines, making it unsuitable for use in the visible region. Also shown in Figure 5.2(a) and Figure 5.2(b) is the higher spectral distribution of a xenon-arc source below 400 nm compared to that of a QTH source, which makes a xenon-arc source appropriate for use in the UV wavelength region.

Two wavelength regions were considered for the characterisation of spectral power responsivity in this study, namely UV or 200 nm to 400 nm, and visible to near-IR or 600 nm to 1 100 nm. For the UV wavelength region, a xenon-arc source was used. A LDLS was experimented with in this region for its higher spectral radiance than a xenon-arc source; refer to Appendix F for this discussion. For the visible to near-IR wavelength region, a QTH source was used.

## **5.2 Uncertainty contributors**

Factors related to sources of optical radiation that contribute to measurement uncertainty associated with the spectral power responsivity measurement of a detector are discussed below. The effect of these uncertainty contributors was determined for the spectral power responsivity calibrations performed in this study and is discussed in detail in Section 8.4.

### **5.2.1 Source stability**

Sources may experience power fluctuations and time-dependent drift in radiant power during the measurement. To correct for these effects, a monitor detector may be used to continuously measure the incident optical power and can be placed in the optical system using a beam splitter to divert some of the light from the detector being measured. The ratio of the standard and test detectors' meas-

ured output signals and the monitor detector's output signal can be calculated to perform the correction. Equation 4.4 will then be modified to

$$s_T(\lambda) = s_S(\lambda) \frac{V_T(\lambda)/V_{MT}(\lambda)}{V_S(\lambda)/V_{MS}(\lambda)}, \quad (5.1)$$

where  $V_{MT}(\lambda)$  and  $V_{MS}(\lambda)$  are the output signals measured with the monitor detector simultaneously with the output signals of the test detector and standard detector, respectively.

Some sources may be equipped with an intensity controller which corrects the output power to the preset power level in real-time to supply constant output. This was the case when the QTH source was used in the visible to near-IR region, see Section 8.1.1.

If it is not possible to use a monitor detector or intensity controller, the stability of the source may be measured empirically. The effect should be quantified and added to the uncertainty of measurement. Such an empirical measurement was performed when the xenon-arc source was used in the UV region, a description is provided in Section 8.1.1.

## 5.2.2 Uniformity

The monochromatic radiation exiting the monochromator is not uniformly distributed over the area of the measurement spot, causing a non-uniform beam profile [Gardner *et al.*, 2011]. For example, if the source used has a coiled filament, the filament will be imaged onto the entrance slit and the irradiance at the entrance slit will not be uniform. Subsequently, the image at the detector surface will not be uniform either.

The non-uniformity of the beam at the detector surface may be characterised by measuring the irradiance field spatially with a small detector. This is especially

important if a detector is being overfilled, such as when measuring spectral irradiance responsivity. However, since the detector is underfilled for spectral power responsivity measurements, this effect of non-uniformity may be minimised by rotating the detector about the optical axis and averaging the measurements.

### **5.2.3 Polarisation**

Polarisation is a wavelength-dependent property of the source, transferred to the monochromator system. This is an important effect to consider if the responsivity of the detector is dependent on polarisation. The sensitivity of a detector to polarisation is mainly a result of an angled optical interface. Therefore polarisation sensitivity should be considered if the incident flux is not perpendicular to the detector surface, or if it has angular divergence [Gardner *et al.*, 2011], since the responsivity of a detector to a divergent beam is not similar to that of a parallel beam. Refer to Section 6.5.2 which discusses beam divergence.

According to the CCPR-K2.b intercomparison report on responsivity, for incident flux perpendicular to the detector surface, single photodiodes are not significantly sensitive to polarisation effects, whereas trap detectors may show some sensitivity [Goebel and Stock, 2004b].

To eliminate polarisation effects on a detector, an integrating sphere, which depolarises the incident flux, may be used [Hengstberger, 1984]. Typically the requirement for spectral power responsivity measurements is the use of such unpolarised radiation. Another way to minimise or quantify polarisation effects is to integrate polarisation components. This can be done by rotating the detector about the optical axis of the incident flux at specified angles between measurement sets and averaging the results.

## Chapter 6

# The monochromator system

The typical monochromator system consists of a monochromator which includes dispersive elements and internal optics, and is combined with sources of optical radiation. Such a system includes order-sorting filters if required and imaging optics. Each of these components is discussed below.

### 6.1 Basic operation of a monochromator

A monochromator is an instrument that disperses optical radiation from a broadband source into its constituent wavelengths, allowing monochromatic light to be measured. A monochromator typically consists of a collimator, a dispersing element and a focusing mirror. A collimator may be a mirror, that collects the optical radiation of the source and collimates it onto a dispersing element, usually an optical prism or diffraction grating. The dispersing element separates that optical radiation spatially as a function of wavelength. A focusing mirror is then used to focus and image the dispersed light onto the exit slit of the monochromator.

The most commonly used monochromator configuration for spectral power responsivity measurement is the Czerny-Turner layout in a “W” configuration. This configuration was used in this study and is shown in Figure 6.1.

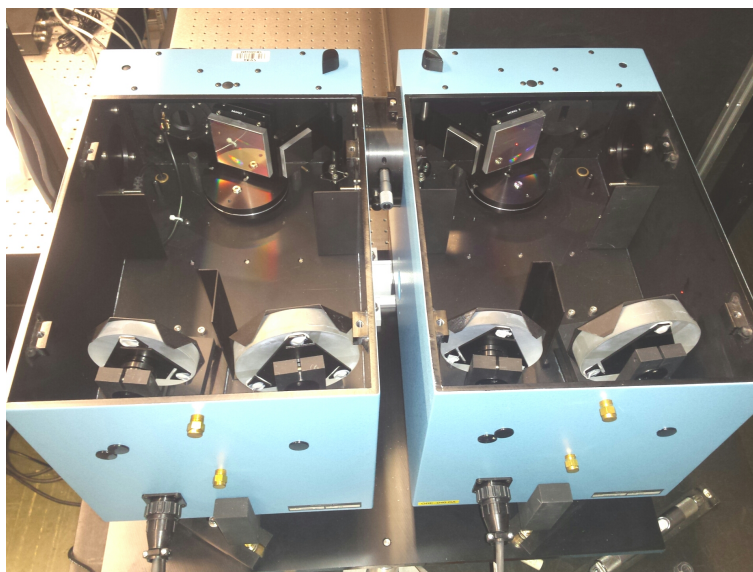


Figure 6.1: The “W” configuration of the Czerny-Turner monochromator mounting used.

A single Czerny-Turner monochromator consists of an entrance slit at the focal point of a collimating spherical mirror, which collimates the optical radiation from the entrance slit onto a diffraction grating. The diffracted light is imaged onto an exit slit using a focusing spherical mirror of the same focal length as the collimating spherical mirror. In a double Czerny-Turner monochromator, another single monochromator is connected in series to the exit slit of the first monochromator. The diffracted light from the first monochromator is dispersed again in the second monochromator.

## 6.2 Dispersive elements

The dispersive element in a monochromator is either an optical prism or a diffraction grating and governs the spectral range of the monochromator. Optical prisms are less costly than diffraction gratings, but it produces non-linear dispersion, *i.e.* the bandwidth does not remain constant for a constant slit width when scanned

through a wavelength range. See section 6.5.3 for the discussion on bandwidth.

In this study ruled diffraction gratings are used. A diffraction grating consists of an optical substrate, such as a mirror, with a reflective coating and machined grooves or rulings. The dispersion of a diffraction grating is linear but higher orders of wavelengths are produced [Sanders, 1984]. Diffraction gratings should therefore be used in combination with order-sorting filters to eliminate these higher orders.

The ideal situation is to have a prism-grating double monochromator to combine the advantages of both dispersing elements, *i.e.* considering that optical prisms disperse light non-linearly in wavelength but linearly in energy, and *vice versa* for diffraction gratings. Typically, double monochromators are grating-grating monochromators.

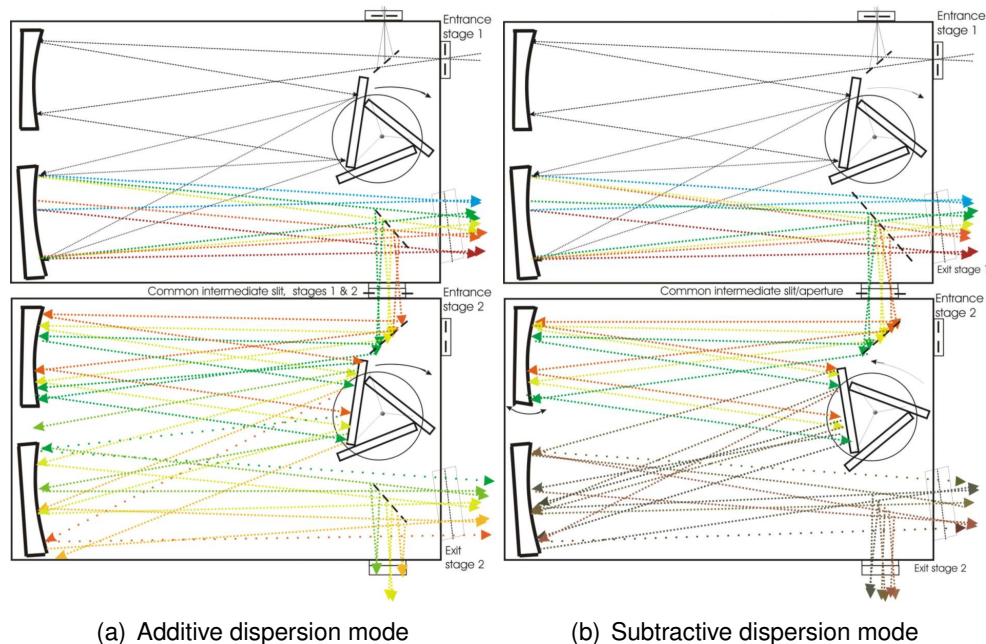


Figure 6.2: Illustration of a double monochromator in additive and subtractive dispersion mode [Neumann, 2014].

A double monochromator can be configured for additive dispersion or subtractive dispersion, depending on the application. In additive dispersion mode, Figure 6.2(a), the rotation of the two gratings is in the same direction, therefore the dispersion from the gratings in the two monochromators is in the same direction. This increases the dispersion, providing better resolution, but causes a non-uniform dispersion at the exit slit, *i.e.* containing some shorter wavelengths from the one side and some longer wavelengths towards the other. Additive dispersion double monochromators are commonly used, however, the non-uniform dispersion can cause errors if the detector of which the responsivity is being measured is not uniform. A typical application of additive dispersion double monochromators is therefore source characterisation such as spectral irradiance responsivity.

In subtractive dispersion mode, Figure 6.2(b), the gratings in the two monochromators are arranged to rotate in the opposite direction, such that the dispersion in the second monochromator reverses the dispersion of the first, mixing the wavelengths at the exit slit to produce uniform dispersion. A typical application of subtractive dispersion double monochromators is detector standardisation such as spectral power responsivity. The monochromator used for spectral power responsivity measurement in this study is therefore a subtractive double grating monochromator.

### **6.2.1 The grating equation**

The light dispersion caused by a diffraction grating is described by the grating equation. Figure 6.3 shows an incident beam of monochromatic light [Ientillucci, 2006]. A difference in the path length for ray 1 and ray 2 can be observed. This path length difference is given by  $d\sin\theta_i$  for the incident beam, and  $d\sin\theta_d$  for the diffracted beam, where  $d$  is the distance between the adjacent grooves or rulings



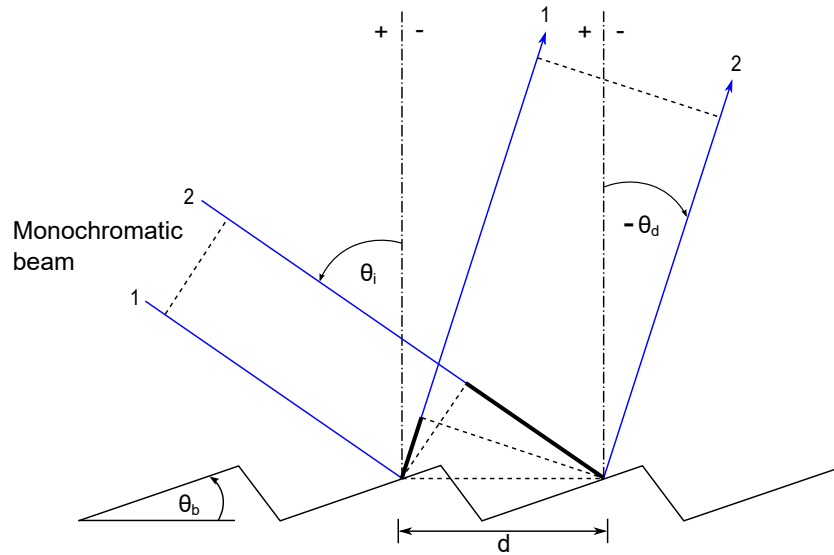


Figure 6.3: A schematic representation of the derivation of the grating equation [Lentillucci, 2006].

of the grating,  $\theta_i$  is the angle of incident flux and  $\theta_d$  is the angle of diffracted flux to the normal of the grating. For constructive interference to occur for the diffracted flux of the adjacent grooves, the total difference in path length must be an integer multiple of the wavelength,  $\lambda$ , producing the grating equation

$$m\lambda = d(\sin\theta_i \pm \sin\theta_d), \quad (6.1)$$

where  $m$  is the order of diffraction. A negative sign implies that the incident and diffracted flux are on opposite sides of the normal to the grating [Kostkowski, 1997].

## 6.2.2 Grating efficiency

A ruled grating specification will include the groove density [g/mm], and a blaze wavelength. The blaze wavelength is where the grating has its maximum effi-

ciency, this is the wavelength with the highest reflection and it is determined by the blaze angle,  $\theta_b$ . By general approximation, the efficiency of the grating will reduce by 50 % at two thirds of the blaze wavelength [Lerner and Thevenon, 1996].

Generally, the grating efficiency is determined in Littrow configuration. The Littrow condition occurs when the first order diffracted flux returns along the same path as the incident flux [Shimadzu, 2020]. The grating efficiency can be expressed as absolute or relative efficiency. The absolute grating efficiency is the ratio of the diffracted flux to the incident flux, for a given diffraction order. The relative grating efficiency is the absolute grating efficiency divided by the reflectance of the grating coating.

The polarisation of incident flux can cause a change in grating efficiency. For S-polarisation, where the oscillation direction of the electric field vectors is perpendicular to the grating grooves or rulings, large fluctuations may be observed in the grating efficiency curve. In the case of P-polarisation, where the oscillation direction of the electric field vectors is parallel with the grating grooves or rulings, a smooth curve will be observed [Shimadzu, 2020].

Figure 6.4 gives an example of a grating efficiency curve, obtained from the manufacturer, for a grating with a groove density of 600 g/mm blazed at 800 nm.

### 6.2.3 Dispersion

The dispersion specification of diffraction gratings is used to set the bandwidth of the monochromator.

The angular dispersion of the grating is obtained by differentiating the grating equation, 6.1, with respect to wavelength, for a constant angle of incidence,

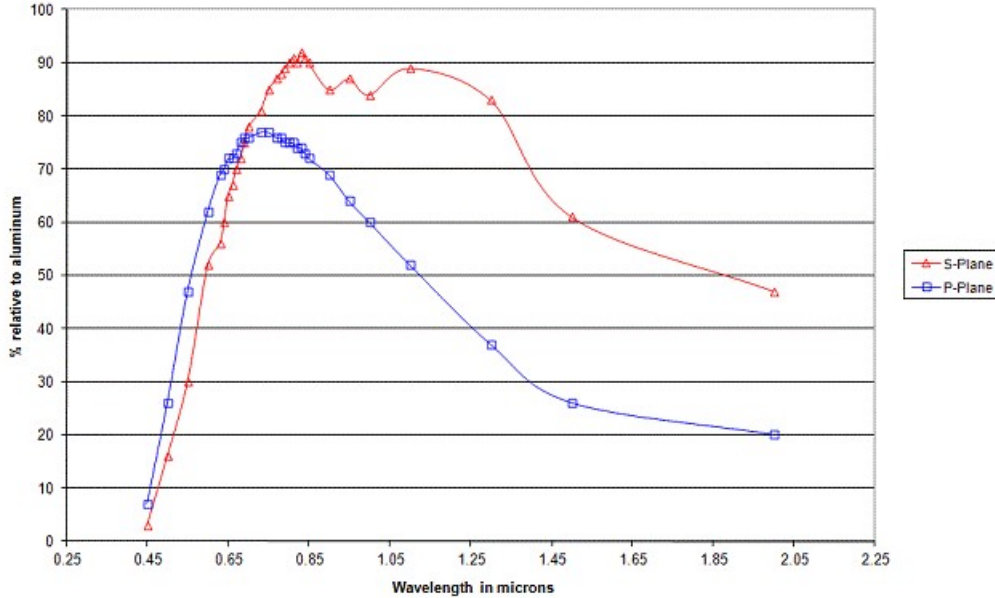


Figure 6.4: Example of a grating efficiency curve indicating the relative efficiency for a grating with a groove density of 600g/mm blazed at 800 nm with an aluminium coating [McPherson, 2017].

$$\frac{d\theta_d}{d\lambda} = \frac{m}{d\cos\theta_d}, \quad (6.2)$$

which indicates the change in the angle of diffraction,  $d\theta_d$ , with a change in wavelength,  $d\lambda$ . The unit for angular dispersion is [rad/nm] [Kostkowski, 1997].

The linear dispersion,  $\frac{dL}{d\lambda}$ , where  $L$  is the position along the spectrum, will vary with the focal length of the monochromator and angle of diffraction, and is obtained by multiplying the angular dispersion with the focal length,  $f$ ,

$$\frac{dL}{d\lambda} = f \frac{d\theta_d}{d\lambda} = \frac{fm}{d\cos\theta_d}. \quad (6.3)$$

The unit for linear dispersion is [mm/nm].

Generally, the reciprocal linear dispersion is used for the wavelength dispersion specification of the diffraction grating with the unit of nm/mm. The bandwidth

of the monochromator is selected by using this wavelength dispersion specification and a fixed slit width.

For example, a bandwidth of 4 nm was used for the calibration performed in the region of 600 nm to 1 100 nm. The set of gratings used has a groove density of 600 g/mm and is blazed at 800 nm. The dispersion of these gratings is 4 nm/mm. Therefore, the slit width was set to 1 mm to achieve a bandwidth of 4 nm. Similarly, a slit width of 2 mm may be used to achieve a bandwidth of 8 nm.

### **6.3 Order-sorting filters**

To suppress the higher orders produced by the diffraction gratings, *i.e.*  $m = 2$ ,  $m = 3$ , and so on, order-sorting filters are used. These are filters that have a near zero transmittance up to, and a near full transmittance above a specified wavelength.

Order-sorting filters are chosen based on the source used and the wavelength region being measured. Typically, a set of order-sorting filters are selected to cover the entire measurement range and inserted into a filter wheel. The filter wheel is placed at the entrance slit of the monochromator and may be externally controlled via a computer.

For example, consider the wavelength region of 400 nm to 650 nm to be measured using a QTH source. A QTH source typically starts to emit optical radiation between 250 nm and 300 nm. This means multiples of these wavelengths will start to be detectable at around 500 nm to 600 nm, which is within the wavelength range being measured.

To suppress these unwanted wavelengths, the order sorting filter GG395 may be used. This filter has a transmittance of approximately 50 % at 395

nm. The filter will have near zero transmittance below this wavelength and near 100 % transmittance above, see Figure 6.5. This means that any multiple of the wavelength region below 400 nm will be suppressed. It also means that any multiple from about 400 nm will be detectable, and therefore another order sorting filter will be required if measurements must be performed from approximately 800 nm.

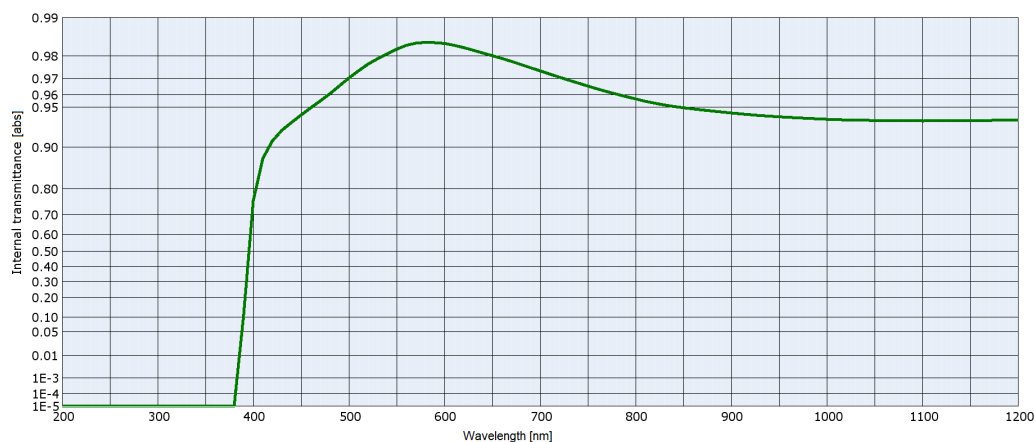


Figure 6.5: Transmittance of the order sorting filter GG395 [Schott, 2014].

## 6.4 Imaging optics

In this study, imaging optics refer to input optics that image the source onto the entrance slit of the monochromator, and output optics that focus the light emerging from the exit slit of the monochromator on the detector.

The selection of imaging optics depends greatly on the required aperture ratio. Figure 6.6 is used to explain the concept of aperture ratio and shows a lens with diameter,  $D$ , collimating light from a source. The focal length,  $f$ , is defined as the distance at which an optical component focuses the image of the source.

The aperture ratio of an optical component, or F-number ( $F/\#$ ), is defined

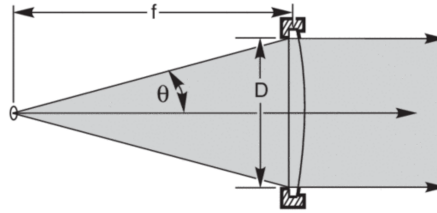


Figure 6.6: Illustration of a lens collecting and collimating light from a source [Newport, 2021c].

as

$$F/\# = \frac{1}{2n\sin\theta}, \quad (6.4)$$

where  $n$  is the refractive index of the ambient air and  $\theta$  is the half angle of the acceptance cone of optical radiation also known as the acceptance angle, see Figure 6.6.

For small angles,  $\theta \leq 15^\circ$ , the approximation of the ratio of the focal length of the optical component to the diameter of the effective aperture (typically the mask over a mirror or grating) is commonly used:

$$F/\# \approx \frac{f}{D} \quad (6.5)$$

To optimise the throughput of the monochromator system (how much light passes through the system), the  $F/\#$  of the input optics must match the  $F/\#$  of the monochromator [Newport, 2021c]. The optical radiation exiting the monochromator has the same  $F/\#$  as the monochromator.

Lenses or mirrors may be used as imaging optics. The advantages of mirrors are that they have no internal reflections or chromatic aberration. Though spherical aberration may be present in mirrors, it is typically negligible for mirrors with an aperture ratio of  $F/8$  or greater [Gardner *et al.*, 2011].

An aperture ratio of  $F/8$  or larger should be used when imaging the exit slit

of the monochromator onto the detector. If not, the angular divergence of the beam will be significant and may change the response of the detector [Gardner *et al.*, 2011].

## 6.5 Uncertainty contributors

Uncertainty contributors related to the monochromator system are discussed below and were determined for the uncertainty associated with the spectral power responsivity calibrations performed in this study. See Section 8.4 for a detailed discussion.

### 6.5.1 Inter-reflections between detector and exit slit of the monochromator

Detector surfaces may have high reflectance which causes inter-reflections between the exit slit of the monochromator and the detector being measured. Such inter-reflections may be detected with a monitor detector or reduced by blackening the slits. Typically these inter-reflection effects are negligible when the slits are blackened.

### 6.5.2 Beam divergence and vignetting

The divergence of a light beam is dependent on the  $F/\#$  of an optical component. As illustrated in Figure 6.7, an optical component with a high  $F/\#$  will produce a beam divergence with a small divergence angle,  $\theta_1$ , as opposed to an optical component with a low  $F/\#$  that will produce a beam divergence with a large divergence angle,  $\theta_2$ . Since the responsivity of a detector has angular dependence, the effect of beam divergence should be considered when determining the meas-

urement uncertainty.

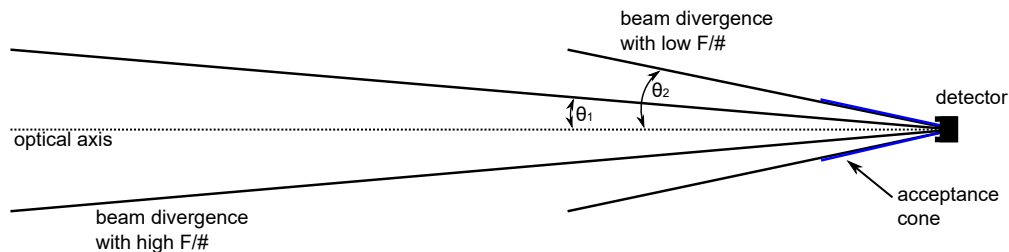


Figure 6.7: Illustration of beam divergence for a high vs low  $F/\#$ .

The technical report CIE 202:2011 [Gardner *et al.*, 2011] prescribes that the acceptance angle of a detector must be large enough not to cause vignetting (darkening or blurring at the periphery of the image) of the incident light beam. Vignetting is related to the  $F/\#$  of an optical component. Refer to Figure 6.7, if a low  $F/\#$  optical component with large beam divergence is used, the light might be blocked by the edges of the detector aperture or the acceptance cone of the detector.

The CCPR-K2.c key comparison report [Werner, 2014], specifies that the effect of beam divergence and vignetting is negligible if the beam divergence is within the acceptance angle of the detector. To minimise this effect, the typical requirement given in technical protocols for spectral power responsivity measurement is to use an optical component with  $F/8$  or higher to focus the light beam onto the detector surface. This requirement was met in the measurement setup used in this study and is discussed in Section 8.1.2.

### 6.5.3 Passband, bandpass and bandwidth

The technical report, CIE 214:2014 [Gardner *et al.*, 2014], best describes each of these terms when referring to a spectral interval to be isolated with a monochromator.



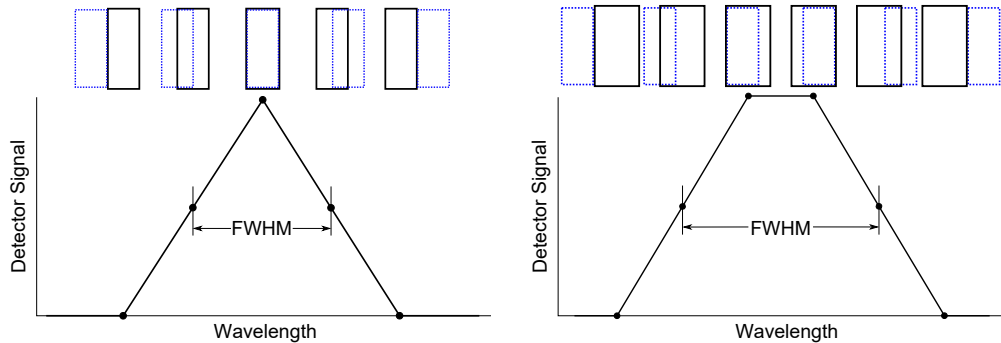
A monochromatic light source with wavelength  $\lambda_0$  analysed by an ideal monochromator, should produce output identical to the spectrum of the light source, *i.e.* a perfect line at  $\lambda_0$ .

However, a real monochromator includes the selected wavelength,  $\lambda_0$ , as well as the narrow band of wavelengths around this wavelength, the light from the monochromator is therefore referred to as quasi-monochromatic light. This real spectrum of the source that is selectively transmitted through the monochromator, taking into account the optical extent, transmission and reflection losses, grating efficiency and aberrations of the monochromator, is called the instrumental passband.

The line spread function or slit function is defined by CIE 214:2014 as the convolution of the distribution of light over the entrance and exit slits. With a monochromator, the entrance slit is imaged onto the exit slit and the exit slit determines the portion of the image that is transmitted, *i.e.* the signal on the detector. For a monochromatic source, a scan may be performed by changing the wavelength setting of the monochromator and measuring the signal on the detector as the image passes along the exit slit. Such a scan indicates the slit function and is illustrated in Figure 6.8.

The rectangles at the top of in Figure 6.8 indicate the exit slit (black rectangle) and the relative position of the image that is passed along the exit slit (blue dotted rectangle), and the extent to which they overlap. When the entrance and exit slits are of equal width, the slit function is triangular, see Figure 6.8(a), when the slit widths are unequal, the slit function is trapezoidal, shown in Figure 6.8(b).

The spectrum recorded through the monochromator is a convolution of the passband and the slit function and is called the instrumental bandpass. It is



(a) Slit function and bandwidth for slits of equal width (b) Slit function and bandwidth for slits of unequal width

Figure 6.8: Illustration of a triangular slit function and bandwidth for slits of equal width and a trapezoidal slit function and bandwidth for slits of unequal width. The black rectangles represent the exit slit and the blue dotted rectangles represent the relative position of the image that is passed along the exit slit. [Gooch and Housego, 2013]

defined as the range of wavelengths passed by an instrument in the interval  $(\lambda_0 - \Delta \leq \lambda \leq \lambda_0 + \Delta)$ , where  $\Delta$  is the bandwidth.

For a triangular or trapezoidal bandpass shape, the bandwidth is defined as the full width at half of maximum (FWHM) of the bandpass curve about the nominal wavelength,  $\lambda_0$ , or half the full base-width of the bandpass curve. The bandpass function is therefore zero outside the above-mentioned interval.

The bandwidth is determined by the size of the slits or the slit width. In subtractive double monochromators, the dispersion is entirely that of the first monochromator, the bandwidth is therefore controlled by the entrance and intermediate slits. For additive double monochromators, since the dispersion is in the same direction and therefore increased over a single monochromator, the bandwidth is controlled by the entrance and exit slits [Gardner *et al.*, 2011].

When measuring the spectral power responsivity of detectors, a subtractive double monochromator with equal slit widths may be used to provide maximum throughput and narrow bandpass.

Bandwidth effects are typically negligible in comparison with other uncertainty contributions if the relative spectral responsivity curves of detectors being compared have similar shapes.

#### **6.5.4 Resolution**

The resolution is the ability of a monochromator to separate wavelengths. Diffraction gratings with higher groove densities have higher reciprocal dispersion and higher resolution. Resolution specifications are typically provided by the manufacturer and are used in particular when performing the wavelength calibration of the monochromator and for the determination of the measurement uncertainty.

When determining the wavelength interval at which a measurement should be performed, the resolution must be considered. For example, if the resolution of a diffraction grating is 0,1 nm, it is not meaningful to have a wavelength interval of 0,05 nm.

#### **6.5.5 Stray light**

Stray light in a monochromator may refer to the effective transmission of wavelengths outside the bandpass [[Gardner et al., 2011](#)]; flux scattered from the diffraction grating, the focusing mirror and the monochromator housing [[Kostkowski, 1997](#)]; and spectral impurity, which is any stray light not accounted for by multiple order diffraction. Stray light is a property of grating monochromators [[Davis, 2000](#)]. This spectral impurity may be caused by errors in groove spacing or ghosts, errors or variations in groove locations, surface roughness, scratches or dust and variation in ruling depth.

The effect of stray light is worse where grating efficiency is low and at short wavelengths where the responsivity of the detector and spectral distribution of

the source are low.

As mentioned in Section 6.1, a single monochromator can be connected in series with a second monochromator, creating a double monochromator that disperses the light from the first monochromator a second time. This reduces stray light significantly and the use of a double monochromator is common practice in laboratories where low measurement uncertainty is required. According to Gardner *et al.*, 2011, a single monochromator has a typical stray light contribution of  $10^{-4}$ , where a double monochromator can reduce this contribution to  $10^{-8}$ .

Other ways to reduce stray light is to make sure the grating efficiency is not low at the wavelengths at which measurements are taken and to use a detector that has zero responsivity for most of the stray light.

Kostkowski [1997] describes a method for experimentally checking for out-of-band stray light in a monochromator system using order-sorting filters. An order sorting filter with very low or zero transmittance in the wavelength region to be checked for stray light, is placed at the entrance slit of the monochromator. Placing the filters at the entrance of the monochromator will reduce the amount of optical radiation inside the monochromator that may contribute to stray light. If the output signal drops to close to zero, or the same level as when the optical shutter is closed, then the effect of stray light is insignificant. To quantify the effect of stray light, the ratio of the output signal with the optical shutter closed, with and without the filter may be calculated. An example of this method can be seen in the paper Kruger and Sieberhagen [2015], where the stray light of an array spectroradiometer was investigated.

For this study, two terms will be used for the evaluation of their uncertainty contributions, namely internal and external stray light. Internal stray light refers to the stray light at out-of-band wavelengths, scattered light and spectral impurity

caused by the internal optical components of the monochromator. External stray light refers to scattered light from reflections outside the monochromator. This effect can be corrected with the use of an optical shutter at the entrance slit of the monochromator. A dark signal is measured with the optical shutter closed and subtracted from the light signal measured when the optical shutter is open.

### **6.5.6 Wavelength accuracy**

It is critical to have good wavelength accuracy for a double monochromator. For applications where a low uncertainty of measurement is required, a wavelength calibration must be performed to determine the true position of the wavelength spectrum. Refer to Section 7 for a detailed description of how to perform such a calibration and the wavelength calibrations performed for the double monochromator.

## Chapter 7

# The wavelength calibration

The wavelength calibration should be performed before any measurement is done on the double monochromator and with each change in the monochromator setup, such as a change in diffraction gratings. The wavelength calibration produces a wavelength calibration equation, which may be used by the monochromator software when scanning through a wavelength region to record data.

### 7.1 Wavelength standards

Atomic emission spectral lines of spectral line sources are typically used as wavelength standards. These spectral line sources are lamps that contain specific elements and through the electrical discharge in such gas or vapour, emissions lines occur at known wavelengths [Kostkowski, 1997]. The NIST Atomic Spectra Database [NIST, 2019] lists the wavelengths of these emissions and also indicates the stronger emission spectral lines.

The atomic emission spectral lines in vacuum are typically selected from the NIST Atomic Spectra Database and are corrected for ambient air using the NIST Engineering Metrology Toolbox [NIST, 2004]. See Section 7.2 for a description of

how this correction is performed. Figure 7.1 provides an example of the emission spectral lines of the argon spectral line source used in this study.

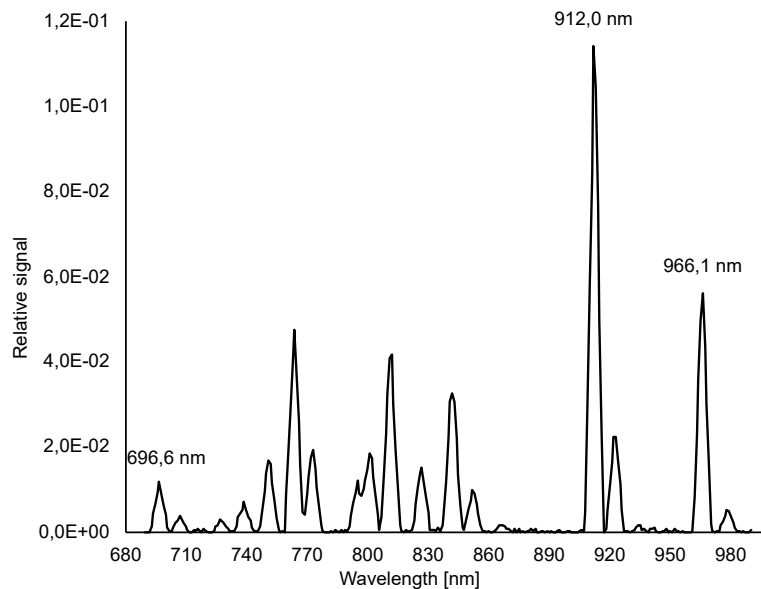


Figure 7.1: Emission spectral lines in ambient air of the argon spectral line source used for the wavelength calibration in the visible to near-IR region.

As mentioned in Section 6.2, diffraction gratings produce higher order wavelengths, causing second or higher orders of spectral lines to appear. Though these higher orders of spectral lines may be useful for the wavelength calibration, they can also cause line blending. This is when two or more spectral lines are too close to each other to be spectrally resolved. Order-sorting filters may be used to eliminate the unwanted higher orders of spectral lines. For example, mercury has an emission spectral line at 275,3591 nm, in vacuum, and will have a second order spectral line, in vacuum, at 550,7182 nm. This second order spectral line is close to the spectral line at 546,22675 nm and may cause line blending.

The wavelength region in which the wavelength calibration is to be performed and the spectral responsivity of the detector should be considered to determine whether the use of order-sorting filters is really necessary. For example,

## *The wavelength calibration      Determining the wavelength calibration equation*

---

a mercury spectral line source has an emission spectral line at 253,7283 nm, in vacuum, and will have a second order spectral line, in vacuum, at 507,4566 nm. If a wavelength calibration is performed from 200 nm to 400 nm, no order-sorting filters will be required. Another example is when a silicon photodiode detector is used to perform the wavelength calibration. Typically, the responsivity of silicon drops after 1 100 nm and other detectors, such as an indium gallium arsenide (InGaAs) detector, will be used at longer wavelengths. A mercury spectral line source has an emission spectral line at 546,22675 nm, in vacuum, and will have a second order spectral line, in vacuum, at 1 092,4535 nm. It is unlikely that this second order spectral line will be observed by the silicon photodiode detector.

## **7.2 Determining the wavelength calibration equation**

The appropriate spectral line source should be selected for the wavelength region in which the calibration is to be performed. The spectral line source is measured on the monochromator using the same bandwidth as to be used for the spectral power responsivity calibration. At first, a large spectral area scan should be performed to determine which spectral lines to use, refer to Figure 7.1. Good spectral lines will be those free of line blending. Spectral lines that are in the noise level should also be avoided.

At least three spectral lines should be selected in the wavelength region to be measured to provide sufficient data for a good statistical fit. Each chosen spectral line should be scanned at least three times. The wavelength of the peak of the spectral line may be determined using the steep-side method described in [Kostkowski \[1997\]](#). This method determines the wavelength of the peak of the



*The wavelength calibration      Determining the wavelength calibration equation*

---

spectral line by averaging the wavelengths at the steep sides of the spectral line at 10 % of the maximum signal,  $\lambda_1$  and  $\lambda_2$ , see Figure 7.2. The wavelength of the peak or centre wavelength is given by

$$\lambda_c = \frac{\lambda_1 + \lambda_2}{2}. \tag{7.1}$$

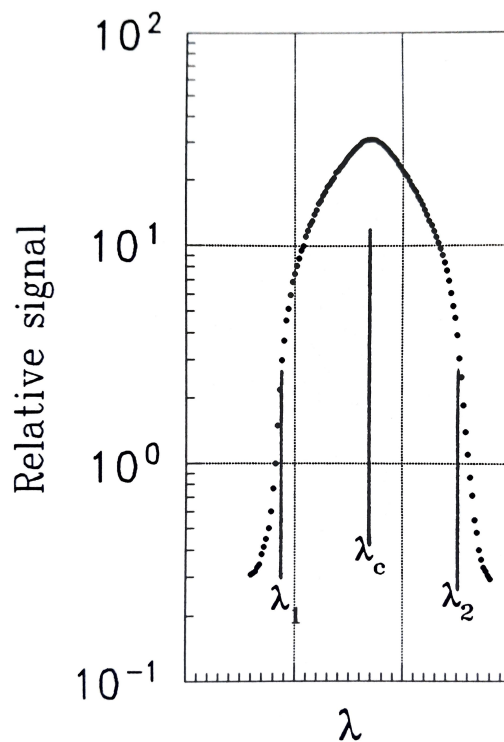


Figure 7.2: Excerpt from [Kostkowski \[1997\]](#) indicating the steep-side method for wavelength calibration.

The monochromator steps corresponding to the wavelength of the peak of each spectral line are used to determine the wavelength calibration equation, but first, the atomic emission spectral lines in vacuum should be corrected for ambient conditions using the NIST Engineering Metrology Toolbox.

This Toolbox utilises the modified Edlén equation to calculate the index of refraction of ambient air,  $n$ , from the supplied laboratory air temperature, relative humidity and air pressure. It then calculates the wavelength in ambient air,  $\lambda_{air}$ , from the wavelength in vacuum,  $\lambda_{vac}$ , and the refractive index using the relationship:

$$\lambda_{air} = \frac{\lambda_{vac}}{n} \quad (7.2)$$

The index of refraction calculated using this Toolbox is the phase refractive index but will be referred to as the refractive index in this study.

Once the spectral lines in ambient air are obtained, the monochromator steps versus the wavelength of the peak of each corrected spectral line are plotted. The appropriate fit for the data is derived for the expected wavelength calibration equation.

### **7.3 Method**

The internal optics of the double monochromator were aligned with two low-power Helium/Neon (HeNe) lasers, one at the input side and one at the output side of the double monochromator, see Appendix B for a detailed description. Optimised alignment of each of the optical components ensures maximum throughput for the monochromator system. The initial alignment was checked and minor adjustments were performed when other gratings were installed for operation in a different wavelength region.

A wavelength calibration was performed for the double monochromator in the wavelength regions of 200 nm to 400 nm and 600 nm to 1 100 nm using the standard laboratory procedure. The relevant spectral line sources were used, together with silicon photodiode detectors and a variable gain low noise current

amplifier connected to a multimeter operated with the monochromator software. The spectral lines were obtained from the NIST Atomic Spectra Database. To find the monochromator steps corresponding to each spectral line wavelength, the steep-side method as described in Section 7.2 was used. The ambient conditions were measured during each calibration and a correction was applied for temperature, atmospheric pressure and relative humidity, to each spectral line wavelength using the Engineering Metrology Toolbox of NIST.

As mentioned in Section 6.5.3, for a subtractive double monochromator maximum throughput is achieved with equal slit widths. Therefore, for the calibrations performed, the entrance, intermediate and exit slits of the monochromator were all set to equal widths. See Appendix E for an experimental demonstration of slit functions for monochromator slits set to equal and unequal widths.

### **7.3.1 Wavelength region of 200 nm to 400 nm**

A set of 1 200 g/mm ruled gratings blazed at 300 nm was installed in the double monochromator. A mercury spectral line source was used and to achieve stable emission the spectral line source was allowed to warm up for at least 20 minutes; a warm-up time of 10 minutes is recommended by the manufacturer.

A scan was performed with the monochromator from 233 nm to 552 nm in 1 nm intervals. From this scan, the spectral lines used for this calibration were selected. These spectral lines, in vacuum, were 253,7283 nm, 296,8149 nm and 435,9560 nm. Each of these spectral lines was scanned using a wavelength interval of 0,2 nm. This is not the smallest wavelength resolution allowed for this set of gratings, but it was found to be sufficiently small for this wavelength calibration. Smaller wavelength intervals are selected if the spectral lines cannot be resolved. In this case, the spectral lines could be resolved well enough and with a

sufficiently small contribution to the measurement uncertainty using an interval of 0,2 nm, and it was decided that the use of a smaller interval was not necessary.

The scans were performed over a wavelength range of  $\pm 5$  nm of the spectral line. To achieve higher throughput, a bandwidth of 5 nm was used for this wavelength calibration. The dispersion of these gratings is 2 nm/mm, so the width of each of the slits was set to 2,5 mm to achieve the selected bandwidth.

Each spectral line was scanned with the monochromator. To determine the monochromator steps of the peak of the spectral line, the steep-side method was used. The monochromator steps at the steep sides of each spectral line corresponding to 10 % of the maximum signal were determined. However, when 10 % of the maximum signal is calculated, it does not necessarily correspond to the exact monochromator steps recorded during the scan. Instead of selecting the closest value of monochromator steps, a linear fit was used on each steep side of the spectral line to calculate the monochromator steps corresponding to the calculated 10 % of the maximum signal.

The recorded signal closest to the calculated 10 % of the maximum signal was used as the midpoint of five data points on each steep side of the spectral line, respectively. The five data points were used to determine a linear fit on each steep side of the spectral line, shown in blue in Figure 7.3. The linear fits were used to calculate the monochromator steps corresponding to the calculated 10 % of the maximum signal on each steep side of the spectral line. The average of these calculated monochromator steps was used to determine the monochromator steps of the peak of the spectral line.

In Figure 7.3, it can be observed that the five data points on the right steep-side have a different slope than the data points directly above them. This asymmetry may be caused by poor monochromator alignment and optical aberrations

in the monochromator optics. This asymmetry problem was not addressed in this study and is discussed in Section 11 as further research.

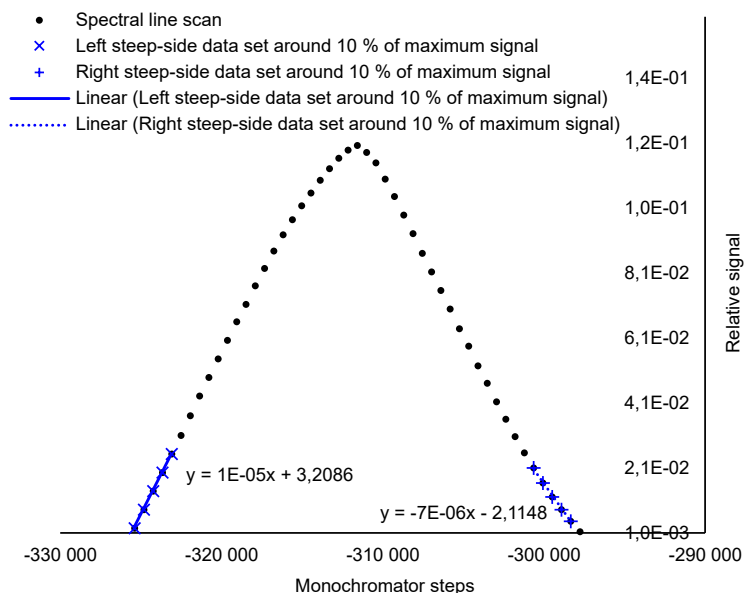


Figure 7.3: An example of the steep-side method and linear fits of data points around 10 % of maximum signal to determine the monochromator steps of the peak of a spectral line.

Three scans were performed for each spectral line and the same process was followed to calculate the monochromator steps of the peak of the spectral line. The average of the monochromator steps calculated for each of the three scans was used as the monochromator steps of the peak of the spectral line.

For the spectral line at 253,7283 nm in vacuum, 15 % of the maximum signal was used to determine the monochromator steps of the peak of the spectral line. This was because the range of the scan performed did not include 10 % of the maximum signal. For the same reason, 30 % of the maximum signal was used for one of the three scans performed for the spectral line at 435,9560 nm.

The selected spectral lines were corrected for ambient air using the ambient conditions recorded during the wavelength calibration. Corrections for ambi-

ent air using the NIST Engineering Metrology Toolbox [NIST, 2004] is limited to the wavelength region of 300 nm to 1 700 nm. Two of the wavelengths selected to determine the wavelength calibration equation in this wavelength region, 253,7283 nm and 296,8149 nm, therefore fall outside this range. The correction applied to these two wavelengths was the refractive index determined for the ambient air as specified in the laboratory procedure for temperature,  $24\text{ }^{\circ}\text{C} \pm 2\text{ }^{\circ}\text{C}$ , relative humidity,  $50\text{ \%RH} \pm 15\text{ \%RH}$ , and an atmospheric pressure of 86 kPa at 300 nm. This approximation was done as a best estimate and found to be sufficient as the results were within the stated uncertainty for the verification performed.

The monochromator steps were plotted against each corrected spectral line and a linear fit was applied to the data to obtain the wavelength calibration equation. The origin in the monochromator software was set to zero monochromator steps at the corrected wavelength of the spectral line 296,8149 nm, in vacuum.

A verification was performed by using the wavelength calibration equation 7.3 to calculate the corresponding monochromator steps and move the scan controllers of the monochromator to a laser line at 543 nm. The peak signal of the laser line was found at the monochromator position within the stated wavelength uncertainty.

### **7.3.2 Wavelength region of 600 nm to 1 100 nm**

A set of 600 g/mm gratings blazed at 800 nm was installed in the double monochromator. An argon spectral line source was used and to achieve stable emission the spectral line source was allowed to warm up for at least 20 minutes.

A scan was performed with the monochromator from 690 nm to 990 nm in 1 nm intervals. From this scan, the spectral lines used for this calibration were

selected. These spectral lines, in vacuum, were 696,7352 nm, 912,5471 nm and 966,0435 nm. Each of these spectral lines was scanned using a wavelength interval of 0,1 nm, which is the smallest wavelength resolution allowed for this set of gratings. The scans were performed over a wavelength range of  $\pm 5$  nm of the spectral line. A bandwidth of 4 nm was used for this wavelength calibration, since that was the bandwidth to be used for the spectral power responsivity calibration. The dispersion of these gratings is 4 nm/mm, so the width of each of the slits was set to 1 mm to achieve the selected bandwidth.

Each spectral line was scanned once with the monochromator and to determine the monochromator steps of the peak of the spectral line, the steep-side method was used. The monochromator steps at the steep sides of each spectral line corresponding to 10 % of the maximum signal were determined. For this wavelength region, the value of monochromator steps closest to the corresponding 10 % of the maximum signal was used, instead of a linear fit of the data points around the 10 % of the maximum signal to calculate the corresponding monochromator steps. The largest difference between the closest value and calculated value of monochromator steps using the linear fits, was approximately 36 monochromator steps. This is equal to approximately 0,025 nm, which is very small in comparison with the wavelength uncertainty of  $\pm 0,2$  nm obtained.

The selected spectral lines were corrected for ambient air using the ambient conditions recorded during the wavelength calibration and the NIST Engineering Metrology Toolbox [NIST, 2004]. The monochromator steps were plotted against each corrected spectral line. A linear fit was applied to the data to obtain the wavelength calibration equation. The origin in the monochromator software was set to zero monochromator steps at the corrected wavelength of the spectral line 696,7352 nm, in vacuum.

A verification was performed by using the wavelength calibration equa-

tion 7.4 to calculate the corresponding monochromator steps and move the scan controllers of the monochromator to the HeNe laser line at 632,8 nm. The peak signal of the laser line was found at the monochromator position within the stated wavelength uncertainty.



## 7.4 Results

### 7.4.1 Wavelength region of 200 nm to 400 nm

The wavelength calibration equation was found to be

$$y(\lambda) = 288,047\lambda - 855\,187, \quad (7.3)$$

where  $y(\lambda)$  is the monochromator steps and  $\lambda$  is the wavelength in angstrom [Å], see Figure 7.4. Also shown in the figure is the R-squared value as an indication of how well the linear model fits the data set.

The uncertainty of measurement in wavelength was  $\pm 0,3$  nm. See Section 7.5 for a detailed description of the uncertainty of measurement analysis and Appendix G for the uncertainty budget.

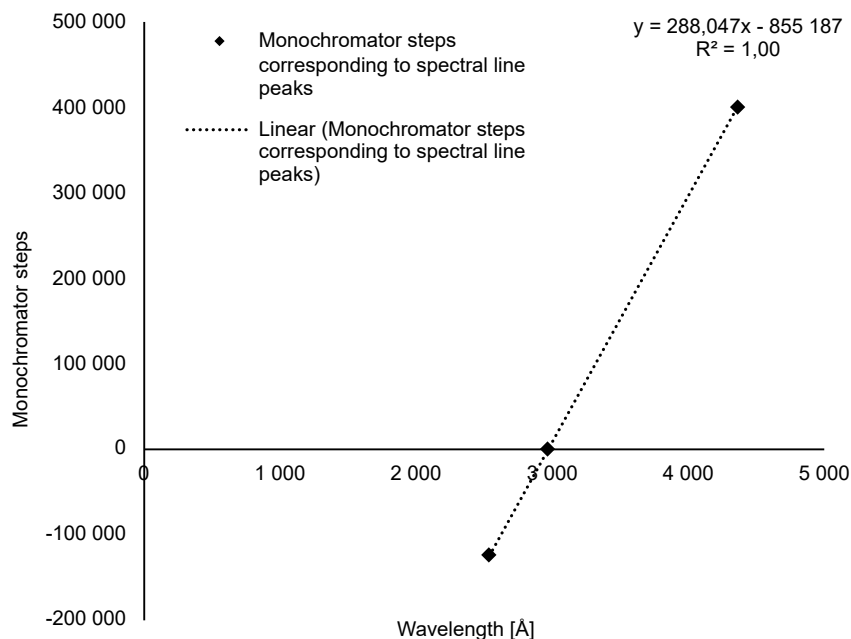


Figure 7.4: A plot of the monochromator steps corresponding to spectral lines peaks with a linear fit for the wavelength calibration in the region 200 nm to 400 nm.

## 7.4.2 Wavelength region of 600 nm to 1 100 nm

The wavelength calibration equation was found to be:

$$y(\lambda) = 144,028\lambda - 1\,003\,276, \quad (7.4)$$

where  $y(\lambda)$  is the monochromator steps and  $\lambda$  is the wavelength angstrom [ $\text{\AA}$ ], see Figure 7.5. The R-squared value determined shows a good fit of the linear model to the data set.

The uncertainty of measurement in wavelength was  $\pm 0,2$  nm. See Section 7.5 for a detailed description of the uncertainty of measurement analysis and Appendix H for the uncertainty budget.

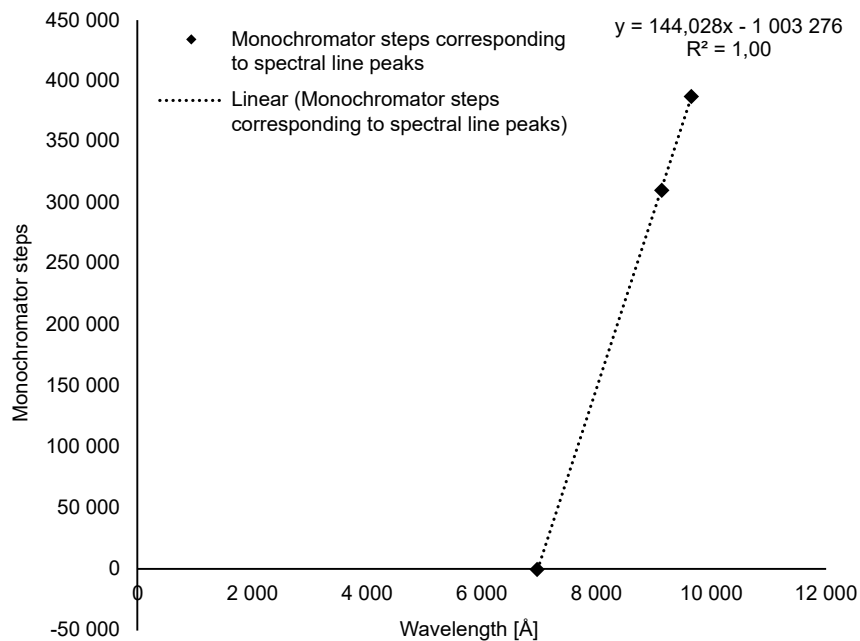


Figure 7.5: A plot of the monochromator steps corresponding to spectral lines peaks with a linear fit for the wavelength calibration in the region 600 nm to 1 100 nm.

## 7.5 Uncertainty analysis

The following uncertainty contributors were considered and quantified for the wavelength calibrations performed in both the ultraviolet and visible to near-infrared wavelength regions. Refer to Appendix G for the uncertainty budget for the ultraviolet wavelength region (200 nm to 400 nm) and Appendix H for the uncertainty budget for the near-infrared wavelength region (600 nm to 1 100 nm).

### 7.5.1 Theoretical value of the spectral line in vacuum, $U_{sl}$

The NIST Atomic Spectra Database [NIST, 2019] provides an uncertainty associated with the spectral line in vacuum. The uncertainty associated with each spectral line used to determine the wavelength calibration equation, was added in quadrature to determine the combined uncertainty,  $U_{sl}$ . A coverage factor of  $k = 1$  was used, as a Gaussian probability distribution is assumed for the uncertainty. The sensitivity coefficient is  $c_{sl} = 1$ , since the uncertainty contribution is already in the desired unit for wavelength, [nm].

### 7.5.2 Uncertainty in modified Edlén equation calculation, $U_{Ed}$

The NIST Engineering Metrology Toolbox [NIST, 2004] uses the modified Edlén Equation to calculate the wavelength in ambient air,  $\lambda_a$ , *i.e.* the laboratory conditions recorded for temperature, relative humidity and atmospheric pressure, for the spectral lines used. The NIST Engineering Metrology Toolbox also calculates the refractive index of air,  $n_a$ , and the estimated expanded uncertainty of the calculated index for a coverage factor of  $k = 2$ .

This estimated expanded uncertainty of the calculated index,  $\pm 0,000000043$  in Figure 7.6, was added to the refractive index calculated

### Index of Refraction of Air

Jack A. Stone and Jay H. Zimmerman

#### Wavelength in Ambient Air and Refractive Index of Air Based on Modified Edlén Equation

Input	Amount
Vacuum Wavelength:	300 Nanometers [nm]*
Air Temperature:	24 Degrees Celsius
Atmospheric Pressure:	86 Kilopascals [kPa]
Air Humidity:	50 Relative Humidity, Percent
* Extreme input parameter value. Check to be sure that entry is correct.	

Output	Result
Wavelength in Ambient Air:	299.928181 Nanometers [nm]**
Refractive Index of Air <sup>1</sup> :	1.000239454**
Uncertainty of Calculated Index <sup>2</sup> :	0.000000043
<sup>1</sup> This is the phase refractive index, appropriate for typical displacement measuring interferometers but not appropriate for many ranging instruments. See documentation for details. <sup>2</sup> Estimated expanded uncertainty (coverage factor of k=2) from Edlen calculation, but not including uncertainties of the input parameters.	
** Calculated results are potentially suspect due to extreme value of input parameter.	

Figure 7.6: Visual representation of the wavelength and refractive index calculated for ambient conditions using the NIST Engineering Metrology Toolbox based on the modified Edlén equation. [NIST, 2004].

for each wavelength in ambient air, or 1,000239454 in Figure 7.6, to obtain the refractive index with the uncertainty included,  $n_u$ . The latter was used to calculate the wavelength in ambient air,  $\lambda_u$ , from the spectral line in vacuum. The difference between  $\lambda_a$  and  $\lambda_u$ , and  $n_a$  and  $n_u$  was calculated respectively, to determine the sensitivity coefficient  $c = \Delta\lambda/\Delta n$  at each wavelength. This process was followed to calculate  $\lambda_u$  for each spectral line. The estimated expanded uncertainty of each spectral line was added in quadrature and used as the combined uncertainty contributor,  $U_{Ed}$ . The average of the sensitivity coefficients calculated at each wavelength was taken as  $c_{Ed}$ .

Also shown in Figure 7.6 is the refractive index calculated for 300 nm, the extreme input parameter, in ambient conditions. As mentioned in Section 7.3.1, the modified Edlén Equation is limited to the wavelength region of 300 nm to

1 700 nm. For the two spectral lines that fall outside this range, this refractive index was used to correct these spectral lines for ambient conditions.

### **7.5.3 Laboratory temperature effect, $U_T$**

The NIST Engineering Metrology Toolbox [NIST, 2004] was used to calculate the wavelength in ambient conditions for each spectral line used, and for 435,9560 nm in the ultraviolet region. The atmospheric pressure used in the calculations was 86 kPa. The laboratory's Quality System procedure [NMISA, 2014a] provides the relative humidity range of 50 %RH  $\pm$  15 %RH, and temperature range of 24 °C  $\pm$  2 °C that must be maintained in the laboratory. The humidity used in the calculations was 50 %RH. To determine the uncertainty due to the effect of temperature, the upper and lower limits of the laboratory temperature range were used to calculate the wavelength in ambient conditions,  $\lambda_{T_{up}}$  and  $\lambda_{T_{lw}}$ , respectively. The difference in these wavelengths, and the difference in the upper and lower limits of the temperature range were used to calculate the sensitivity coefficient at each wavelength. The average of the sensitivity coefficients was used,  $c_T = \Delta\lambda_T/\Delta T$ . The uncertainty contributor,  $U_T$ , was taken as  $\Delta T$  or 4 °C, assuming any deviation in temperature during the calibration is maintained in this range. A triangular probability distribution with a coverage factor of  $k = \sqrt{6}$  was used, since it is more likely that the temperature will be close to the centre of the limits of its range.

### **7.5.4 Laboratory humidity effect, $U_{RH}$**

The NIST Engineering Metrology Toolbox was used to calculate the wavelength in ambient conditions for each spectral line used, and for 435,9560 nm in the ultraviolet region. An atmospheric pressure value of 86 kPa and a temperature

value of 24 °C were used in the calculations. The upper and lower limits of the laboratory relative humidity range was used to calculate the wavelength in ambient conditions,  $\lambda_{RH_{up}}$  and  $\lambda_{RH_{lw}}$ , respectively. The difference in these wavelengths, and the difference in the upper and lower limits of the relative humidity range were used to calculate the sensitivity coefficient at each wavelength. The average of the sensitivity coefficients was used,  $c_{RH} = \Delta\lambda_{RH}/\Delta RH$ . The uncertainty contributor,  $U_{RH}$ , was taken as  $\Delta RH$  or 30 %RH, assuming any deviation in relative humidity during the calibration is maintained in this range.

A U-shaped probability distribution with a coverage factor of  $k = \sqrt{2}$  was used, since the relative humidity is cycled sinusoidally between the limits of its range. This is because the humidifier that controls the laboratory's relative humidity switches off when the upper limit is reached, and switches back on when the relative humidity has dropped to the lower limit of the specified range.

### **7.5.5 Laboratory air pressure effect, $U_{ap}$**

Similarly to the temperature and humidity uncertainty contributions, The NIST Engineering Metrology Toolbox was used to calculate the wavelength in ambient conditions for each spectral line used, and for 435,9560 nm in the ultra-violet region. The temperature and relative humidity used in the calculations were 24 °C and 50 %RH, respectively. The atmospheric pressure was measured by the NMISA Flow and Pressure laboratory to be 86 kPa  $\pm$  2 kPa. The upper and lower limits of the atmospheric pressure range was used to calculate the wavelength in ambient conditions,  $\lambda_{ap_{up}}$  and  $\lambda_{ap_{lw}}$ , respectively. The difference in these wavelengths, and the difference in the upper and lower limits of the atmospheric pressure range were used to calculate the sensitivity coefficient at each wavelength. The average of the sensitivity coefficients was used,

$c_{ap} = \Delta\lambda_{ap}/\Delta ap$ . The uncertainty contributor,  $U_{ap}$ , was taken as  $\Delta ap$  or 4 kPa, assuming any deviation in atmospheric pressure during the calibration is maintained in this range. A rectangular probability distribution with a coverage factor of  $k = \sqrt{3}$  was used, since it is unknown which values of atmospheric pressure between the limits are more or less likely.

### **7.5.6 Steep-side method offset, $U_{ssmo}$**

For the wavelength calibration in the visible to near-infrared region, the steep-side method was applied to determine the monochromator steps of the peak of each spectral line. The value of monochromator steps closest to the corresponding 10 % of the maximum signal was used, instead of a linear fit of the data sets around the 10 % of the maximum signal to calculate the corresponding monochromator steps. The largest difference between the closest value and calculated value of monochromator steps using the linear fits, approximately 36 monochromator steps, was added to the uncertainty calculation as a possible offset that may be present.

A Gaussian probability distribution was used with a coverage factor of  $k = 1$ . The sensitivity coefficient  $c_{ssmo}$  was the same as the sensitivity coefficient calculated in Section 7.5.11 for the repeatability uncertainty.

### **7.5.7 Wavelength calibration equation offset, $U_o$**

When the wavelength calibration equation is obtained, a verification is performed. Typically, this is done using the wavelength calibration equation to move to the wavelength position of a spectral line source. The offset that exists must be within the uncertainty determined for the wavelength calibration. Instead of correcting for this offset during the spectral power responsivity measurements performed

with the double monochromator, the offset is included in the uncertainty calculation. As described in CIE 198-SP1.2 [2011], if the standard deviation in the measured offset is significantly larger than the resolution, it may be taken as the uncertainty contribution, with a coverage factor of  $k = 1$ . Since in this case, the offset was measured only once, the offset itself is taken as the uncertainty contribution, as  $U_o$ . A Gaussian probability distribution was used with a coverage factor of  $k = 1$ . The sensitivity coefficient  $c_o$  was the same as the sensitivity coefficient calculated in Section 7.5.11 for the repeatability uncertainty.

### **7.5.8 Wavelength reproducibility, $U_\lambda$**

The wavelength reproducibility uncertainty contribution of the double monochromator was obtained from the manufacturer's specifications [McPherson, 2015] and is  $\pm 0,005$  nm. The sensitivity coefficient is  $c_\lambda = 1$ , since the uncertainty contribution is already in the desired unit for wavelength, [nm]. A rectangular probability distribution was used with a coverage factor of  $k = \sqrt{3}$ . This is because the value of the wavelength reproducibility quantity is given as an accuracy statement and the value is expected to lie anywhere within the specified limits.

### **7.5.9 Mechanical resolution of monochromator, $U_{Mres}$**

The resolution specification of the 1 200 g/mm gratings blazed at 300 nm and the 600 g/mm gratings blazed at 800 nm is 0,05 nm and 0,1 nm, respectively, and was obtained from the manufacturer's specifications. The semi-range of the resolution specification was used as the uncertainty contribution,  $U_{Mres}$ , for each wavelength range. This is because the wavelength can be anywhere within the interval of the resolution specification. For example, if the resolution is 0,05 nm, the wavelength can lie within the interval  $\pm 0,025$  nm. The sensitivity coefficient



used was  $c_{Mres} = 1$ , because the uncertainty contribution was already in the desired unit for wavelength, [nm].

Typically, tolerance limits provided in manufacturer specifications with a given coverage probability, have a Gaussian distribution. However, the coverage probability is not stated for the mechanical resolution and therefore a rectangular probability distribution with a coverage factor of  $k = \sqrt{3}$  was used.

#### **7.5.10 Resolution used in the calibration, $U_{Cres}$**

The resolution used to perform the wavelength calibrations may not be the same as the mechanical resolution of the monochromator. Larger wavelength intervals, found to be sufficiently small to perform a wavelength calibration, were used in the ultraviolet region. The uncertainty contributions due to this resolution or wavelength interval used in each of the wavelength regions, were taken as the semi-range of the wavelength intervals. The sensitivity coefficient was  $c_{Cres} = 1$ . A rectangular probability distribution was used with a coverage factor of  $k = \sqrt{3}$ , since the wavelength was expected to lie anywhere within the specified limits.

#### **7.5.11 Repeatability, $U_r$**

For the wavelength calibration in the ultraviolet region, each of the spectral lines was measured three times and the positions of the peaks were determined by calculating the average of the three sets, respectively. The standard deviation between each of the three measurements was calculated for each wavelength and the worst case was used as the uncertainty contribution,  $U_r$ . The unit of this contribution is in monochromator steps, therefore a sensitivity coefficient was calculated. The wavelength calibration equation obtained was used to calculate the corresponding wavelength, in [nm], of the peak positions measured in mono-

chromator steps for the first two measurements of the spectral line in vacuum, 435,9560 nm. The difference in these wavelengths,  $\Delta\lambda$ , and the difference in monochromator steps in the two peaks,  $\Delta steps$ , were used to determine the sensitivity coefficient,  $c_r = \Delta\lambda/\Delta steps$ .

For the wavelength calibration in the visible to near-infrared region, each spectral line was measured only once. To estimate a repeatability uncertainty contribution in this wavelength region, the new origin position, *i.e.* the spectral line in vacuum, 696,7352 nm, was measured again after the wavelength calibration was performed. The difference in monochromator steps from the origin position *i.e.* 0 steps, was taken as the uncertainty contribution,  $U_r$ . This difference in monochromator steps, and the origin position, was used in the wavelength calibration equation obtained to calculate the corresponding wavelength, in [nm], of the two peak positions. The difference in these wavelengths,  $\Delta\lambda$ , and the difference in monochromator steps of the two peaks,  $\Delta steps$ , were used to determine the sensitivity coefficient,  $c_r = \Delta\lambda/\Delta steps$ .

This uncertainty contribution is also an indication of the error that may be caused by the use of the steep-side method to determine the position of a single wavelength [Kostkowski, 1997]. This error may be due to the grating drive mechanism, noise in the output signal caused by the detector and instability of the spectral line source.

In a set of repeated measurements, the values are more likely to fall near the average, therefore a Gaussian distribution with a coverage factor of  $k = 1$  was used.

## Chapter 8

# The spectral power responsivity calibrations

### 8.1 Measurement system

Refer to Figure A.1 in Appendix A for a schematic representation of the spectral power responsivity measurement system. A selection guide to sources, diffraction gratings, detectors and order-sorting filters that are used at NMISA for measurement or calibration of spectral power responsivity is given in Table 8.1 for a wavelength range from 200 nm to 1 600 nm. The spectral power responsivity setup was characterised in the ultraviolet wavelength region, 200 nm to 400 nm, and in the visible to near-infrared wavelength region, 600 nm to 1 100 nm.

#### 8.1.1 Sources of optical radiation

Both the xenon arc and QTH sources were mounted in their own chimney-style lamp housings that fit onto the entrance slit mount of the double monochromator. These lamp housings contain the required optics and adjusters for aligning the sources and focusing the light onto the entrance slit. The lamp housings also include a fan operated by a power supply to ensure adequate cooling.

Table 8.1: The selection of sources, diffraction gratings based on their efficiency range discussed in Section 6.2.2, detectors and order-sorting filters for the operation wavelength ranges.

Operational wavelength range			Grating							
Start [nm]	End [nm]	Source	Detector		Groove density [g/mm]	1st order Littrow blaze [nm]	Dispersion [nm/mm]	Efficiency range		Order sorting filter
			Working standard	Primary standard				Start [nm]	End [nm]	
200	400	Xe	PtSi	UV enhanced Si	1 200	300	2	200	400	No filter/ N-WG280
400	600	QTH	Si	Si-trap (Pyro-electric)	1 200	500	2	333	667	GG395
600	1 100	QTH	Si	Si-trap (Pyro-electric)	600	800	4	533	1 067	OG550
900	1 600	QTH		InGaAs	600	1 250	4	833	1 667	RG850

The stability of the QTH source was controlled with an intensity controller. A UV-enhanced, temperature-stabilised, silicon detector, mounted against a small opening in the lamp housing, monitored the output of the lamp. The controller constantly compared the measured signal with the preset power level to make any required changes to the power supply output of the lamp [Newport, 2021a].

The xenon arc source was not compatible with the intensity controller. Instead, the xenon arc source was monitored by the same UV-enhanced, temperature-stabilised, silicon detector. The signal was measured every 5 seconds for one hour, the approximate duration for a calibration of spectral power responsivity in this wavelength region. This drift in the source was quantified and added to the uncertainty of measurement.

### **8.1.2 Imaging optics**

All optical components were mounted on an optical breadboard placed on a bench next to the double monochromator.

The setup used dedicated input optics mounted in the lamp housings of the sources. These input optics consist of mirrors, collimating and focusing lenses, that image the source onto the entrance slit with a focal length matching that of the monochromator.

The double monochromator has a built-in optical shutter at the entrance slit. The optical shutter is connected to a controller and is used to perform dark readings to correct for the effect of external stray light and the offset of the output voltage of the detector-amplifier combination.

Two spherical collimating mirrors and two spherical focusing mirrors were used as the output optics to focus the quasi-monochromatic light beam onto the detectors with an aperture ratio of  $F/8$ . The aperture ratio was calculated using

Equation 6.5, using the diameter of the light beam incident on the focusing mirror and the focal length of the mirror.

The first collimating mirror was placed at the exit slit of the double monochromator and collimated the exiting light beam onto the first focusing mirror. For measurements with the pyroelectric detector where an optical chopper was used, the optical chopper was placed at the focal point of the first focusing mirror. Due to the construction of the monochromator, the lamp housings are mounted against the entrance slit of the monochromator. This means that there is no space to mount the optical chopper at the input side of the monochromator, which is the preferred position to limit acoustic noise at the pyroelectric detector. At first, the optical chopper was placed near the exit slit, but as a consequence of the construction of the optical chopper wheel holder, a large portion of the divergent light beam was cut off. It is for this reason that a second set of collimating and focusing mirrors was used.

After the focal point of the first focusing mirror, the light beam diverged onto the second collimating mirror, which produced a collimated light beam on the second focusing mirror. This mirror then imaged the square exit slit onto the detector. The spot size of the focused beam had an approximate square cross-section of  $2 \text{ mm} \times 2 \text{ mm}$ .

The HeNe alignment laser at the input-side of the double monochromator was used to align the above-mentioned output-mirrors and detectors. This was done by following the same process used to align the internal optical components of the double monochromator. The alignment laser was switched on and to allow for the initial laser beam drift to stabilise, approximately 30 minutes was allowed for warm-up time. The laser beam exiting the double monochromator was aligned with the centre of the first collimating mirror. Each mirror was consecutively positioned such that the reflected laser beam was at the centre of the next mirror and

ultimately on the centre of the detector.

The output optics, optical chopper and detectors were mounted in a light-tight enclosure to reduce stray light, acoustic noise and air flow disturbance from the nearby air conditioning duct on the pyro-electric detector.

### **8.1.3 Diffraction gratings and order-sorting filters**

Plane ruled diffraction gratings were used as the dispersive elements in the double monochromator. They were selected based on their grating efficiencies in the desired wavelength ranges. The wavelength regions in which they were to be used, were determined using the general approximation given in Section 6.2.2 or  $\pm 1/3$  of the blaze wavelength. These wavelength regions are shown in Table 8.1.

A set of order-sorting filters was chosen based on the spectral distributions of the sources used and the wavelength regions being measured, see Section 6.3 for such a selection example. The selected filters for the various wavelength regions are listed in Table 8.1.

These filters fit in a filter wheel that can be mounted on the double monochromator. The filter wheel can hold five filters and can be controlled manually or with a device controller to select the required filter. The filter wheel is mounted on the double monochromator, between the entrance slit and the lamp housing.

### **8.1.4 Optical detectors and traceability chain**

See Figure 8.1 and Figure 8.2 for schematic representations of the traceability chain for spectral power responsivity in the relevant wavelength regions.

In the wavelength region of 200 nm to 400 nm, a PtSi photodiode detector was calibrated against a UV-enhanced Si photodiode detector for spectral power

responsivity. The UV-enhanced Si photodiode detector has been calibrated for absolute spectral power responsivity by NPL.

The PtSi photodiode detector was previously calibrated by PTB. As verification of the results, the spectral power responsivity obtained from the calibration was compared to the spectral power responsivity values of the PTB calibration certificate.

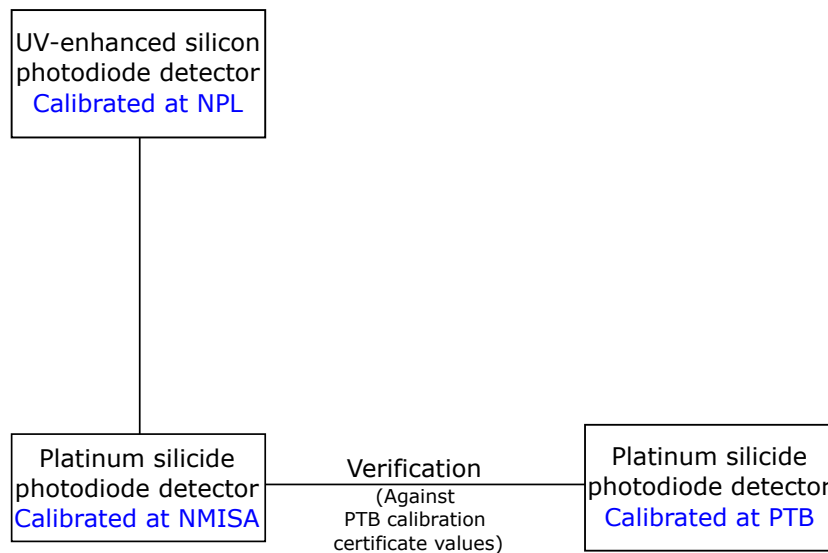


Figure 8.1: A schematic representation of the traceability chain for spectral power responsivity in the wavelength region of 200 nm to 400 nm.

In the wavelength region of 600 nm to 1 100 nm, a Si photodiode detector was calibrated for spectral power responsivity. This was done by first calibrating the Si photodiode detector for absolute spectral power responsivity, at 632,8 nm, against the national measurement standard for radiant power and spectral response, a Si-trap detector. The Si-trap detector has been calibrated against the electrical substitution cryogenic radiometer at NPL.

Secondly, the relative spectral power responsivity of the Si photodiode de-



tector was determined using a pyro-electric detector and the double monochromator setup. The measured relative spectral power responsivity curve was made absolute using the absolute calibration point at 632,8 nm.

The Si photodiode detector was also calibrated for absolute spectral power responsivity using a different standard, the UV-enhanced Si photodiode detector calibrated by NPL. The results of the two calibrations were compared as verification.

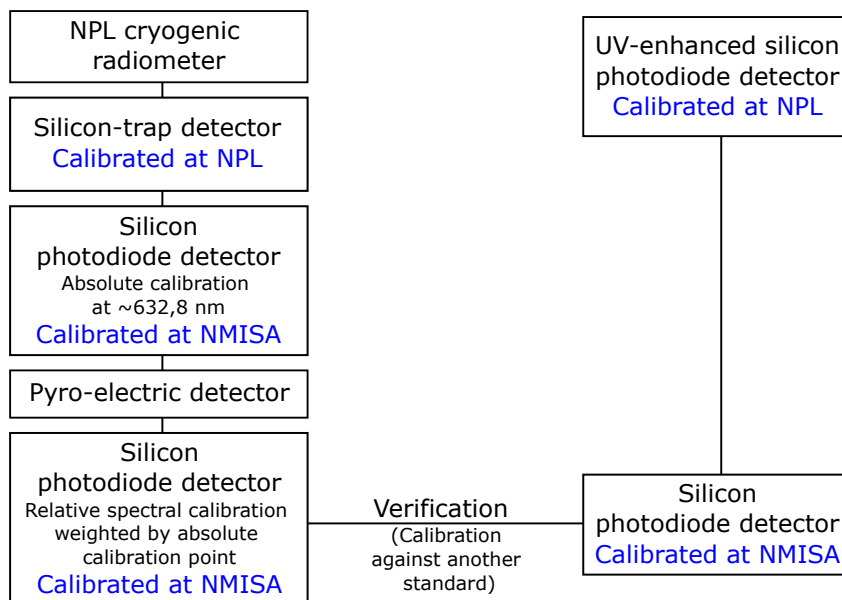


Figure 8.2: A schematic representation of the traceability chain for spectral power responsivity in the wavelength region of 600 nm to 1 100 nm.

## 8.2 Method

The measurement system makes use of control software, described in Appendix C, which allows the user to set the double monochromator to a specific wavelength, or to scan a wavelength region while recording data. The optical

detectors were mounted on x- and y-translation stages with their own control software. For a detailed description of how the optical detectors were mounted, refer to Appendix D.

The spectral power responsivity measurement setup was characterised using the standard laboratory procedure NMISA [2014b]. The laboratory's environmental conditions were recorded during the calibrations and were within the range specified in the standard laboratory procedure for environmental conditions [NMISA, 2014a], *i.e.*  $24\text{ }^{\circ}\text{C} \pm 2\text{ }^{\circ}\text{C}$  for temperature, and  $50\text{ \%RH} \pm 15\text{ \%RH}$  for relative humidity.

### **8.2.1 Wavelength region of 200 nm to 400 nm**

The absolute spectral power responsivity of the PtSi photodiode detector was determined through direct comparison against the standard UV-enhanced Si photodiode detector, using the substitution method.

No order-sorting filters were required, since the spectral distribution of the Xenon-arc source causes no additional orders in this wavelength region. Using the monochromator software and the relevant wavelength calibration equation, the monochromator was set to a wavelength where the light beam was visible. The detectors were mounted at the focal point of the second focusing mirror at the output side of the monochromator. The spot created by the light beam was aligned to the centre of each detector, respectively. The detector positions were optimised using the software of the translation stages which allowed for fine position adjustment.

The detectors were connected to a calibrated variable gain low noise current amplifier and a calibrated multimeter. To determine instrument settings such as amplifier gain, the monochromator software was used to scan through the

wavelength region and check the signal of each detector on the multimeter in DC voltage mode. The same amplifier gain setting was chosen for both detectors. A bandwidth of 5 nm was used for this calibration.

The monochromator software and wavelength calibration equation were used to scan through and record readings from the multimeter for the standard UV-enhanced Si photodiode detector from 200 nm to 400 nm in 10 nm intervals. The recorded readings included the average and standard deviation of 20 measurements taken with the multimeter at each wavelength. After this, the optical shutter at the entrance slit of the monochromator was closed, and readings were taken for the same wavelength region and interval. The readings obtained with the optical shutter closed, were subtracted from those obtained with the optical shutter open, to determine the net value of the output signal at each wavelength, see equation 8.1.

$$V_S(\lambda) = V_{S_{open\ shutter}}(\lambda) - V_{S_{closed\ shutter}}(\lambda) \quad (8.1)$$

The same method was used to record the output signal of the PtSi photodiode detector.

The absolute spectral power responsivity of the PtSi photodiode detector,  $s_T(\lambda)$ , was calculated using equation 4.8 and from the output signal recorded for the standard UV-enhanced Si photodiode detector,  $V_S(\lambda)$ , its known absolute spectral power responsivity,  $s_S(\lambda)$ , and the output signal recorded for the PtSi photodiode detector,  $V_T(\lambda)$ .

The PTB calibration of the PtSi photodiode detector was performed at a temperature of 25,2 °C. The average laboratory temperature recorded during the calibration against the UV-enhanced Si photodiode detector was 23,5 °C. The PTB calibration values were therefore corrected for the temperature deviation

using the spectral temperature coefficients given in the CCPR-K2.c key comparison report for a PtSi photodiode detector [Werner, 2014]. The corrected PTB calibration values were used as a verification of the measurement results obtained.

The deviation between the PTB calibration values and the temperature-corrected PTB values for spectral power responsivity ranges between 0,1 % and 0,3 % in the wavelength region of 200 nm to 400 nm. The contribution from this effect is small with respect to the uncertainty of measurement determined for this region, but it is considered a good measurement practise to apply such a correction.

## **8.2.2 Wavelength region of 600 nm to 1 100 nm**

### **Obtaining the absolute tie point:**

The absolute power responsivity of the Si photodiode detector was determined at 632,8 nm by calibrating it against a Si-trap detector using the substitution method. A HeNe laser source was stabilised with a laser power controller at approximately 200  $\mu$ W. The laser beam was conditioned with a spatial filter, collimated and centred on and perpendicular to each detector surface, underfilling each detector, respectively. An optical shutter was placed in the path of the laser beam for dark signal measurements.

Since the relative spectral power responsivity calibration was to be performed with chopped radiation, it was decided to also perform this calibration with AC signal to match the similar measurement procedure to be used.

For the calibration using a DC signal, both detectors were connected to a calibrated variable gain low noise current amplifier and used the same amplifier gain setting. For the AC signal calibration, an optical chopper set to a frequency

of 135 Hz was used with a lock-in amplifier, and both detectors were again connected to a calibrated variable gain low noise current amplifier. The same lock-in amplifier sensitivity setting was used for both detectors.

The detectors were connected to a calibrated multimeter. The output signals of each detector were recorded by the multimeter by placing each detector in the laser beam path, respectively.

Equation 4.8 was used to calculate the absolute spectral power responsivity of the Si photodiode detector from the output signals recorded for each detector and the known absolute spectral power responsivity of the Si-trap detector.

For the AC signal calibration, the duty cycle,  $D_c$ , was determined and included in Equation 4.8 to determine the absolute spectral power responsivity of the Si photodiode detector:

$$s_T(\lambda) = s_S(\lambda) \frac{V_T(\lambda)}{V_S(\lambda)} D_c \quad (8.2)$$

The duty cycle in Equation 8.2 was calculated using a thermopile detector and the optical chopper with a frequency set to 135 Hz. The same stabilised laser source was used with a beam power of approximately 298  $\mu$ W. Measurements were performed with the optical chopper on (AC signal) and again with it off (DC signal). The ratio of the AC signal and DC signal was calculated and used as the duty cycle.

This calibration provided the absolute tie point that was used to convert the relative spectral calibration to an absolute spectral calibration.

Three methods of verification of the measurement result obtained were used. First, the absolute power responsivity of the Si photodiode detector at 632,8 nm obtained with the DC signal calibration was compared to that of the

AC signal calibration.

Second, the same calibration described above using DC signal, was repeated against another Si-trap detector used as a verification standard, which was also calibrated against the ESCR at NPL.

Third, the measurement result obtained was compared to a previous calibration for absolute spectral power responsivity of the Si photodiode detector performed in 2003 [Botha, 2003].

### **Spectral power responsivity calibration:**

The relative spectral power responsivity of the Si photodiode detector was measured on the double monochromator with a bandwidth of 4 nm, using a pyroelectric detector as the spectrally flat, wavelength extending transfer detector. The surface coating of the pyroelectric detector has been characterised by the manufacturer and measured for spectral absorptance.

Two order-sorting filters were used together with the QTH source, namely OG550 for 600 nm to 950 nm and RG850 for 950 nm to 1 100 nm. An optical chopper was used in this setup to provide chopped radiation for the pyroelectric detector and was set to a frequency of 135 Hz. The same method was followed as described in Section 8.2.1 to align the detectors with the measurement spot. An additional baffle was placed in front of the detectors to reduce acoustic noise produced by the optical chopper.

The Si photodiode detector was connected to a calibrated variable gain low noise current amplifier and a calibrated multimeter. The pyroelectric detector was connected to a lock-in amplifier which was connected to the calibrated variable gain low noise current amplifier and calibrated multimeter. The gain setting on the variable gain low noise current amplifier and sensitivity setting on the lock-in amplifier were determined using the same procedure described in Section 8.2.1.

The output signals of each detector were recorded from 600 nm to 1 100 nm in 10 nm intervals in the same way as described in Section 8.2.1. Four independent sets of data were recorded and the average of the sets used to determine the relative spectral power responsivity.

The output signals of the respective detectors were recorded in smaller wavelength sections, each section consisting of five wavelengths. For example, the Si photodiode detector was placed in position and its output signal recorded from the multimeter in the wavelength section of 600 nm to 640 nm in 10 nm intervals. The Si photodiode detector was substituted with the pyroelectric detector and the same process was followed. This process was repeated for the next wavelength section until the entire wavelength range was completed. The reason for using smaller wavelength sections was to reduce the effect of drift in the source on the detectors during the calibration.

The relative spectral power responsivity was calculated for the Si photodiode detector using Equation 4.8. This was converted to absolute spectral power responsivity,  $s_T(\lambda)$ , using the absolute tie point,  $s_S(632,8 \text{ nm})$ , and correcting for the absorptance of the pyroelectric detector's surface coating,  $A_S(\lambda)$ :

$$s_T(\lambda) = s_S(632,8 \text{ nm}) \frac{V_r(\lambda)}{V_r(632,8 \text{ nm})} A_S(\lambda), \quad (8.3)$$

where  $V_r(\lambda)$  is the ratio of the output signal of the Si photodiode detector,  $V_T(\lambda)$ , and the pyroelectric detector,  $V_S(\lambda)$ .

Two methods of verification of the measurement results obtained were used. First, the absolute spectral power responsivity determined for the Si photodiode detector was compared to its previous calibration, [Botha \[2003\]](#).

Second, the Si photodiode detector was also calibrated against the UV-enhanced Si photodiode detector using the same monochromator measurement

system. Since the UV-enhanced Si photodiode detector has already been calibrated for absolute spectral power responsivity, the normal substitution method, Equation 4.8, was used and there was no need for a wavelength extending transfer detector.

## 8.3 Results

### 8.3.1 Wavelength region of 200 nm to 400 nm

Figure 8.3 provides a graph of the output signal of the standard UV-enhanced Si photodiode detector with the optical shutter open (light signal) and closed (dark signal). As seen in the graph, below 260 nm the light signal was very low or similar to the dark signal measured.

See Section 8.4.1 for the detailed analysis of the uncertainty of measurement, which was determined to range from  $\pm 4,3 \%$  at 260 nm to  $\pm 2,6 \%$  at 400 nm as shown in Appendix I. The ratio of the dark signal to the light signal was calculated and found to be larger than the uncertainty of measurement below 260 nm. It was therefore decided that it was not meaningful to report the spectral power responsivity below 260 nm. To extend the measurement capability for spectral power responsivity below 260 nm, the use of the LDLS must be investigated, see Section 11.



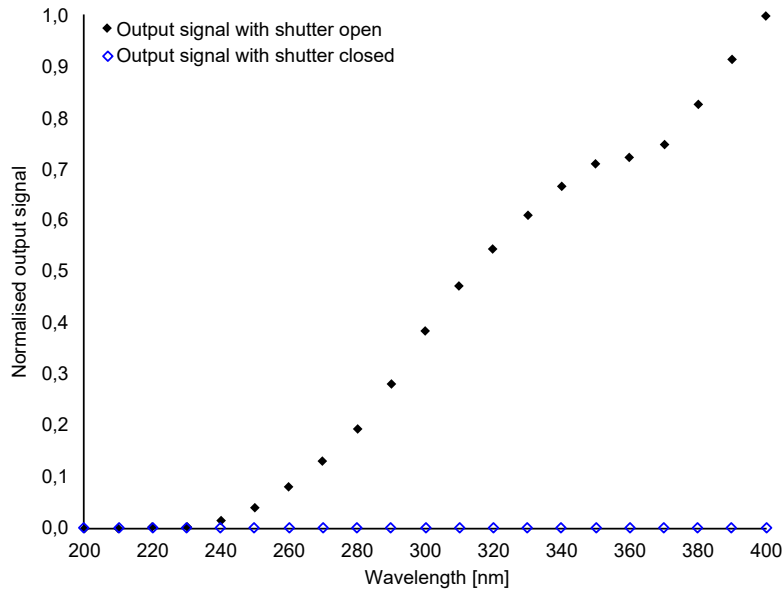


Figure 8.3: Normalised output signal of the standard UV-enhanced Silicon photodiode detector indicating the low signal level below 260 nm.

Figure 8.4 shows the absolute spectral power responsivity calculated for the PtSi photodiode detector in the calibration against the UV-enhanced Si photodiode detector, its associated uncertainty of measurement indicated as error bars, and the absolute spectral power responsivity of the PtSi photodiode detector determined by the PTB. This data is also reported in Table 8.2 along with the deviation from the PTB calibration and the  $E_n$  score calculated using Equation 2.2.

The deviation between the results of the two calibrations was within the calculated uncertainty of measurement, seen in Figure 8.4, and the results are therefore considered verified. The  $E_n$  score was smaller than 1,0 at all reported wavelengths, also indicating satisfactory performance.

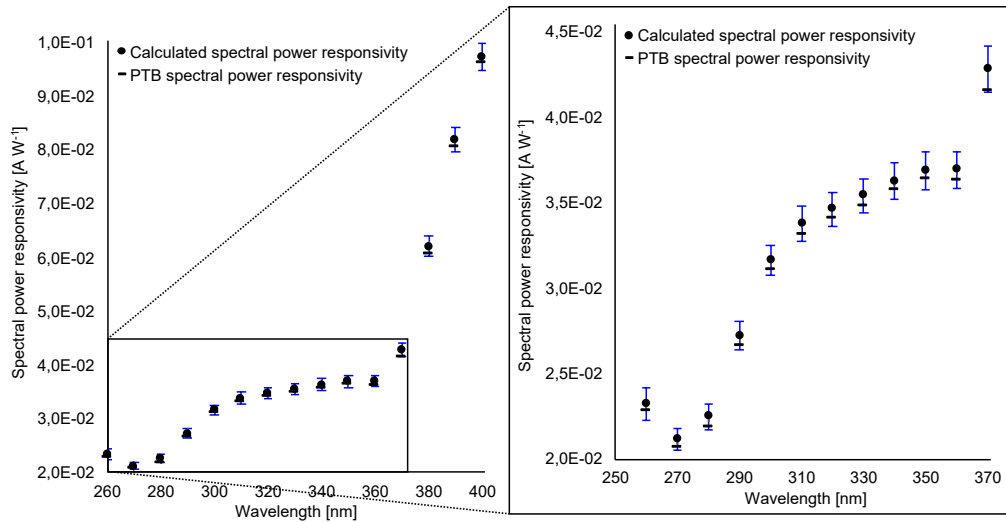


Figure 8.4: Calculated spectral power responsivity and PTB determined spectral power responsivity for the PtSi photodiode detector in the wavelength region 260 nm to 400 nm (the panel on the right is a zoom-in of the rectangle in the left panel).

Table 8.2: The absolute spectral power responsivity of a PtSi detector and comparison with the PTB calibration.

Wavelength [nm]	UV-enhanced Si photodiode detector as standard		PTB calibration	Deviation between calibrations [%]	$E_n$ score
	Absolute spectral power responsivity [A W <sup>-1</sup> ]	Uncertainty of measurement [%]	Absolute spectral power responsivity [A W <sup>-1</sup> ]		
260	0,022 74	4,3	0,022 36	1,7	0,38
270	0,020 64	3,1	0,020 22	2,1	0,65
280	0,021 98	3,4	0,021 42	2,6	0,73
290	0,026 72	3,1	0,026 12	2,3	0,72
300	0,031 14	2,9	0,030 56	1,9	0,64
310	0,033 3	3,2	0,032 67	1,9	0,58
320	0,034 16	2,9	0,033 57	1,8	0,59
330	0,034 9	2,9	0,034 34	1,7	0,58
340	0,035 8	3,0	0,035 29	1,4	0,47
350	0,036 4	3,0	0,035 93	1,2	0,41
360	0,036 4	3,0	0,035 81	1,8	0,57
370	0,042 3	3,2	0,041 07	3,0	0,90
380	0,061 6	3,0	0,060 19	2,4	0,75
390	0,081 5	2,8	0,080 30	1,5	0,52
400	0,096 9	2,6	0,095 80	1,1	0,43

### 8.3.2 Wavelength region of 600 nm to 1 100 nm

#### The absolute tie point:

The absolute power responsivity of the Si photodiode detector determined at 632,8 nm with DC and AC signals is reported in Table 8.3. The uncertainty of measurement in the absolute spectral power responsivity of the Si-trap detectors at the time of the calibration was  $\pm 0,44$  %, see Appendix K and Section 8.4.2 for a detailed description of the uncertainty of measurement analysis. The deviation between the results obtained from the DC and AC signal calibrations was 0,11 % and is therefore within the uncertainty of the Si-trap detectors and considered verified. The result obtained with the AC signal was used as the absolute tie point for the relative spectral power responsivity calibration.

Table 8.3: The absolute power responsivity of the Si photodiode detector obtained with DC and AC signals.

Wavelength [nm]	Absolute power responsivity of Si photodiode detector [A W <sup>-1</sup> ]		Deviation [%]	Uncertainty of measurement in Si-trap detectors [ $\pm$ %]
	With standard Si-trap detector			
	DC signal	AC signal		
632,8	0,3510	0,3506	0,11	0,44

The absolute power responsivity calculated for the Si photodiode detector using DC signal and both the standard and verification standard Si-trap detectors at 632,8 nm is reported in Table 8.4. The deviation in the results obtained from the two Si-trap detectors was 0,018 %, which is within the  $\pm 0,44$  % uncertainty of measurement of the Si-trap detectors. The results obtained for the Si photodiode detector are therefore considered verified.

Table 8.4: The absolute power responsivity of the Si photodiode detector obtained with the standard Si-trap detector and verification standard Si-trap detector.

Wavelength [nm]	Absolute power responsivity of Si photodiode detector [A W <sup>-1</sup> ]		Deviation [%]	Uncertainty of measurement in Si-trap detectors [± %]
	With standard Si-trap detector	With verification standard Si-trap detector		
	DC signal	DC signal		
632,8	0,3510	0,3510	0,018	0,44

Table 8.5 reports the results of the verification with the previous calibration of the Si photodiode detector. In the previous calibration, the absolute spectral power responsivity was determined for the wavelength range of 600 nm to 1 100 nm in wavelength intervals of 10 nm, with a measurement uncertainty of ± 2,6 %. Interpolating the results obtained at 630 nm and 640 nm, the absolute power responsivity of the Si photodiode detector at 632,8 nm was 0,3490 A W<sup>-1</sup>.

The deviation between the previous calibration result and the absolute spectral power responsivity of 0,3506 A W<sup>-1</sup> obtained for the Si photodiode detector is 0,46 %. This deviation may be due to the difference in traceability routes used for the two calibrations. The previous calibration was traceable to the previous ESCR used at NMISA, and as mentioned, this calibration is traceable to the ESCR at NPL. Drift in the reference detector might have also played a role. However, the deviation is within the uncertainty of measurement reported in the previous calibration certificate and the results are considered verified.

Table 8.5: The absolute power responsivity of the Si photodiode detector compared to its previous calibration.

Wavelength [nm]	Absolute power responsivity of Si photodiode detector [A W <sup>-1</sup> ]		Deviation [%]	Si photodiode detector uncertainty of measurement from its previous calibration [± %]
	With standard Si-trap detector	From previous calibration		
	AC signal			
632,8	0,3506	0,3490	0,46	2,6

### Spectral power responsivity calibration:

A plot of the absolute spectral power responsivity calculated for the Si photodiode detector is given in Figure 8.5, along with the measurement results from its previous calibration and the verification performed by calibrating the Si photodiode detector against the UV-enhanced Si photodiode detector.

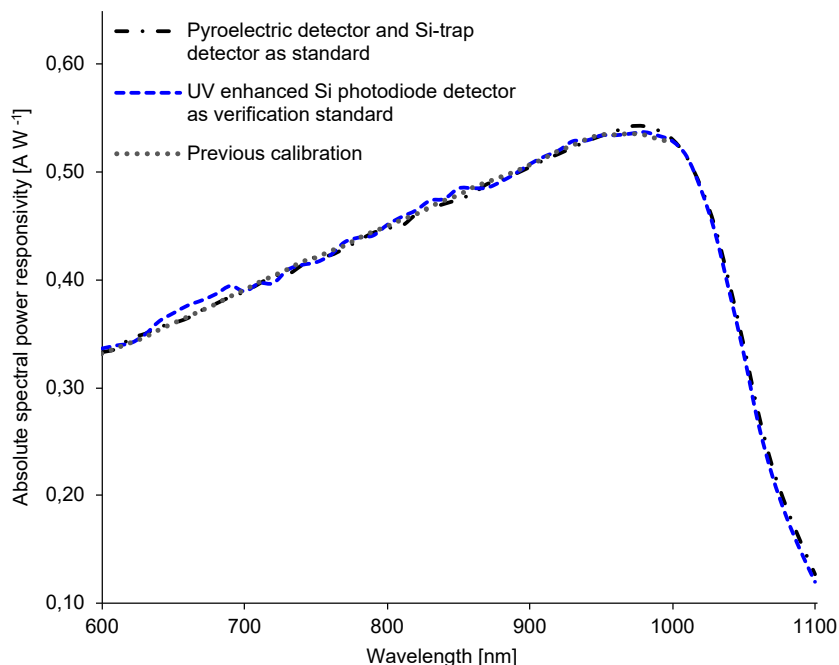


Figure 8.5: Absolute spectral power responsivity of the Si photodiode detector determined using the pyroelectric detector and Si-trap detector as standard, from its previous calibration, and using the UV-enhanced Si photodiode detector as verification standard.

The uncertainty of measurement associated with the calibration performed using the pyroelectric detector and Si-trap detector as standard was determined to be  $\pm 2,7$  %, see Section 8.4.2 and Appendix K.

The Si photodiode detector was calibrated for absolute spectral power responsivity in 2003 from 600 nm to 1 000 nm in 10 nm intervals, therefore the verification with its previous calibration could only be performed up to 1 000 nm. The uncertainty of measurement of this previous calibration was  $\pm 2,6$  %.

Table 8.6 provides the measurement results of this verification, *i.e.* the absolute spectral power responsivity of the Si photodiode detector determined using the pyroelectric detector and Si-trap detector as standard and that of its previous calibration.

The deviation between these calibration results was calculated and found to be smaller than the uncertainty of measurement,  $\pm 2,6$  %, at all wavelengths reported. This can also be seen in Figure 8.6 which shows the absolute spectral power responsivity of the Si photodiode and its associated uncertainty of measurement determined in the previous calibration, indicated as error bars. It is clear that the absolute spectral power responsivity of the Si photodiode detector determined using the pyroelectric detector and Si-trap detector as standard lies within the uncertainty of measurement of the previous calibration. The results are therefore considered verified.

The  $E_n$  score was also determined and is reported in Table 8.6. It was found to be smaller than 1,0 at all reported wavelengths, thus also indicating successful verification.

Table 8.6: The absolute spectral power responsivity of a Si photodiode detector compared with its previous calibration's measurement results.

Wavelength [nm]	Absolute power responsivity of Si photodiode detector [A W <sup>-1</sup> ]		Deviation [%]	$E_n$ score
	Using method described in Section 8.2.2	From previous calibration		
600	0,332 9	0,332	0,26	0,07
610	0,336 1	0,337	0,26	0,07
620	0,345 9	0,342	1,15	0,30
630	0,350 0	0,347	0,87	0,23
640	0,356	0,354	0,61	0,16
650	0,360	0,360	0,02	0,00
660	0,365	0,366	0,38	0,10
670	0,372	0,372	0,01	0,00
680	0,378	0,378	0,03	0,01
690	0,384	0,385	0,16	0,04
700	0,389	0,391	0,47	0,13
710	0,396	0,398	0,39	0,11
720	0,404	0,404	0,02	0,00
730	0,405	0,410	1,21	0,32
740	0,414	0,417	0,80	0,21
750	0,422	0,421	0,15	0,04
760	0,423	0,427	0,93	0,25
770	0,429	0,432	0,62	0,17
780	0,437	0,439	0,50	0,13
790	0,444	0,445	0,28	0,08
800	0,448	0,450	0,43	0,11
810	0,450	0,456	1,30	0,35
820	0,461	0,461	0,05	0,01
830	0,466	0,468	0,34	0,09
840	0,471	0,474	0,69	0,19
850	0,475	0,479	0,87	0,23
860	0,480	0,486	1,18	0,32
870	0,489	0,491	0,38	0,10
880	0,493	0,496	0,66	0,18
890	0,499	0,501	0,47	0,13
900	0,505	0,507	0,42	0,11
910	0,511	0,513	0,31	0,08
920	0,517	0,520	0,59	0,16
930	0,523	0,525	0,38	0,10
940	0,529	0,531	0,40	0,11
950	0,534	0,535	0,21	0,05
960	0,538	0,535	0,61	0,16
970	0,543	0,536	1,22	0,32
980	0,543	0,535	1,47	0,39
990	0,539	0,531	1,50	0,40
1 000	0,531	0,528	0,49	0,13

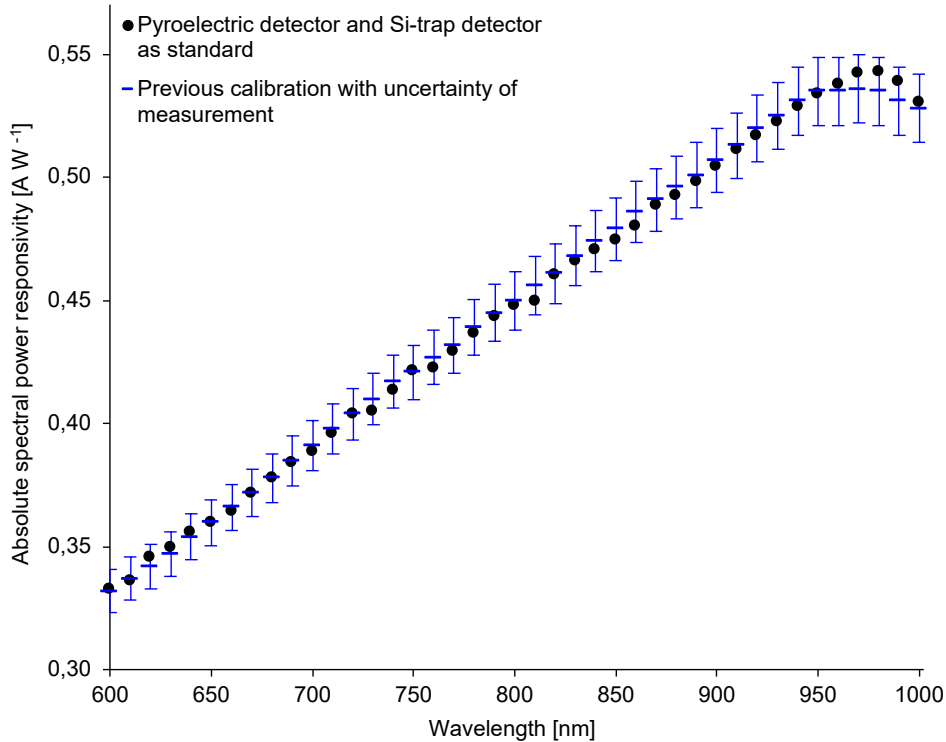


Figure 8.6: Verification of the calculated spectral power responsivity of the Si photodiode detector with its previous calibration.

The results of the verification by calibrating the Si photodiode detector against the UV-enhanced Si photodiode detector are shown in Table 8.7. A spectral uncertainty of measurement analysis was performed for this calibration and the calculated uncertainty was found to range from  $\pm 1,3 \%$  to  $\pm 3,6 \%$  in the wavelength range of 600 nm to 1 100 nm, see Table 8.7. Refer to Appendix J and Section 8.4.1 for a detailed description of the uncertainty of measurement analysis.

The deviation between the calibrations of the Si photodiode detector using the pyroelectric detector and Si-trap detector as standard and the UV-enhanced Si photodiode detector as verification standard, as well as the calculated  $E_n$  score are shown in Table 8.7.



*The spectral power responsivity calibrations*

*Results*

Table 8.7: Absolute spectral power responsivity of the Si photodiode detector as determined using the method described in Section 8.2.2 and using the UV-enhanced Si photodiode detector as a verification standard. The measurement results in blue and bold indicate wavelengths at which the verification was not successful.

Wavelength [nm]	Using method described in Section 8.2.2	UV-enhanced Si photodiode detector as verification standard		Deviation [%]	$E_n$ score
	Absolute spectral power responsivity [A W <sup>-1</sup> ]	Absolute spectral power responsivity [A W <sup>-1</sup> ]	Uncertainty of measurement [%]		
600	0,332 9	0,336 0	2,5	0,94	0,26
610	0,336 1	0,338 8	2,7	0,78	0,21
620	0,345 9	0,341 0	1,9	1,44	0,43
630	0,350 0	0,349 0	1,6	0,31	0,10
640	0,356	0,361 3	1,5	1,42	0,46
650	0,360	0,368 8	1,5	2,41	0,79
660	0,365	0,375 9	1,4	3,00	1,01
670	0,372	0,380 7	1,4	2,28	0,76
680	0,378	0,386 6	1,4	2,20	0,74
690	0,384	0,394 0	1,3	2,44	0,83
700	0,389	0,389 0	1,5	0,05	0,02
710	0,396	0,396 4	1,8	0,00	0,00
720	0,404	0,396 6	1,3	1,85	0,61
730	0,405	0,408 9	1,6	0,94	0,30
740	0,414	0,413 5	1,3	0,05	0,02
750	0,422	0,415 9	1,5	1,38	0,44
760	0,423	0,422 5	1,5	0,12	0,04
770	0,429	0,434 6	1,3	1,21	0,41
780	0,437	0,438 8	1,3	0,46	0,16
790	0,444	0,440 7	1,6	0,69	0,22
800	0,448	0,450 7	2,6	0,59	0,16
810	0,450	0,458 0	3,1	1,73	0,42
820	0,461	0,464 0	3,2	0,70	0,17
830	0,466	0,473 2	3,0	1,44	0,36
840	0,471	0,474 7	2,9	0,83	0,21
850	0,475	0,484 5	3,3	1,98	0,47
860	0,480	0,484 6	3,1	0,89	0,22
870	0,489	0,485 1	3,1	0,84	0,20
880	0,493	0,490 9	3,0	0,37	0,09
890	0,499	0,498 4	2,9	0,05	0,01
900	0,505	0,507 0	3,1	0,41	0,10
910	0,511	0,513 9	3,6	0,48	0,11
920	0,517	0,519 4	3,6	0,47	0,10
930	0,523	0,528 1	3,3	0,97	0,23
940	0,529	0,528 9	3,6	0,00	0,00
950	0,534	0,533 5	3,6	0,07	0,02
960	0,538	0,533 7	3,6	0,85	0,19
970	0,543	0,535 1	3,5	1,40	0,32
980	0,543	0,536 6	3,3	1,17	0,27
990	0,539	0,533 3	3,4	1,06	0,24
1 000	0,531	0,528 2	3,3	0,45	0,11
1 010	0,514	0,514 0	2,7	0,02	0,01
1 020	0,486	0,483 5	3,3	0,57	0,13
1 030	0,448	0,443 0	3,3	1,23	0,29
1 040	0,396	0,388 0	3,3	2,16	0,50
1 050	0,339 5	0,331 1	3,2	2,53	0,60
1 060	0,277 8	0,267 6	3,2	3,79	0,89
1 070	0,226 9	0,218 2	3,0	4,01	0,97
1 080	0,188 7	0,179 7	3,2	5,03	1,18
1 090	0,156 5	0,147 9	3,4	5,82	1,31
1 100	0,126 6	0,119 6	3,3	5,84	1,34

Two comparisons were performed for this verification. First, as shown in Figure 8.7, a check was performed to determine whether the absolute spectral power responsivity of the Si photodiode detector obtained from the calibration against the UV-enhanced Si photodiode detector was within the uncertainty of measurement associated with the calibration against the pyroelectric detector and Si-trap detector, *i.e.*  $\pm 2,7\%$ .

It can be seen in Figure 8.7 that at 660 nm and 1 060 nm to 1 100 nm the measurement results are not within the stated uncertainty of measurement. These measurement results are indicated in Table 8.7 (in bold and blue font) where it is reported that the deviation between the calibrations ranges from  $\pm 3,00\%$  to  $\pm 5,84\%$ . It is also shown that the  $E_n$  score is larger than 1,0 at some of the wavelengths.

Second, as shown in Figure 8.8, a check was performed to determine whether the absolute spectral power responsivity of the Si photodiode detector obtained from the calibration against the pyroelectric detector and Si-trap detector was within the spectral uncertainty of measurement associated with the calibration against the UV-enhanced Si photodiode detector.

As seen in Figure 8.8 and as reported in Table 8.7 (in blue, and bold and blue font), some measurement results in the ranges of 650 nm to 720 nm and 1 060 nm to 1 100 nm are not within the spectral uncertainty of measurement associated with the calibration against the UV-enhanced Si photodiode detector. Similarly, the  $E_n$  scores at some of these wavelengths are larger than 1,0.

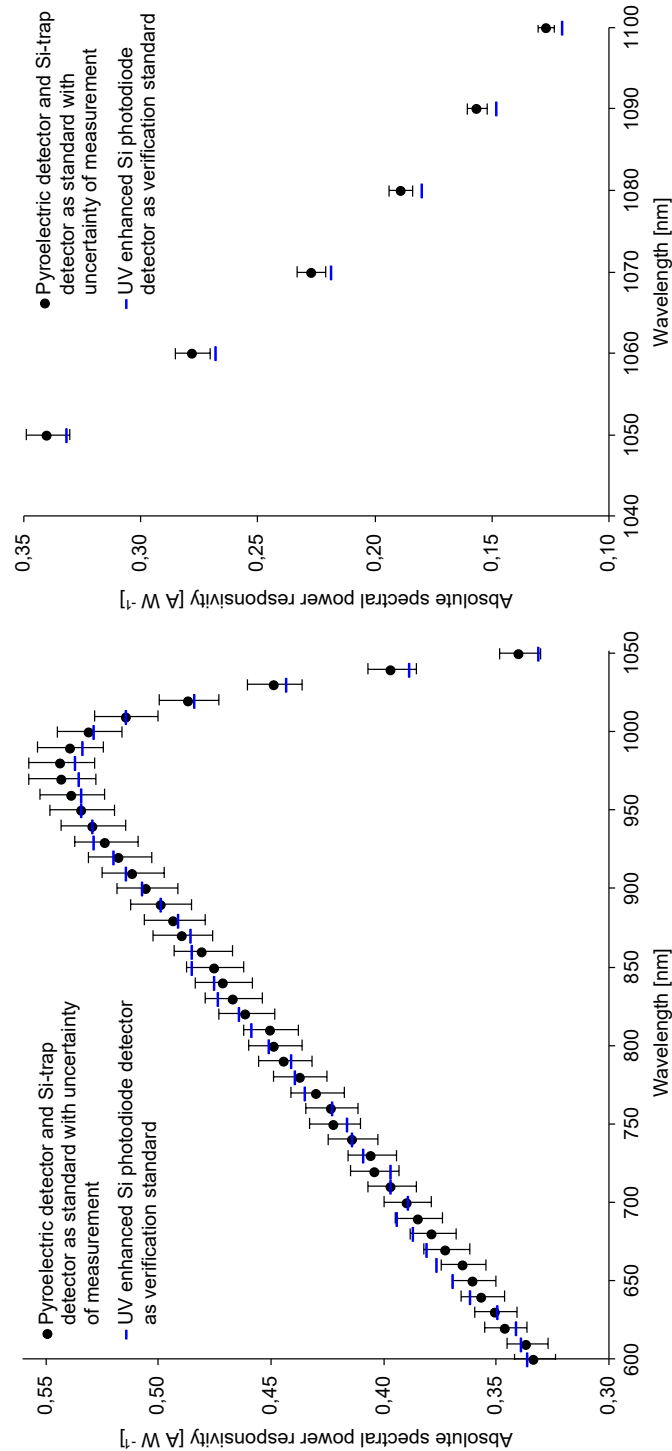


Figure 8.7: Absolute spectral power responsivity of the Si photodiode detector as determined using the method described in Section 8.2.2 with its associated uncertainty of measurement, and using the UV-enhanced Si photodiode detector as a verification standard.

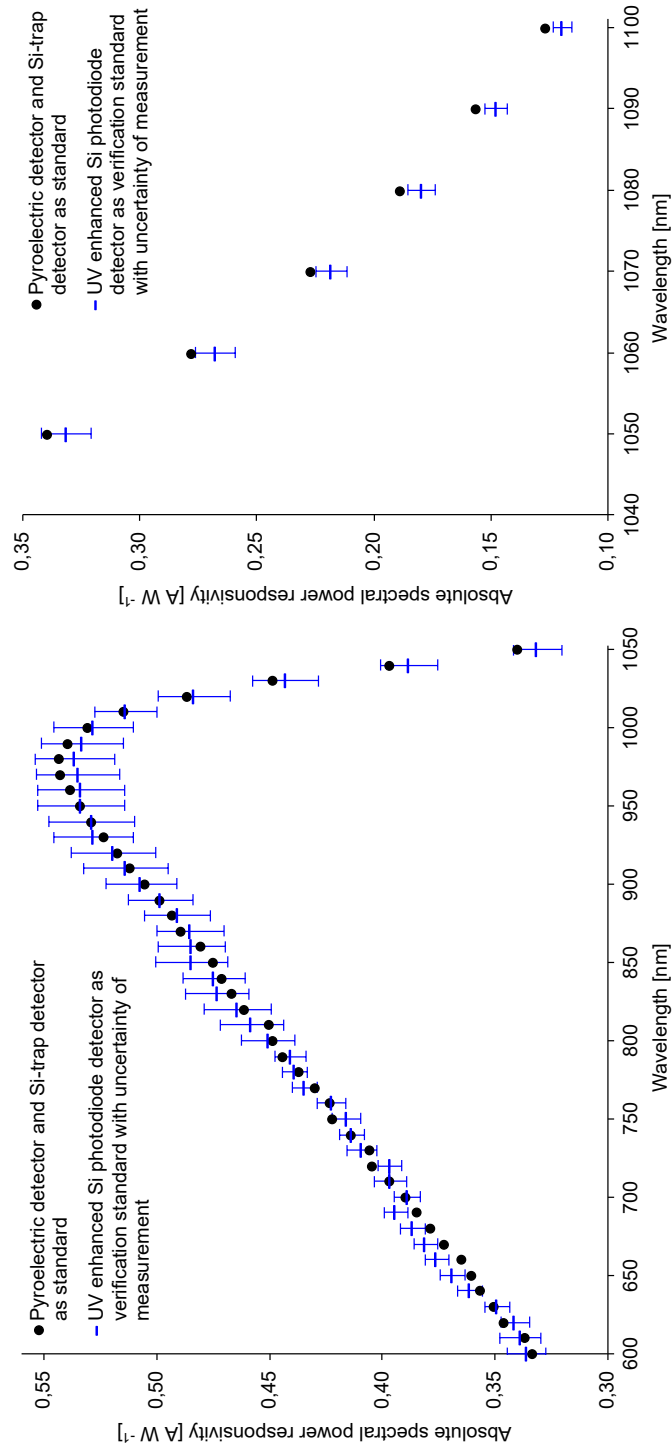


Figure 8.8: Absolute spectral power responsivity of the Si photodiode detector as determined using the method described in Section 8.2.2, and using the UV-enhanced Si photodiode detector as a verification standard with its associated uncertainty of measurement.

The unsuccessful verification of the measurement results at the wavelengths indicated in blue in Table 8.7 above 1 050 nm is considered to be caused by low signal issues due to the sharp decrease in detector responsivity after 1 000 nm and decreasing grating efficiency. As shown in Table 8.1, the grating efficiency of the diffraction gratings used in this wavelength region, is estimated to drop below 50 % at 1 067 nm. Both these factors could cause significantly lower throughput above 1 000 nm influencing the measurement results and leading to the larger deviation observed above 1 000 nm.

For the larger deviation observed between 650 nm to 720 nm, considerations for causes are the reflectance coating of the output optic mirrors, source instability due to possible power fluctuations and external stray light on the detectors, which are larger at the lower end of the 600 nm to 1 100 nm region. However, these factors are all common to the two calibrations performed and would have likely cancelled in the ratio.

A factor that is not common to the two calibrations, is the absorptance of the pyroelectric detector surface coating. It would be prudent to measure the surface coating internally to determine whether there might be an anomaly in the 650 nm to 720 nm region.

As mentioned in Chapter 3, Si photodiode detectors are susceptible to change when exposed to UV radiation. It could be that the UV-enhanced Si photodiode detector is showing signs of such degradation. In this case, a recalibration of the detector will be required.

All the above-mentioned factors require further investigation and are discussed in Section 11

Since the verification of the measurement results against the previous calibration was successful, and since all measurement results from the calibration

against the UV-enhanced Si photodiode detector below 1 060 nm, with the exception of 660 nm, lie within the uncertainty of measurement of  $\pm 2,7$  % associated with the calibration against the pyroelectric detector and Si-trap detector, the measurement results between 600 nm and 1 050 nm are considered verified.

## **8.4 Uncertainty analysis**

### **8.4.1 Spectral analysis of uncertainty**

Spectral analyses of the uncertainty of measurement were performed for the calibration of the PtSi photodiode detector in the wavelength region of 200 nm to 400 nm (see Appendix I for the calculated uncertainty of measurement) and the calibration of the Si photodiode detector against the UV-enhanced Si photodiode detector as verification standard in the wavelength region of 600 nm to 1 100 nm (see Appendix J for the calculated uncertainty of measurement).

The relative uncertainty of measurement for the aforementioned calibrations was determined from the uncertainty contributors described below. In this section, the UV-enhanced Si photodiode detector will be referred to as the standard detector and the PtSi photodiode detector and Si photodiode detector as the test detectors.

The key comparison reports on spectral responsivity, CCPR-K2.c (200 nm to 400 nm) [Werner, 2014] and CCPR-K2.b (300 nm to 1 000 nm) [Goebel and Stock, 2004a] were used to obtain estimates of some uncertainty contributors. This was possible, because the detectors used in the key comparisons were of similar types as the detectors used in this calibration.

Unless otherwise specified, Gaussian distributions with a coverage factor of  $k = 1$  and sensitivity coefficients equal to 1 were used for the uncertainty contributors described below. This was done as a best estimate and may be investigated in future to improve the uncertainty of measurement calculations.

#### **8.4.1.1 Absolute spectral power responsivity of the standard detector, $u_S$**

The standard, UV-enhanced Si photodiode detector was calibrated for absolute spectral power responsivity by NPL [Winkler, 2018]. This calibration certificate reports the relative spectral expanded uncertainty with a Gaussian distribution and a coverage factor of  $k = 2$ .

#### **8.4.1.2 Drift in the standard detector, $u_{Sd}$**

A paper published in the 2014 NEWRAD conference proceedings [Littler *et al.*, 2014] describes the predicted wavelength-dependent drift in responsivity in silicon. The paper provides a model that predicts the relative drift per annum:

$$\text{Drift}(\lambda_{nm}) = \frac{-0,184}{1 + \frac{(\lambda_{nm} - 365)^2}{1\,691}} \%, \quad (8.4)$$

and the wavelength-dependent standard deviation in the drift rate:

$$\sigma(\lambda_{nm}) = 1,89 \times 10^{-7} \lambda_{nm}^2 - 2,71 \times 10^{-4} \lambda_{nm} + 0,0987 \% \quad \text{for } \lambda_{nm} < 716,9 \text{ nm}$$

$$\sigma(\lambda_{nm}) = 0,00156 \% \quad \text{for } \lambda_{nm} > 716,9 \text{ nm}. \quad (8.5)$$

This model was applied to calculate the drift for the standard detector. The wavelength-dependent standard deviation in the drift rate was also calculated according to Equation 8.5. The drift and the standard deviation in the drift rate were added in quadrature for the total spectral drift contribution.

#### **8.4.1.3 Spatial uniformity of the standard detector, $u_{SSu}$**

The spatial uniformity of detectors similar to the standard detector and test detector used in the 200 nm to 400 nm region was determined for the CCPR-K2.c



key comparison. Measurements were performed by the pilot laboratory by measuring the surface of the detectors at a wavelength of 253,7 nm with a small beam diameter in 0,5 mm steps. The results include the effects of varying measurement spot diameters, deviation of the measurement spot position from the centre of the detectors and varying measurement spot profiles. The largest contribution reported was used as an estimate of the relative standard uncertainty contribution associated with the spatial uniformity of the standard detector in the 200 nm to 400 nm region.

An empirical test [NMISA, 2003] was previously performed at NMISA for the spatial uniformity of the Si photodiode detectors. The result of this empirical test was used as the standard uncertainty contribution associated with the spatial uniformity of the standard detector in the 600 nm to 1 100 nm region.

#### **8.4.1.4 Linearity of the standard detector, $u_{slin}$**

The CCPR-K2.c report indicates that the detectors are linear in the UV and visible wavelength range for an optical beam power below 500  $\mu\text{W}$  and similar beam spot sizes used in the key comparison, and provides an associated relative standard uncertainty contribution. The beam cross-section used by the pilot laboratory of this key comparison was near circular with a diameter of approximately 3,2 mm. This claim is supported by linearity measurements performed on similar Si photodiode and PtSi photodiode detectors in [Lei and Fischer \[1993\]](#) and [Richter \*et al.\* \[2002\]](#).

The maximum beam power used for the calibration in the 200 nm to 400 nm region was found to be approximately 37  $\mu\text{W}$ . The measurement spot on the detectors' surfaces was square with a cross-section of approximately 2 mm  $\times$  2 mm. Since the beam power and spot size meet the above-mentioned

requirement, the uncertainty contribution provided in CCPR-K2.c report was used as an estimate.

The CCPR-K2.b report states that non-linearity effects are negligible compared to other uncertainty contributions for a similar beam size and power as used for these calibrations and do not provide an uncertainty estimate. However, to avoid an underestimation of this uncertainty contribution, an empirical test that was previously performed at NMISA to determine the non-linearity effect for a similar detector was used. This estimate was used as the relative standard uncertainty contribution of non-linearity for the standard detector in the 600 nm to 1 100 nm region.

#### **8.4.1.5 Temperature coefficient of the standard detector, $u_{Stempc}$**

The temperature coefficients for the standard detector as a function of wavelength were obtained from its manufacturer's specification [Hamamatsu, 2015] and the Optical Radiometry book by Parr *et al.* [2005]. The difference in temperature reported on its calibration certificate and measured in the laboratory during the calibrations in the two wavelength regions was used to determine the effect of temperature on the spectral power responsivity of the standard detector. This quantification was used as the relative standard uncertainty contribution.

#### **8.4.1.6 Temperature dependence of the standard detector, $u_{Stempd}$**

The relative standard uncertainty contribution associated with the temperature dependence of the standard detector was obtained from estimates reported in the Optical Radiometry book [Parr *et al.*, 2005] for the 200 nm to 400 nm region and the NIST special publication on Spectroradiometric Detector Measurements [Larason and Houston, 2008] for the 600 nm to 1 100 nm region.

#### **8.4.1.7 Effect of the amplifier, $u_a$**

The same calibrated variable gain low noise current amplifier was connected to the standard detector and test detectors in both wavelength regions. Since the same gain setting was used in each calibration for both the standard and test detectors, the effect from the amplifier cancels in the ratio when calculating the spectral power responsivity of the test detector using Equation 4.6.

Both CCPR-K.2c and CCPR-K.2b reports indicate that the same gain setting was used for the detectors being compared and therefore the effect of the amplifier on the spectral power responsivity of the detectors is negligible.

For the 200 nm to 400 nm region, no standard uncertainty contribution associated with the amplifier was added to the combined standard uncertainty. However, for the 600 nm to 1100 nm region, the uncertainty reported in the calibration certificate of the amplifier was added as a standard uncertainty contribution. As a future improvement of measurement uncertainty, the uncertainty of the amplifier used should be taken into consideration in all wavelength regions. Omitting this contribution may cause an underestimation of the measurement uncertainty.

#### **8.4.1.8 Effect of the multimeter on the standard detector's output signal, $u_{sm}$**

The multimeter was calibrated for, among others, voltage measurements at various voltage ranges. An expanded uncertainty with a Gaussian distribution and a coverage factor of  $k = 2$  was reported in its calibration certificate. This reported uncertainty was used as the standard uncertainty contribution,  $u_{mc}$ , of the multimeter calibration.

In the calibration certificate of the multimeter, the uncertainty is reported in voltage, [V], for each voltage range. The relative contribution,  $u_{mc}$ , to the meas-

ured output signal of the standard detector in each wavelength region,  $V_S(\lambda)$ , was calculated by dividing the reported uncertainty by the coverage factor  $k = 2$  to obtain the standard uncertainty contribution for  $k = 1$ , and then determining the percentage contribution of this uncertainty to the measured signal.

The calibration of the multimeter was performed to confirm whether the multimeter meets the manufacturer's accuracy specification, therefore no correction was reported in the calibration certificate. For this reason, the accuracy specification,  $u_{ma}$ , was also added to the standard uncertainty contribution associated with the multimeter.

The accuracy specification of the multimeter is  $\pm$  (% of reading + % of range) at each voltage range, [Agilent, 2007]. For example, at the 1 V range the accuracy specification is  $\pm$  (0,002 % of reading + 0,0006 % of range). These accuracy specifications were used to determine the relative contribution,  $u_{ma}$ , to the measured output signal of the standard detector in each wavelength region,  $V_S(\lambda)$ , for each voltage range used. Since this is an accuracy specification, a rectangular probability distribution was used with a coverage factor of  $k = \sqrt{3}$ .

To obtain the combined relative standard uncertainty contribution associated with the effect of the multimeter on the standard detector's output signal,  $u_{Sm}$ , the contributions  $u_{mc}$  and  $u_{ma}$  were added in quadrature as a function of wavelength.

#### **8.4.1.9 Effect of resolution of the multimeter on the output signal of the standard detector, $u_{Sres}$**

The resolution of the output signal measured with the multimeter for the standard detector in each wavelength region was determined from the recorded values. As described in Section 7.5.9, the semi-range of the resolution is used as the

uncertainty contribution. Therefore, this spectral resolution was divided by 2 to obtain the semi-range.

A rectangular probability distribution with a coverage factor of  $k = \sqrt{3}$  was used, since the value is expected to lie anywhere within the limits specified by the semi-range. The semi-range values were therefore divided by  $\sqrt{3}$  and the ratio of these spectral values and the output signal measured for the standard detector was used as the relative standard uncertainty contribution,  $u_{Sres}$ .

In future, this contribution may be omitted, since it is negligible in comparison with other uncertainty contributors.

#### **8.4.1.10 Source stability, $u_{ss}$**

The standard uncertainty contribution for the stability in the xenon arc source was determined empirically, since it could not be monitored with the intensity controller. A calibration such as the one performed typically takes one hour to complete. The xenon source was therefore measured with a monitor detector for one hour in five-second intervals, see Section 8.1.1. The deviation in the minimum and maximum values recorded was calculated as the standard uncertainty contribution.

As mentioned in Section 8.1.1, the QTH source was monitored with an intensity controller. Therefore, for this wavelength region, the manufacturer specification of the intensity controller stability was used as the standard uncertainty contribution.

A rectangular distribution with a coverage factor of  $k = \sqrt{3}$  was used.

#### **8.4.1.11 Polarisation and non-uniform beam profile, $u_{pnb}$**

The CCPR-K2.c report describes the measurement method of the relevant detectors. To eliminate beam polarisation effects on the responsivity of the detectors, the detectors were rotated about the optical axis of the incident light beam between measurements. The uncertainty in the average measurements taken for the relevant detectors by the key comparison participants was calculated as the standard deviation of the mean and includes the uncertainty contribution associated with polarisation effects of the source and a non-uniform beam profile. For the uncertainty contribution in the 200 nm to 400 nm region, the largest contribution was selected from the CCPR-K2.c report as an estimate.

The CCPR-K2.b report indicates that polarisation effects for single element Si photodiode are negligible when it is aligned perpendicularly to the incident beam axis. However, to avoid an underestimation of measurement uncertainty, an estimate sourced from previous calibrations was used for the 600 nm to 1 100 nm region.

#### **8.4.1.12 Inter-reflections between detector and exit slit of the monochromator, $u_{refl}$**

The CCPR-K2.b report indicates that inter-reflection effects are negligible when the exit slit is blackened. Therefore, this standard uncertainty contribution was taken from the CCPR-K2.c report as a worst-case estimate for both wavelength regions. This estimate applies when the exit slit of the double monochromator is blackened to reduce inter-reflections. Since the exit slit of the double monochromator used in these calibrations is not blackened, this estimate may be an underestimation and requires further investigation, see Section 11.

#### **8.4.1.13 Beam divergence and vignetting, $u_{bdv}$**

According to the CCPR-K2.c and CCPR-K2.b reports, the effect of beam divergence and vignetting is negligible if the beam divergence is within the acceptance angle of the detectors. As prescribed in the CCPR-K2.b technical protocol [BIPM, 2001], an aperture ratio of F/8 or larger must be used. This ensures that the angle at which the focused light converges onto the detector is smaller than the acceptance angle of the detector.

Since the mirror that focuses the light beam onto the detector surface has an aperture ratio of F/8, the beam divergence is small enough for this effect to be negligible. However, an estimate based on what other laboratories use in the UV region was taken as an uncertainty contribution for the 200 nm to 400 nm region.

#### **8.4.1.14 Internal stray light, $u_{isl}$**

The specification of the McPherson monochromator [McPherson, 2015] includes a contribution of internal stray light which was used as an estimate for the relative standard uncertainty associated with internal stray light of the measurement setup. The method described in Section 6.5.5 was used by the manufacturer to determine the internal stray light of the double monochromator. The output signal with the shutter closed was measured at several wavelengths with and without the appropriate order-sorting filter. The internal stray light was found to be within the requirement specified by NPL, [McPherson, 2015].

#### **8.4.1.15 Effect of external stray light on the standard detector, $u_{sesl}$**

The relative standard uncertainty associated with the external stray light was estimated from the ratio of the output signal measured for the standard detector with the shutter closed (dark signal) and with the shutter open (light signal). In

the calculation of the spectral power responsivity, the dark signal was subtracted from the light signal, therefore this contribution might be an overestimation, but is still included in the combined standard uncertainty.

#### **8.4.1.16 Spectral wavelength calibration, $u_\lambda$**

The wavelength calibrations performed provided the expanded uncertainties of  $\pm 0,3$  nm and  $\pm 0,2$  nm for 200 nm to 400 nm and 600 nm to 1 100 nm, respectively, with a Gaussian distribution and a coverage factor of  $k = 2$ .

This standard uncertainty contribution of wavelength to the measured spectral power responsivity was calculated using two methods for each wavelength region. First from the spectral power responsivity of the test detector,  $s_T(\lambda)$ , using Equation 8.6, and second from the ratio of the output signals from the test and standard detectors, using Equation 8.9.

For the first method, the uncertainty was added to each wavelength, e.g.  $\lambda_+ = 200$  nm + 0,3 nm = 200,3 nm. A cubic spline interpolation was performed to calculate the spectral power responsivity of the test detector at these new wavelengths,  $s_{T_+}(\lambda)$ . The uncertainty was also subtracted from each wavelength, e.g.  $\lambda_- = 200$  nm - 0,3 nm = 199,7 nm, and the same interpolation was performed to calculate the spectral power responsivity of the test detector at these wavelengths,  $s_T(\lambda)$ . The spectral sensitivity coefficient,  $c_{\lambda_i}(\lambda)$ , was calculated from this data:

$$c_{\lambda_i}(\lambda) = \frac{\delta s_T}{\delta \lambda}(\lambda) = \frac{s_{T_+} - s_T}{\lambda_+ - \lambda_-}(\lambda) \text{ [A W}^{-1} \text{ nm}^{-1}] \quad (8.6)$$

This spectral sensitivity coefficient was divided by the spectral power responsivity



of the test detector to obtain the relative standard uncertainty contribution:

$$\frac{c_{\lambda_1}(\lambda)}{s_T(\lambda)} \text{ [nm}^{-1}\text{]} \quad (8.7)$$

For the second method, the standard uncertainty contribution was calculated from the ratio of the detectors' output signals:

$$V_r(\lambda) = \frac{V_T(\lambda)}{V_S(\lambda)} \quad (8.8)$$

The output signals of the detectors were determined for the wavelengths  $\lambda_+$  and  $\lambda_-$  in the same way as described above, using cubic spline interpolation, to determine the spectral sensitivity coefficient,  $c_{\lambda_2}(\lambda)$ :

$$c_{\lambda_2}(\lambda) = \frac{\delta V_r}{\delta \lambda}(\lambda) = \frac{V_{r+} - V_{r-}}{\lambda_+ - \lambda_-}(\lambda) \text{ [V V}^{-1}\text{ nm}^{-1}\text{]} \quad (8.9)$$

The spectral sensitivity coefficient was divided by the ratio of the detectors' output signals,  $V_r(\lambda)$ , to obtain the relative standard uncertainty contribution:

$$\frac{c_{\lambda_2}(\lambda)}{V_r(\lambda)} \text{ [nm}^{-1}\text{]} \quad (8.10)$$

The relative spectral standard uncertainty contributions were calculated by dividing the wavelength uncertainty, e.g.  $\pm 0,3$  nm, by the coverage factor  $k = 2$ , multiplying with spectral sensitivity coefficients calculated in Equation 8.7 and Equation 8.10, respectively, and multiplying by a 100.

The larger spectral uncertainty contribution obtained between the two methods was used to determine the combined standard uncertainty.

#### **8.4.1.17 Repeatability of the standard detector, $u_{Sr}$**

As described in Section 8.2.1 and Section 8.2.2, 20 readings were recorded with the multimeter at each wavelength for each detector in both wavelength regions, and the average and standard deviation of these 20 readings were recorded. To determine the relative standard uncertainty contribution associated with the repeatability of the standard detector, the percentage contribution of the standard deviation to the average was calculated as a function of wavelength.

#### **8.4.1.18 Bandwidth effects on the test detector, $u_{Tb}$**

For the calibrations in the two wavelength regions, the same bandwidth was used for the standard and test detectors, respectively. The sources used also did not have any rapid changes in their spectral distributions in the wavelength regions measured. Therefore the effect of bandwidth on the spectral power responsivity of the detectors was estimated to be small.

The CCPR-K2.c report, calculated an uncertainty associated with bandwidth effects when comparing a PtSi photodiode detector against a Si photodiode detector with a rectangular probability distribution, *i.e.* a coverage factor of  $k = \sqrt{3}$ . This spectral uncertainty contribution was used as an estimate for the relative standard uncertainty.

The CCPR-K2.b report estimated the bandwidth effects to be negligible for the detectors compared. However, to avoid the underestimation of this effect, an estimate from previous calibrations was used as a relative standard uncertainty contribution. A rectangular probability distribution with a coverage factor of  $k = \sqrt{3}$  was used.

#### **8.4.1.19 Spatial uniformity of the test detector, $u_{Tsu}$**

Refer to Section 8.4.1.3 describing the spatial uniformity measurements performed for similar detectors in the CCPR-K2.c key comparison [Werner, 2014]. The largest spatial uniformity contribution reported for PtSi photodiode detectors was used as an estimate of the relative standard uncertainty contribution associated with the spatial uniformity of the test detector in the 200 nm to 400 nm region.

The same empirical test [NMISA, 2003] used for the standard uncertainty contribution associated with the spatial uniformity of the standard detector, was also used as an estimate of the standard uncertainty contribution associated with the spatial uniformity of the test detector in the 600 nm to 1 100 nm region.

#### **8.4.1.20 Linearity of the test detector, $u_{Tlin}$**

Refer to Section 8.4.1.4 where the linearity of the detectors used in the CCPR-K2.c key comparison was discussed. The uncertainty contribution provided in the CCPR-K2.c report was used as an estimate of the relative standard uncertainty contribution of the test detector in the 200 nm to 400 nm region.

The same empirical test used in Section 8.4.1.4 for the standard detector in the 600 nm to 1 100 nm region was used to provide the estimate of the relative standard uncertainty contribution for non-linearity of the test detector.

#### **8.4.1.21 Temperature coefficient of the test detector, $u_{Tempc}$**

The pilot laboratory of the CCPR-K2.c key comparison provided temperature coefficients for the PtSi photodiode detectors [Werner, 2014]. These temperature coefficients and the difference in laboratory temperature recorded during calibration in the 200 nm to 400 nm region and the PTB calibration of the PtSi photo-

diode detector were used to determine the effect of this temperature change on the spectral power responsivity of the test detector. This result was used as an estimate of the relative standard uncertainty contribution due to the temperature change. In future, this uncertainty may be omitted, since it causes an overestimation of uncertainty. This uncertainty contribution is not required for the test detector. The temperature effect on the test detector on the spectral power responsivity is already taken into account in the temperature dependence standard uncertainty contribution.

For this same reason, no uncertainty contribution due to the temperature coefficient of the test detector in the 600 nm to 1 100 nm region was considered.

#### **8.4.1.22 Temperature dependence of the test detector, $U_{Tempd}$**

The CCPR-K2.c report describes that the pilot laboratory performed measurements at recorded temperatures that spread over an interval. An associated standard uncertainty was calculated for this temperature spread assuming a rectangular probability distribution, *i.e.* a coverage factor of  $k = \sqrt{3}$ . This relative standard uncertainty was used as an estimate of temperature dependence of the test detector in the 200 nm to 400 nm region, or the effect of the change in temperature during the calibration on the spectral power responsivity of the test detector.

For the 600 nm to 1 100 nm region, an estimate of the temperature dependence of the test detector was obtained from NIST special publication on Spectroradiometric Detector Measurements [Larason and Houston, 2008] and used as a relative standard uncertainty contribution.

#### **8.4.1.23 Effect of the multimeter on the test detector's output signal, $u_{Tm}$**

This relative standard uncertainty contribution was calculated in the same way as described in Section 8.4.1.8 for the standard detector. The uncertainty contributions from the calibration of the multimeter and its accuracy specification were determined and added in quadrature as a function of wavelength to obtain the combined relative standard uncertainty contribution associated with the effect of the multimeter on each test detector's output signal,  $u_{Tm}$ .

#### **8.4.1.24 Effect of resolution of the multimeter on the output signal of the test detector, $u_{Tres}$**

The relative standard uncertainty contribution associated with the resolution of the multimeter on the output signal of the test detector in each wavelength region was determined using the same method described in Section 8.4.1.9.

#### **8.4.1.25 Effect of external stray light on the test detector, $u_{Tesl}$**

The relative standard uncertainty associated with the effect of external stray light on the test detector in the 600 nm to 1 100 nm region was determined using the same method described in Section 8.4.1.15. This effect was not taken into account for the test detector in the 200 nm to 400 nm region.

Since the inclusion of this contribution for the standard detector might already be an overestimation, the omission of the effect on the test detector in the 200 nm to 400 nm region will not lead to an underestimation of the combined uncertainty of measurement.

#### **8.4.1.26 Repeatability of the test detector, $u_T$**

As described in Section 8.4.1.17, 20 readings were recorded with the multimeter at each wavelength for each detector in both wavelength regions, and the average and standard deviation of these 20 readings were recorded. To determine the relative standard uncertainty contribution associated with the repeatability of the test detectors in both wavelength regions, the percentage contribution of the standard deviation to the average was calculated as a function of wavelength.

## **8.4.2 Uncertainty analysis for calibration of the Si photodiode detector against the pyroelectric detector and Si-trap detector as standard in the wavelength region of 600 nm to 1 100 nm**

An uncertainty of measurement analysis was performed for the calibration of the Si photodiode detector against the pyroelectric detector and Si-trap detector as standard in the wavelength region of 600 nm to 1 100 nm, see Appendix K for the calculated uncertainty of measurement.

The relative uncertainty of measurement of this calibration, including both the absolute tie point and spectral power responsivity calibration, was determined from the uncertainty contributors described below. In this section, the Si-trap detector will be referred to as the standard detector and the Si photodiode detector as the test detector.

Unless otherwise specified, Gaussian distributions with a coverage factor of  $k = 1$  and sensitivity coefficients equal to 1 were used for the uncertainty contributors described below. This was done as a best estimate and may be investigated in future to improve the uncertainty of measurement calculations.

### **8.4.2.1 Absolute calibration uncertainty contributors**

#### **8.4.2.1.1 Absolute spectral power responsivity of the standard detector, $u_s$**

The uncertainty of measurement in the absolute spectral power responsivity of the standard detector at 632,8 nm was obtained from its calibration certificate. This certificate reports the relative expanded uncertainty with a Gaussian distribution and a coverage factor of  $k = 2$ .

#### **8.4.2.1.2 Drift in the standard detector, $u_{Sd}$**

The drift in the absolute spectral power responsivity of the standard detector was determined from its calibration history. Sufficient data were available to calculate the drift in absolute spectral power responsivity at 632,8 nm per calibration interval of the standard detector to use as the relative standard uncertainty contribution.

#### **8.4.2.1.3 Spatial uniformity of the standard detector, $u_{Ssu}$**

The alignment position of the standard detector was optimised for maximum signal from the incident laser beam, since the standard detector was originally calibrated following the same alignment procedure. The deviation in signals measured around this position was used as a standard uncertainty contribution.

#### **8.4.2.1.4 Linearity of the standard detector, $u_{Sin}$**

As mentioned in Section 8.4.1.4, the CCPR-K2.b report states that non-linearity effects are negligible compared to other uncertainty contributions for a similar beam size and power as used for the calibrations discussed in Section 8.4.1. However, for the absolute tie point calibration, the laser beam power was higher than that used in the CCPR-K2.b key comparison and therefore the same assumption could not be made.

The same empirical test used in Section 8.4.1.4 for the non-linearity effect was also used as the relative standard uncertainty contribution of this standard detector with a Gaussian distribution and a coverage factor of  $k = 2$ .

#### **8.4.2.1.5 Effect of the amplifier, $u_a$**

Both CCPR-K.2c and CCPR-K.2b reports indicate that if the same gain settings are used for the detectors being compared, the effect of the amplifier on the



spectral power responsivity of the detectors is negligible. This was also the case for the absolute tie point calibration. However, to avoid an underestimation of this uncertainty contribution, the uncertainty reported in the calibration certificate of the amplifier with a Gaussian distribution and a coverage factor of  $k = 2$ , was added as a standard uncertainty contribution.

#### **8.4.2.1.6 Effect of the multimeter on the detectors' output signal, $U_{AbsM}$**

As seen in previous similar calibrations performed at NMISA, the method used in Section 8.4.1.8 produces an uncertainty smaller than 0,002 %. Therefore, this uncertainty was taken as the worst case uncertainty contribution associated with the effect of the multimeter on the detectors' output signals. A Gaussian distribution and a coverage factor of  $k = 2$  were used, as reported on the multimeter's calibration certificate.

#### **8.4.2.1.7 Source stability, $U_{AbsSS}$**

The HeNe laser source was stabilised with a laser power controller, as described in Section 8.2.2. This laser power controller's manufacturer's specification for optical ripple was used as the standard uncertainty contribution associated with the source stability with a Gaussian distribution and a coverage factor of  $k = 2$ .

#### **8.4.2.1.8 Stray light and standard detector noise, $U_{Ssl}$**

The ratio of the output signal measured for the standard detector with the shutter closed (dark signal) and with the shutter open (light signal) was calculated and used as the relative standard uncertainty associated with stray light and detector noise. As done for the other calibrations performed, the dark signal was subtracted from the light signal to correct for the effect of external stray light. The calculated standard uncertainty contribution was still included to account for any

other effects related to stray light and detector noise.

#### **8.4.2.1.9 Repeatability of the standard detector, $u_{Sr}$**

Similar to the other calibrations performed, 20 readings were recorded with the multimeter for the standard detector. The average and standard deviation of these 20 readings were recorded. To determine the relative standard uncertainty contribution associated with the repeatability of the standard detector, the percentage contribution of the standard deviation to the average was calculated.

#### **8.4.2.1.10 Spatial uniformity of the test detector, $u_{TSU}$**

The same standard uncertainty contribution reported in Section 8.4.1.19 for the test detector in the 600 nm to 1 100 nm region was used here, since this is the same test detector, *i.e.* the Si photodiode detector.

#### **8.4.2.1.11 Temperature dependence, $u_{temp}$**

The uncertainty due to temperature effects was estimated based on the stability of the environmental conditions. The laboratory's Quality System procedure specifies the temperature range at which the laboratory must be maintained. During the calibration, the laboratory's temperature remained within this temperature range.

#### **8.4.2.1.12 Repeatability of the test detector, $u_{Tr}$**

Similarly to the standard detector, 20 readings were recorded with the multimeter for the test detector, in two sets. The standard deviation between the two sets was divided by the square root of the number of sets, *i.e.*  $\sqrt{2}$ , to obtain the standard deviation of the mean.

To determine the relative standard uncertainty contribution associated with

the repeatability of the test detector, the percentage contribution of the standard deviation of the average was calculated.

#### **8.4.2.2 Spectral calibration uncertainty contributors**

##### **8.4.2.2.1 Pyroelectric detector absorptance, $u_{pa}$**

The spectral absorptance of the pyroelectric detector surface coating was provided by the manufacturer. As a best estimate of the standard uncertainty contribution associated with this spectral absorptance, the relative change in absorptance in the wavelength region of interest was calculated. A rectangular probability distribution with a coverage factor of  $k = \sqrt{3}$  was used.

##### **8.4.2.2.2 Effect of the multimeter on the detectors' output signal, $u_{SpecM}$**

The same standard uncertainty contribution reported in Section 8.4.2.1.6 was used for the uncertainty contribution associated with the effect of the multimeter on both the standard and test detectors' output signal obtained in the spectral calibration.

##### **8.4.2.2.3 Source stability, $u_{SpecSS}$**

As mentioned in Section 8.1.1, the QTH source was monitored with an intensity controller. The manufacturer's specification of the intensity controller stability was used as the standard uncertainty contribution associated with the source stability. A Gaussian distribution with a coverage factor of  $k = 2$  was used.

##### **8.4.2.2.4 Polarisation, diffraction, interference and angular effects $u_{pdia}$**

The CCPR-K2.b report states that polarisation effects for single element Si photodiodes are negligible, however, the same standard uncertainty contribution as determined in Section 8.4.1.11 for the 600 nm to 1 100 nm region was used here,

since the test detector and source used are the same. This uncertainty contribution was assumed to include any diffraction, interference and angular effects on the spectral power responsivity of the test detector.

#### **8.4.2.2.5 Spectral wavelength calibration, $u_{\lambda}$**

The same calculation as described in Section 8.4.1.16 for the 600 nm to 1 100 nm region was used to determine this uncertainty contribution. The largest contribution as a function of wavelength in the 600 nm to 1 100 nm region was selected as the standard uncertainty contribution associated with wavelength. A Gaussian distribution with a coverage factor of  $k = 2$  was used.

#### **8.4.2.2.6 Linearity of the test detector, $u_{Lin}$**

Section 8.4.1.4 describes that an empirical test was previously performed at NMISA to determine the non-linearity effect for a similar detector. The same estimate was used as the relative standard uncertainty contribution of non-linearity for the test detector. A rectangular probability distribution with a coverage factor of  $k = \sqrt{3}$  was used.

#### **8.4.2.2.7 Stray light and test detector noise, $u_{Tsl}$**

The same method as described in Section 8.4.2.1.8 was used to determine the relative standard uncertainty associated with the stray light effect on the pyroelectric and test detectors, as well as the detector noise.

#### **8.4.2.2.8 Repeatability of the test detector, $u_{SpecTr}$**

As described in Section 8.2.2, four independent sets of data were recorded for the spectral power responsivity calibration, and the average of these sets was used. To determine this uncertainty contribution, the relative contribution of the

standard deviation of these four sets to their average was calculated as a function of wavelength. The largest contribution of the spectral data was used as relative standard uncertainty associated with the repeatability of the test detector.

## Chapter 9

### Discussion

A new system for the measurement of spectral power responsivity of detectors, using a scanning double monochromator and a selection of sources, order-sorting filters, diffraction gratings, imaging optics and detectors, was implemented.

A xenon-arc source and a LDLS were experimented with in the UV region. An operational issue caused the LDLS to lose power during its use. This issue must be investigated and is discussed in Chapter 11 as further research. The xenon-arc source was therefore used in the UV region. A QTH source was selected for the visible to near-IR region. No additional input imaging optics were required as the necessary optics were mounted inside the lamp housings of the selected sources.

A set of order-sorting filters and sets of diffraction gratings were selected based on the wavelength region to be measured and the sources used. A set of output optics was selected to image the exit slit onto the detector with an aperture ratio of  $F/8$  or greater, and to allow an optical chopper to be mounted at the output of the monochromator. Optical detectors were selected based on the wavelength region to be measured and traceability routes to be established.

## *Discussion*

---

The implemented measurement system was characterised by a series of calibrations. First, wavelength calibrations were performed in the wavelength regions of 200 nm to 400 nm and 600 nm to 1 100 nm. This was done by measuring the relevant wavelength standards for spectral lines selected from the NIST Atomic Spectra Database, and applying corrections for ambient conditions using the Engineering Metrology Toolbox of NIST.

The monochromator steps corresponding to the spectral peaks measured were determined using the steep-side method. A linear plot of the spectral peaks versus the corresponding monochromator steps was used to obtain the wavelength calibration equations to be used in the respective wavelength regions when operating the monochromator. Uncertainty of measurement analyses were performed for each of the wavelength calibrations.

Verification of the wavelength calibrations was performed by using the obtained wavelength calibration equations to move the monochromator to wavelength positions of laser line sources used in each respective wavelength region. For both wavelength calibration equations used in the respective wavelength regions, the spectral peaks of the laser lines were measured at the expected monochromator position to within the calculated uncertainty of measurement.

A PtSi photodiode detector was calibrated for spectral power responsivity on the new measurement system against a UV-enhanced Si photodiode detector, previously calibrated by NPL for spectral power responsivity, in the 200 nm to 400 nm region using the substitution method. Low signal was measured below 260 nm and it was therefore decided to report the spectral power responsivity from 260 nm to 400 nm only. To address this issue of low signal, the use of the LDLS must be investigated, see Chapter 11. An uncertainty of measurement analysis was performed for this calibration as a function of wavelength.

## *Discussion*

---

The measurement results obtained from this calibration were successfully verified by comparison against the measurement results of the PtSi photodiode detector's previous calibration by PTB for spectral power responsivity.

A Si photodiode detector was calibrated for absolute power responsivity at 632,8 nm against a Si-trap detector using a stabilised HeNe laser source. This calibration was performed using DC signal and then repeated using AC signal since the relative spectral power responsivity calibration performed on the new measurement system was done using a pyroelectric detector and optical chopper. The measurement results obtained from the DC and AC signal calibrations were compared and found to be within the stated measurement uncertainty of the Si-trap detector standard, it was therefore successfully verified.

This absolute tie point calibration was verified by repeating the calibration against another Si-trap detector used as a verification standard and by comparison against a previous calibration of the Si photodiode detector for spectral power responsivity. In both cases, the measurements results obtained successfully verified.

The Si photodiode detector was calibrated for relative spectral power responsivity against a pyroelectric detector, with known spectral absorptance, to extend the absolute power responsivity calibration at 632,8 nm to the wavelength region of 600 nm to 1 100 nm. This was done on the new measurement system using the substitution method. The relative calibration of the Si photodiode detector was converted to absolute spectral power responsivity using the absolute tie point at 632,8 nm. The uncertainty of measurement associated with this calibration was determined.

The measurement results obtained were compared to a previous calibration of the Si photodiode detector for spectral power responsivity and found to be



## *Discussion*

---

within the uncertainty of measurement stated for its previous calibration, therefore providing a successful verification.

The same measurement results were also compared to those obtained from calibrating the Si photodiode detector on the new measurement system against a UV-enhanced Si photodiode detector, previously calibrated by NPL for spectral power responsivity, using the substitution method. An uncertainty of measurement analysis was performed for this calibration as a function of wavelength. The verification was unsuccessful at some wavelengths between 650 nm and 720 nm and 1 060 nm to 1 100 nm.

Since the measurement results at all wavelengths between 600 nm and 1 050 nm, except at 660 nm, were within the uncertainty of measurement associated with the calibration of the Si photodiode detector against the pyroelectric detector and Si-trap detector, the calibration was considered verified between 600 nm and 1 050 nm. The causes of the unsuccessful verification at some wavelengths must be investigated and are discussed in Chapter 11.

Following the implementation of the new measurement system and its characterisation through the mentioned calibrations, it was applied to have the spectral power responsivity measurement capability assessed by SANAS for accreditation.

As a result of the SANAS assessment, the uncertainty of measurement analysis performed for the calibration of the Si photodiode detector against the UV-enhanced Si photodiode detector in the wavelength region of 600 nm and 1 050 nm, was an improvement on the uncertainty of measurement analysis performed for the calibration of the Si photodiode detector against the pyroelectric detector and Si-trap detector.

The improved uncertainty analysis includes several additional uncertainty

## *Discussion*

---

contributors not previously considered. It also determines the uncertainty of measurement as a function of wavelength, thereby providing a more accurate uncertainty estimate.

From the uncertainty analysis performed it can be seen that the largest contributors to the measurement uncertainty for spectral power responsivity of a detector are the effect of external stray light, repeatability of the detector and the absorptance of the pyroelectric detector's surface coating. These are followed by spatial uniformity of the detectors, source stability and the wavelength calibration of the monochromator. These contributions should be considered first when improving the uncertainty of measurement as part of future work, and are discussed in Chapter 11.

Following the clearance of findings raised during this assessment, the spectral power responsivity measurement capability was established for the wavelength regions of 260 nm to 400 nm and 600 nm and 1 050 nm.

## Chapter 10

# Conclusions

A new system for the measurement of spectral power responsivity of detectors was implemented. This measurement system makes use of a scanning double monochromator and other components selected based on the system's requirements. These include sources of optical radiation, order-sorting filters, diffraction gratings, imaging optics and detectors. This measurement system was characterised in the UV region, 200 nm to 400 nm, and in the visible to near-IR region, 600 nm to 1 100 nm.

As the first step of characterisation, wavelength calibrations were performed in the wavelength regions of 200 nm to 400 nm and 600 nm to 1 100 nm. These calibrations produced the wavelength calibration equations used by the double monochromator to scan through the wavelength regions during the spectral power responsivity calibrations. Uncertainty of measurement analyses were performed for these calibrations, producing an uncertainty of measurement of  $\pm 0,3$  nm in the UV region and  $\pm 0,2$  nm in the visible to near-IR region.

The measurement system was then characterised for spectral power responsivity in the wavelength regions of 200 nm to 400 nm and 600 nm to 1 100 nm.

## *Conclusions*

---

Characterisation in the 200 nm to 400 nm region was performed using a xenon-arc source, due to an operational issue with the laser-driven light source. A PtSi photodiode detector was calibrated for spectral power responsivity against a UV-enhanced Si photodiode detector, previously calibrated by NPL for spectral power responsivity, using the substitution method. Due to low signal below 260 nm, measurement results were only reported from 260 nm to 400 nm. A spectral analysis of uncertainty of measurement was performed. An uncertainty of measurement ranging from  $\pm 4,3\%$  at 260 nm to  $\pm 2,6\%$  at 400 nm was obtained. The measurement results obtained from this calibration were successfully verified by comparison against the measurement results of the PtSi photodiode detector's previous calibration by PTB for spectral power responsivity.

For characterisation in the 600 nm to 1 100 nm region, a Si photodiode detector was calibrated for absolute power responsivity at 632,8 nm against a Si-trap detector using a stabilised HeNe laser source. This absolute tie point was used to extend the calibration to the 600 nm to 1 100 nm region using a pyroelectric detector with known spectral absorptance, on the new measurement system using the substitution method. The uncertainty of measurement was calculated for this calibration and found to be  $\pm 2,7\%$ . The measurement results obtained were successfully verified against a previous calibration of the Si photodiode detector for spectral power responsivity.

As an additional verification, the Si photodiode detector was also calibrated on the new measurement system against the UV-enhanced Si photodiode detector using the substitution method. An uncertainty of measurement analysis was performed for this calibration as a function of wavelength, producing an uncertainty of measurement ranging from  $\pm 1,3\%$  to  $\pm 3,6\%$  in the wavelength range of 600 nm to 1 100 nm. The verification was unsuccessful at some wavelengths between 650 nm and 720 nm and 1 060 nm to 1 100 nm. Since

## *Conclusions*

---

the measurement results at all wavelengths between 600 nm and 1 050 nm, except at 660 nm, were within the uncertainty of measurement associated with the calibration of the Si photodiode detector against the pyroelectric detector and Si-trap detector, the calibration was considered verified between 600 nm and 1 050 nm.

Following the characterisation of the new measurement system, the spectral power responsivity measurement capability was assessed by SANAS for accreditation. Accreditation was obtained in the wavelength regions of 260 nm to 400 nm and 600 nm and 1 050 nm.

# Chapter 11

## Further research

Some factors discussed in this study require further investigation. Improvements in the measurement system and uncertainty estimation have also been identified for future research and are discussed.

The output optics used in the measurement system did not match the aperture ratio of the monochromator as is required for maximum throughput. When the measurement system was implemented, the mirrors used were the available output optics. Since the completion of the calibrations performed, new mirrors have been procured that were specifically designed for this measurement system, *i.e.* matching the aperture ratio of the monochromator. Measurements should be repeated with these mirrors as better throughput may be achieved.

The LDLS provides better signal and throughput than the xenon-arc source in the UV region. An operational issue occurred where the LDLS lost power. This will require further investigation to determine the cause and whether the LDLS can still be operated. A factor to consider is the laser source and that it might be faulty. As part of the investigation, the output of the laser source may be measured.

The operation of the LDLS also proved to be challenging. Optimal alignment

### *Further research*

---

is required, since it was observed that even small adjustments in alignment had a large effect on the output signal. Better alignment and improved mounting with opto-mechanical components should be investigated.

Another operational issue of the LDLS is nitrogen purging. When operated, the LDLS depleted the available nitrogen gas faster than the measurement could be completed. A larger nitrogen cylinder may be considered, however, after discussions with other laboratories that also use LDLS's, it was found that these laboratories do not perform purging. It was indicated that this might reduce the lifetime of the source, but had no real effect on measurement results. Operation of the LDLS without purging must be investigated.

With the use of the LDLS, the wavelength region can be extended down to 200 nm, which is required to provide internal traceability for spectral power responsivity of UV detectors.

The verification performed for the measurement results obtained for the Si photodiode detector through calibration against a UV-enhanced Si photodiode detector, was unsuccessful at some wavelengths between 650 nm and 720 nm and 1 060 nm to 1 100 nm. As discussed in Section 8.3.2, this may be due to the rapid decrease in detector responsivity and decreasing grating efficiency after 1 000 nm. It may be considered using another set of diffraction gratings with higher efficiency from 900 nm, such as 600 g/mm blazed at 1 250 nm, to determine if better throughput can be achieved between 1 000 nm and 1 100 nm.

It was observed from the recorded data that the external stray light was higher toward the lower end of the 600 nm to 1 100 nm region. Though measures were taken to reduce external stray light effects, such as baffling, use of a light-tight enclosure and use of thick materials to reduce acoustic noise on the pyroelectric detector, it might not have been adequate. This effect must be

### *Further research*

---

investigated to determine methods for further reducing external stray light.

For this study, the spectral absorptance of the pyroelectric detector surface coating provided by the manufacturer was used in the calculation of spectral power responsivity. In future, the spectral absorptance should be calibrated internally. This will provide confidence in the measurement result since it will be traceable to a national measurement standard. The measurement result will have a better and possibly smaller uncertainty contribution.

Some uncertainty contributions require further investigation for improved quantification, to minimise their contribution and to ensure that their contribution is not overestimated. The uncertainty contributors which have the largest contribution to the combined uncertainty of measurement should be considered first.

The inclusion of the effect of external stray light on the standard and test detectors should be investigated. The contributions added may be overestimations since corrections were already applied for this effect.

The effect of internal stray light is considered in the uncertainty of measurement calculation and is sourced from the manufacturer's specification. This effect is considered to be small because of the second monochromator connected in series to the first. However, the internal stray light of any spectrometer system should be characterised specifically for the instrument in use. The effect may be larger than expected at some wavelengths, especially in the UV region. This uncertainty contribution should therefore be investigated by quantifying the effect for this measurement system using the method prescribed in Section 6.5.5, *i.e.* with order-sorting filters.

The uncertainty contribution from the repeatability of the standard or test detector may be improved by increasing the number of measurements or independent measurement sets to obtain a better average. The standard deviation



### *Further research*

---

should also be divided by the square root of the number of measurements taken to determine the estimated standard deviation in the average. Since this was not done in this study, the uncertainty contribution due to repeatability is likely an overestimation.

The uncertainty associated with the spatial uniformity of a detector surface may be improved through empirical measurement. This may be done by measuring the surface of each detector in a grid formation consisting of small intervals using a stabilised source at one or more wavelengths.

Consider the effect of lamp stability in the UV region. The xenon-arc source could not be controlled with the intensity controller and therefore the source was measured over a period of time, using the measured drift as an uncertainty estimation.

Instead, for future research, the control software should be improved to allow the recording of data from both a monitor detector and the test or standard detector simultaneously. The data recorded with the monitor detector should then be used in equation 5.1, a modified version of equation 4.8, to correct for the effect of drift in the source. Though an uncertainty of measurement estimate must still be included for source stability, the contribution should be much smaller.

The wavelength calibration of the monochromator may also be investigated to improve its uncertainty contribution to the spectral power responsivity measurement results. One of the factors to consider is the measurement interval at which the spectral line sources are scanned. The smallest interval possible for the set of diffraction gratings may be used. As mentioned in Section 7.3.1, this was not the case for the UV region.

Also mentioned in Section 7.3.1, is the asymmetry effect in the measured spectral line in Figure 7.3. This asymmetry may be caused by poor monochro-

### *Further research*

---

mator alignment and optical aberrations in the monochromator optics. As further research, this effect may be addressed by improving the optical alignment of the monochromator or determining the wavelength peak using signals levels other than 10 % of the maximum signal.

Another case where a correction can be applied instead of having a large uncertainty contribution, is the uncertainties obtained for the temperature coefficient of the UV-enhanced Si photodiode detector. Since a temperature correction was not applied to the spectral power responsivity reported in the NPL calibration certificate, an uncertainty contribution had to be added, which was based on the temperature coefficients and temperature difference measured. In future, the temperature correction should be applied, so that this uncertainty contribution may be omitted.

Uncertainty contributions were added for both temperature coefficients and temperature dependence of the test detectors calibrated against the UV-enhanced Si photodiode detector. It may be that the uncertainty due to temperature is considered twice and is therefore an overestimation. The uncertainty contribution described above was necessary for the UV-enhanced Si photodiode detector, but its temperature dependence uncertainty could have been omitted. Since no temperature correction is required for the test detectors, their temperature dependence should still be considered, since there may have been temperature fluctuation during the calibrations. This effect requires further study to confirm whether the correct uncertainty contributions are considered.

The uncertainty of measurement estimate for the effect of polarisation and non-uniform beam profile on spectral power responsivity should be investigated and minimised by either rotating the detectors about the optical axis of the incident light beam during measurement, or using an integrating sphere at the entrance slit of the monochromator [Kostkowski, 1997]. Though these uncertainty

### *Further research*

---

estimates were included for test detectors, it was not determined for the pyroelectric detector. The effect of polarisation, as well as linearity, on the pyroelectric detector should be investigated through empirical measurements.

For the calibrations performed in this study, the detectors were not rotated about the optical axis of the incident light beam and the estimated uncertainty of measurement taken from the CCPR-K2.c report, where this method was used, may be an underestimation. If an integrating sphere is to be considered, additional input optics will be required. Rotating the detector about the optical axis and averaging the measurements will be sufficient to account for this effect, as prescribed in the CCPR-K2.c technical protocol, though this might be time consuming.

Another uncertainty of measurement contribution that could be minimised is the effect of inter-reflections between the detector and exit slit of the monochromator. An estimate of this contribution was taken from the CCPR-K2.c report, but is applicable to a monochromator with blackened slits. The monochromator used in this study does not have blackened slits. It may be considered in future to have the slits of the monochromator black anodised to reduce this uncertainty contribution.

The weighting of the uncertainty contributors should be investigated. In most cases, sensitivity coefficients equal to 1 were used as a best estimate. However, this can either underestimate or overestimate the uncertainty contribution. To determine a more accurate estimate of the measurement uncertainty, further research should be performed to better define the sensitivity coefficients. This may be done through empirical testing or it may be obtained from previous studies performed.

As mentioned in Section 2.8, the individual uncertainty contributions are

### *Further research*

---

combined to obtain the combined standard uncertainty,  $u_c(y)$ . This is done with the law of propagation of uncertainty. In this study, no correlations in uncertainty contributions were considered and only the first term of Equation 2.1 was applied. Some uncertainty contributors considered may be correlated. The effect of this correlation requires further research. Correlated uncertainty contributors should be identified and the effect quantified. Accounting for correlation will provide a better estimate of the uncertainty of measurement.

The new measurement system must still be characterised in the wavelength region of 400 nm to 600 nm. Future work will include using the same methods as described in this study to first calibrate the monochromator for wavelength and then to establish the spectral power responsivity measurement capability in this region. Additionally, following the investigations suggested above, the spectral power responsivity measurement capability should be established in the wavelength regions of 200 nm to 260 nm and 1 050 nm to 1 100 nm.

Once the spectral power responsivity measurement of detectors in the wavelength range of 200 nm to 1 100 nm has been established, the laboratory may participate in available key comparisons such as CCPR to maintain international equivalence.

# Appendices

# Appendix A

## Spectral power responsivity measurement system

*Spectral power responsivity measurement system*

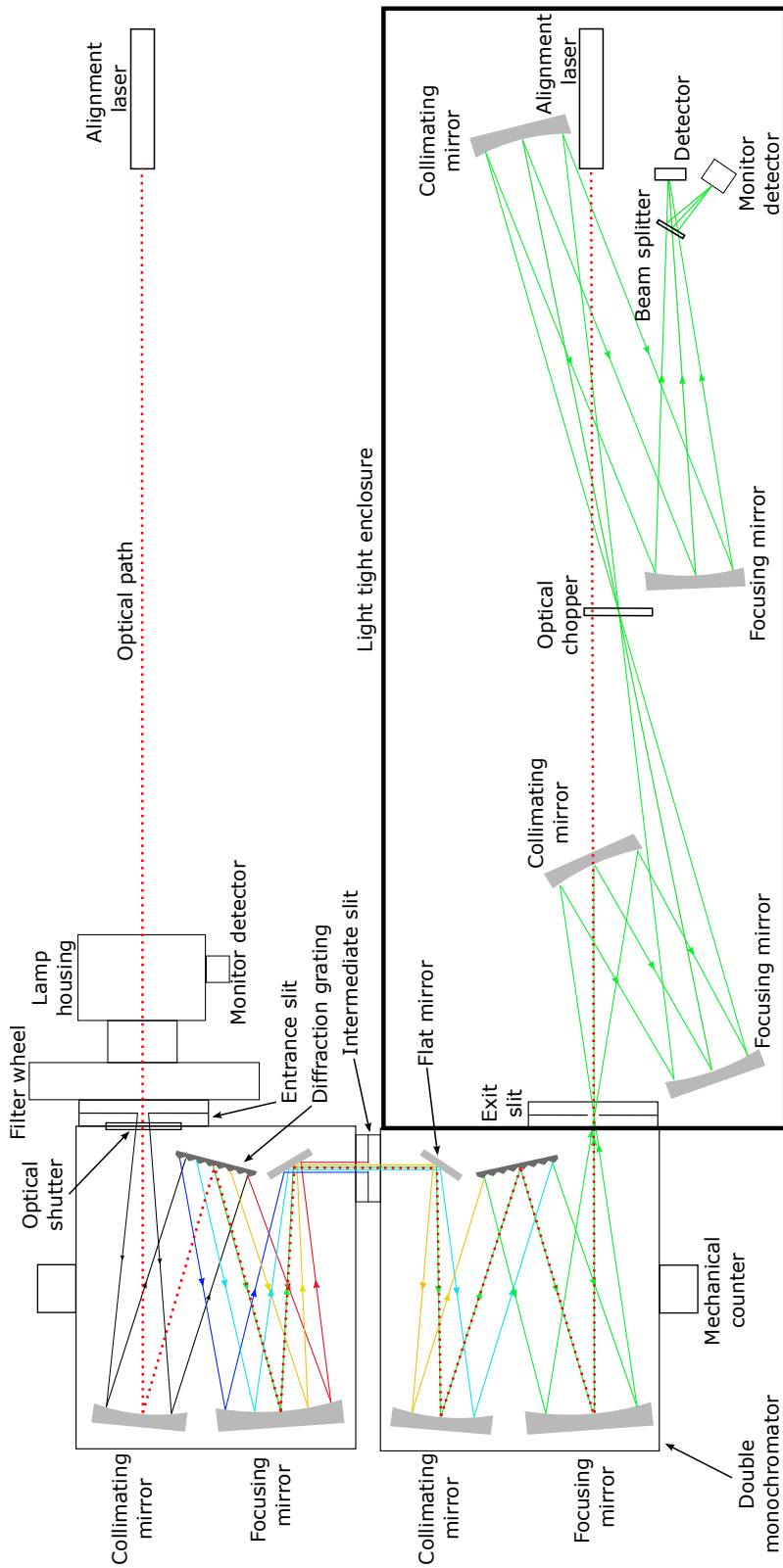


Figure A.1: A schematic representation of the spectral power responsivity measurement system.

## Appendix B

# Alignment of the monochromator

The monochromator was mounted on a bench next to an optical breadboard, on three foot-pieces, with ball head mounts and height adjustment, and was levelled using a spirit level. The horizontal laser line of a laser level was used to align a HeNe alignment laser at the input side of the monochromator, the entrance and exit slits of the monochromator and a HeNe alignment laser at the output side of the monochromator on the same horizontal plane. The two HeNe alignment lasers were mounted on stable mounts that allowed for tip, tilt and two translational adjustments. Both alignment lasers were mounted at the furthest point from the monochromator on the optical bench to allow enough space for the mounting of sources, output optics and detectors. HeNe alignment lasers and laser levels can experience observable beam drift after being switched on and were therefore allowed to stabilise for at least 30 minutes before use.

A set of diffraction gratings with a groove density of 600 g/mm blazed at 800 nm were installed in the scanning double monochromator. The monochromator software was used to move the two individual monochromators to the HeNe laser line, at approximately 632,8 nm. The mechanical wavelength counters of the two individual monochromators were checked to match each other and were both manually adjusted to the HeNe laser line as well. This was done



### *Alignment of the monochromator*

---

because it was noticed during previous use of the monochromator that the mechanical counters move slightly every time the two individual monochromators' scan controllers are switched on and that this mechanical movement is not equal between the two individual monochromators. During a calibration procedure, the scan controllers were therefore not switched off to avoid this mechanical movement which may influence the alignment of the monochromator.

The next step was to align the input-side alignment laser, the internal monochromator optics and the output-side alignment laser such that the two alignment lasers were reflected onto each other through the double monochromator. The input-side alignment laser was adjusted such that the laser beam went through the centre of the entrance slit of the double monochromator and onto the centre of the collimating mirror in the first monochromator. The collimating mirror was adjusted such that the laser beam was aligned in the centre of the diffraction grating. After this, the diffraction grating was adjusted such that the laser beam was aligned in the centre of the focusing mirror, which reflected the laser beam onto a folding mirror and then onto the centre of the middle slit between the two individual monochromators. The folding mirrors in each individual monochromator were adjusted such that the laser beam was reflected onto the centre of the collimating mirror in the second monochromator. This mirror was adjusted to reflect the laser beam to the centre of the diffraction grating in the second monochromator. The second grating was adjusted such that the laser beam was on the centre of the focusing mirror, which was adjusted to reflect the laser beam through the centre of the exit slit of the double monochromator and onto the output-side alignment laser.

This same process was followed with slight adjustments of each optical component until the output-side alignment laser beam travelled through the double monochromator and onto the input-side alignment laser. Two apertures

### *Alignment of the monochromator*

---

were placed in the optical path of the alignment lasers as a reference to the optical axis, each between the alignment laser and entrance and exit slit of the double monochromator, respectively.

Once the alignment was completed, a quartz tungsten halogen lamp, in its lamp housing, was attached to the entrance of the double monochromator. The monochromator software was used to scan through a visible wavelength range to check whether the monochromatic waveband was consistently horizontal over the middle and exit slits of the double monochromator as the gratings were rotated. During alignment, this may also be checked by rotating the gratings and checking whether the different orders of the laser line are also centred on the middle and exit slits of the double monochromator.

After this initial alignment, a verification of alignment was performed as required with a change of optical components, such as gratings for operation in a different wavelength region.

## Appendix C

### Software

The scanning double monochromator has its own control software. Typically, after a double monochromator has been calibrated for wavelength, the wavelength calibration equation is used to calculate the number of steps that the scan controllers of the individual monochromators should move to reach the required wavelength. However, this software does not allow for a wavelength calibration equation input. Instead, the double monochromator manual provides a method for checking the wavelength accuracy.

A laser line, *e.g.* HeNe at approximately 632,8 nm, should be used. The scan controllers or software may then be used to position the two individual monochromators at this wavelength, but such that the laser beam travels from the entrance slit, through the centre of each internal optical component and through the exit slit. This assumes that the double monochromator is aligned and the alignment of the individual internal optical components has not been adjusted. The mechanical wavelength counters on the individual monochromators are then checked. If the wavelength displayed is more than 0,2 nm from the laser line wavelength, the mechanical counters are adjusted to match the laser line wavelength.

## *Software*

---

This method of checking wavelength accuracy is sufficient for most applications in industry. However, at the level of maintaining the national measurement standards, the wavelength error that could be present with this method has a large impact on the measurement uncertainty.

It is for this reason that dedicated control software was written for the double monochromator by a systems engineer at NMISA. The Python program allows the user to move each individual monochromator a number of steps at a time. This is a useful feature when performing the wavelength calibration. Once the wavelength calibration equation has been obtained, it can be used to determine the number of monochromator steps corresponding to a specified wavelength interval and the stepper position of the start wavelength and end wavelength for a specified wavelength region to be measured. The software allows a new origin or home position to be set once the wavelength calibration has been completed.

Additional settings such as scan speed, ramp up and down scan speed, number of measurements, the delay time before measurements are taken and the time interval between measurements can be set using the control software. The software connects to a multimeter to record data for the relevant optical detector and allows the user to enter the text file title in which the measured data should be saved.

During measurements, when returning to the starting wavelength, previous wavelength position or home position, the software automatically performs a mechanical backlash correction. This is done by moving monochromators 10 000 steps past the desired wavelength position, and then moving the 10 000 steps forward so that the monochromators stop at the desired wavelength position again.

The software has a pause function that allows for a waiting period once the

## *Software*

---

required wavelength has been reached on the monochromators. This function was specifically written for when the pyro-electric detector is in use. It was found that the pyro-electric detector takes longer to stabilise once a new wavelength position is set on the double monochromator. This function allows the user to start the measurement sequence once the signal has stabilised.

## Appendix D

### Mounting of optical detectors

The respective optical detectors were mounted on translation stages at the focal point of the monochromatic light beam. Two translation stages, with 100 mm translation each, were mounted on top of each other to achieve translation in the plane perpendicular to the optical axis. The optical axis is defined as the  $x$ -axis. The two axes in the plane perpendicular to the optical axis are defined as the  $y$ -axis, the horizontal axis, and the  $z$ -axis, the vertical axis. Translation of the optical detectors on the optical axis was achieved with a micrometer attached to the  $z$ -axis translation stage. A photo of the detector mounting is given in Figure [D.1](#), indicating the defined axes. Also shown in this figure is a baffle in front of the optical detectors. This additional baffle was used to shield the pyro-electric detector from acoustic noise produced by the optical chopper.

## Mounting of optical detectors

---

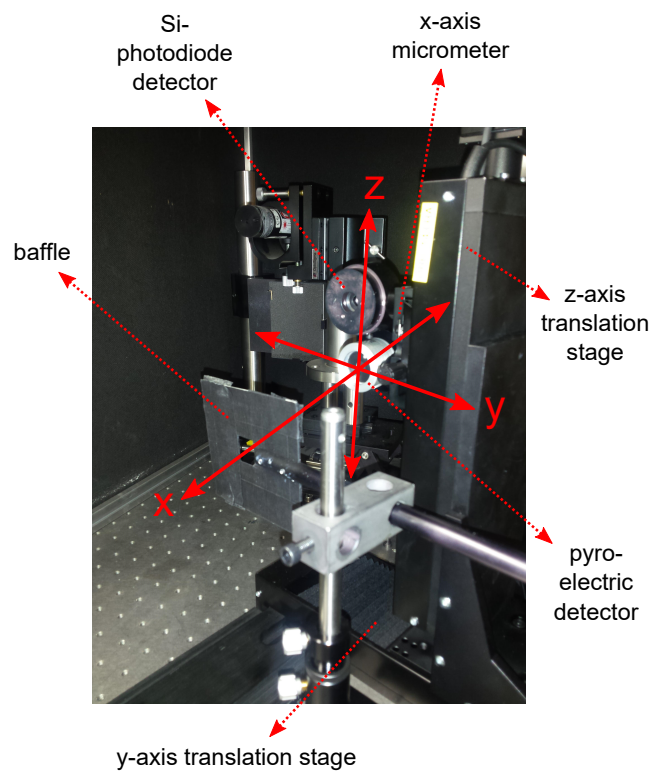


Figure D.1: A picture of the detector mount indicating the translation axes and other components.

## Appendix E

# Experimental demonstration of slit functions

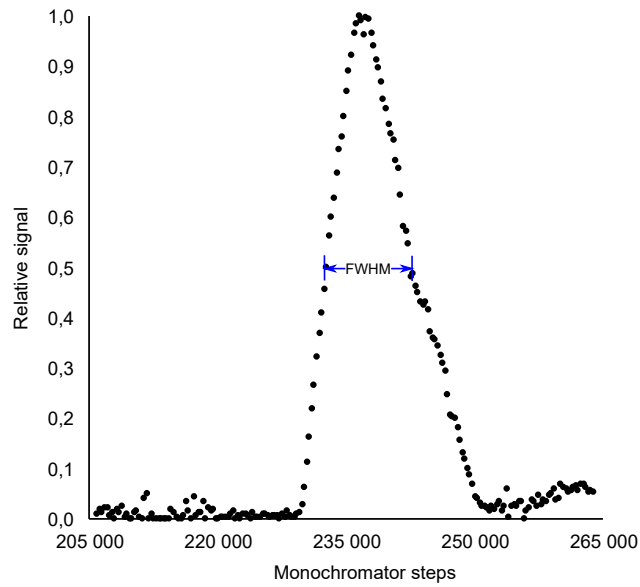
During the selection of spectral line sources for the wavelength calibration of the monochromator, the 823,38964 nm spectral line (in vacuum) of a xenon spectral line source was measured with equal and unequal slit widths, see Figure E.1. Figure E.1(a) shows a triangular slit function obtained when measuring the spectral line with the entrance, intermediate and exit slits all set to equal widths. Figure E.1(b) shows a trapesoidal slit function obtained when measuring the spectral line with the entrance and exit slits set to equal widths, but with the intermediate slit set at a greater width.

As mentioned in Section 6.5.3, for a subtractive dispersion monochromator the entrance and intermediate slits govern the bandwidth. This can be seen in Figure E.1, and determining the FWHM corresponding to the measured monochromator steps using the wavelength calibration equation 7.4, a smaller bandwidth of approximately 7 nm was obtained with a triangular slit function and a larger bandwidth of approximately 21 nm was obtained with a trapesoidal slit function.

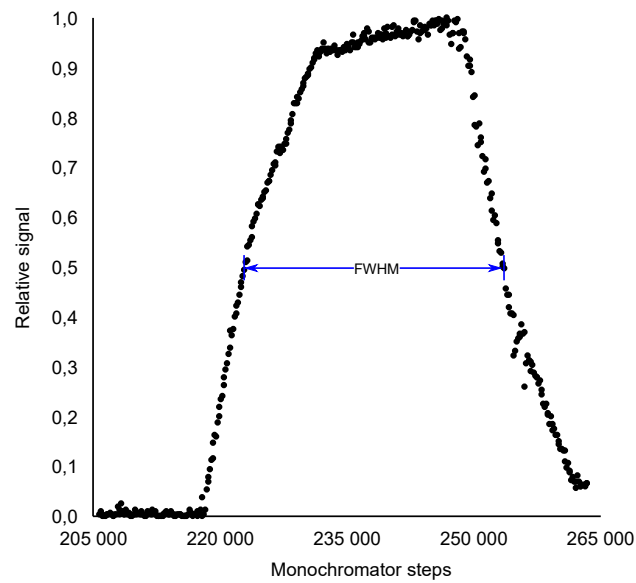


*Experimental demonstration of slit functions*

---



(a) Slit function for equal slits



(b) Slit function for unequal slits

Figure E.1: Graphical illustration of slit functions for equal and unequal slits when measuring the 823,38964 nm spectral line (in vacuum) of a xenon spectral line source.

## Appendix F

### Use of the LDLS

As mentioned in Chapter 5, a LDLS has a higher output power than a xenon-arc source, which makes it the preferred source in the UV region. During measurement with the LDLS, an operational issue occurred where the LDLS lost power. Since this issue requires further investigation, the measurement results obtained using the Xenon arc source were used for determining the spectral power responsivity in the ultraviolet wavelength region.

Other operational issues experienced with the LDLS were alignment and nitrogen gas depletion. The alignment of the LDLS proved to be challenging as even a slight adjustment had a large impact on the signal measured. The LDLS has to be purged with nitrogen gas during operation. It was found that the LDLS depleted the available nitrogen gas cylinder faster than the calibration could be performed. These issues are discussed in Section 11 as further research.

High throughput is an important aspect of a spectral power responsivity calibration, and therefore as described in Section 11, the use of the LDLS should be investigated to improve the spectral power responsivity measurement capability.

## **Appendix G**

# **Uncertainty of measurement for the wavelength calibration in the wavelength region of 200 nm to 400 nm**

*Uncertainty of measurement for the wavelength calibration in the wavelength region of 200 nm to 400 nm*

Table G.1: Uncertainty of measurement calculated for the wavelength calibration in the wavelength region of 200 nm to 400 nm as described in Section 7.5.

No.	Input quantity	Symbol	Value		Estimated uncertainty $u_e(x_i)$	Probability distribution	Coverage factor $k$	Standard uncertainty		Sensitivity coefficient		Uncertainty contribution $u_i(y)$	unit	
			$x_i$	unit				$u(x_i)$	unit	$c_i$	unit			
1	Theoretical value spectral line in vacuum	$u_{sl}$	253,728 296,815 435,956	nm	1,73E-04	Normal	1	1,73E-04	nm	$c_{sl}$	1,00E+00	1,73E-04	nm	
2	Modified Edlen equation calculation	$u_{Ed}$	1,00024E+00	1	7,39E-08	Normal	2	3,70E-08	1	$c_{Ed}$	-3,29E+03	1,21E-04	nm	
3	Laboratory temperature effect	$u_T$	2,33E+01	°C	4,00E+00	Triangular	$\sqrt{6}$	1,63E+00	°C	$c_T$	3,53E-04	5,76E-04	nm	
4	Laboratory humidity effect	$u_{RH}$	5,25E+01	%RH	3,00E+01	U-shaped	$\sqrt{2}$	2,12E+01	%RH	$c_{RH}$	4,50E-06	9,55E-05	nm	
5	Laboratory air pressure effect	$u_{ap}$	8,68E+01	kPa	4,00E+00	Rectangular	$\sqrt{3}$	2,31E+00	kPa	$c_{ap}$	1,17E-03	2,71E-03	nm	
6	Wavelength calibration equation offset	$u_o$	2,87E+02	steps	2,87E+02	Normal	1	2,87E+02	steps	$c_o$	3,47E-04	9,95E-02	nm	
7	Wavelength reproducibility	$u_\lambda$	5,00E-03	nm	5,00E-03	Rectangular	$\sqrt{3}$	2,89E-03	nm	$c_\lambda$	1,00E+00	2,89E-03	nm	
8	Mechanical resolution of monochromator	$u_{Mres}$	5,00E-02	nm	2,50E-02	Rectangular	$\sqrt{3}$	1,44E-02	nm	$c_{Mres}$	1,00E+00	1,44E-02	nm	
9	Resolution used in calibration	$u_{Cres}$	2,00E-01	nm	1,00E-01	Rectangular	$\sqrt{3}$	5,77E-02	nm	$c_{Cres}$	1,00E+00	5,77E-02	nm	
10	Repeatability	$u_r$	8,37E+01	steps	8,37E+01	Normal	1	8,37E+01	steps	$c_r$	3,47E-04	2,91E-02	nm	
												$u_c(y)$	1,20E-01	nm
												$U(k=2)$	0,3	nm

## **Appendix H**

# **Uncertainty of measurement for the wavelength calibration in the wavelength region of 600 nm to 1 100 nm**

*Uncertainty of measurement for the wavelength calibration in the wavelength region of 600 nm to 1 100 nm*

Table H.1: Uncertainty of measurement calculated for the wavelength calibration in the wavelength region of 600 nm to 1 100 nm as described in Section 7.5.

No.	Input quantity	Symbol	Value		Estimated uncertainty $u_e(x_i)$	Probability distribution	Coverage factor $k$	Standard uncertainty $u(x_i)$	Sensitivity coefficient		Uncertainty contribution		
			$x_i$	unit					$c_i$	unit	$u_i(y)$	unit	
1	Theoretical value spectral line in vacuum	$u_{sl}$	696,735 912,547 966,044	nm	1,00E-04	Normal	1	1,00E-04	$c_{sl}$	1,00E+00	1,00E-04	nm	
2	Modified Edlén equation calculation	$u_{Ed}$	1,00023E+00	1	4,20E-08	Normal	2	2,10E-08	$c_{Ed}$	1,00E+00	2,10E-08	nm	
3	Laboratory temperature effect	$u_T$	2,44E+01	°C	4,00E+00	Triangular	$\sqrt{6}$	1,63E+00	$c_T$	6,81E-04	1,11E-03	nm	
4	Laboratory humidity effect	$u_{RH}$	4,21E+01	%RH	3,00E+01	U-shaped	$\sqrt{2}$	2,12E+01	$c_{RH}$	9,29E-06	1,97E-04	nm	
5	Laboratory air pressure effect	$u_{ap}$	8,65E+01	kPa	4,00E+00	Rectangular	$\sqrt{3}$	2,31E+00	$c_{ap}$	2,26E-03	5,21E-03	nm	
6	Steep-side method offset	$u_{ssmo}$	3,60E+01	steps	3,60E+01	Normal	1	3,60E+01	$c_{ssmo}$	6,94E-04	2,50E-02	nm	
7	Wavelength calibration equation offset	$u_o$	7,20E+01	steps	7,20E+01	Normal	1	7,20E+01	$c_o$	6,94E-04	5,00E-02	nm	
8	Wavelength reproducibility	$u_\lambda$	5,00E-03	nm	5,00E-03	Rectangular	$\sqrt{3}$	2,89E-03	$c_\lambda$	1,00E+00	2,89E-03	nm	
9	Mechanical resolution of monochromator	$u_{Mres}$	1,00E-01	nm	5,00E-02	Rectangular	$\sqrt{3}$	2,89E-02	$c_{Mres}$	1,00E+00	2,89E-02	nm	
10	Resolution used in calibration	$u_{Cres}$	1,00E-01	nm	5,00E-02	Rectangular	$\sqrt{3}$	2,89E-02	$c_{Cres}$	1,00E+00	2,89E-02	nm	
11	Repeatability	$u_r$	1,56E+01	steps	1,56E+01	Normal	1	1,56E+01	$c_r$	6,94E-04	1,08E-02	nm	
											$u_c(y)$	7,03E-02	nm
											$U (k=2)$	0,2	nm

## **Appendix I**

# **Uncertainty of measurement for the calibration of the PtSi photodiode detector against the UV-enhanced Si photodiode detector in the wavelength region of 200 nm to 400 nm**

Uncertainty of measurement for the calibration of the PtSi photodiode detector against the UV-enhanced Si photodiode detector in the wavelength region of 200 nm to 400 nm

Table I.1: Standard uncertainty contributions,  $u(x_i)$ , calculated for the PtSi photodiode detector calibration against the UV-enhanced Si photodiode detector in the wavelength region of 200 nm to 400 nm as described in Section 8.4.1.

Wavelength [nm]	Absolute spectral power responsivity of the standard detector $u_s$ [%]	Drift in the standard detector $u_{sd}$ [%]	Spatial uniformity of the standard detector $u_{ssu}$ [%]	Linearity of the standard detector $u_{slin}$ [%]	Temperature coefficient of the standard detector $u_{stempc}$ [%]	Temperature dependence of the standard detector $u_{stempd}$ [%]	Effect of the amplifier $u_a$ [%]	Effect of the multimeter on the standard detector's output signal $u_{mc}$ [%]	$u_{ma}$ [%]	$u_{sm}$ [%]
260	8,30E-01	4,78E-02	8,60E-02	2,00E-02	5,00E-02	2,00E-02	0,00E+00	5,77E-04	9,47E-06	5,77E-04
270	8,20E-01	4,89E-02	8,60E-02	2,00E-02	5,00E-02	2,00E-02	0,00E+00	3,49E-04	1,34E-05	3,50E-04
280	8,15E-01	5,13E-02	8,60E-02	2,00E-02	5,00E-02	2,00E-02	0,00E+00	2,36E-04	1,81E-05	2,37E-04
290	8,20E-01	5,57E-02	8,60E-02	2,00E-02	5,00E-02	2,00E-02	0,00E+00	1,62E-04	2,49E-05	1,64E-04
300	8,15E-01	6,29E-02	8,60E-02	2,00E-02	5,00E-02	2,00E-02	0,00E+00	1,18E-04	3,28E-05	1,23E-04
310	8,15E-01	7,37E-02	8,60E-02	2,00E-02	5,00E-02	2,00E-02	0,00E+00	9,59E-05	3,96E-05	1,04E-04
320	8,15E-01	8,94E-02	8,60E-02	2,00E-02	5,00E-02	2,00E-02	0,00E+00	8,33E-05	4,50E-05	9,47E-05
330	8,15E-01	1,11E-01	8,60E-02	2,00E-02	5,00E-02	2,00E-02	0,00E+00	7,46E-05	4,99E-05	8,97E-05
340	8,15E-01	1,37E-01	8,60E-02	2,00E-02	5,00E-02	2,00E-02	0,00E+00	6,80E-05	5,44E-05	8,71E-05
350	8,15E-01	1,65E-01	8,60E-02	2,00E-02	5,00E-02	2,00E-02	0,00E+00	4,27E-04	6,37E-05	4,32E-04
360	8,15E-01	1,83E-01	8,60E-02	2,00E-02	5,00E-02	2,00E-02	0,00E+00	4,19E-04	6,44E-05	4,24E-04
370	6,65E-01	1,83E-01	8,60E-02	2,00E-02	5,00E-02	2,00E-02	0,00E+00	4,05E-04	6,58E-05	4,11E-04
380	3,95E-01	1,64E-01	8,60E-02	2,00E-02	5,00E-02	2,00E-02	0,00E+00	3,66E-04	7,05E-05	3,72E-04
390	3,25E-01	1,36E-01	8,60E-02	2,00E-02	5,00E-02	2,00E-02	0,00E+00	3,32E-04	7,53E-05	3,40E-04
400	2,45E-01	1,09E-01	8,60E-02	2,00E-02	5,00E-02	2,00E-02	0,00E+00	3,03E-04	8,03E-05	3,13E-04



*Uncertainty of measurement for the calibration of the PtSi photodiode detector against the UV-enhanced Si photodiode detector in the wavelength region of 200 nm to 400 nm*

Table I.2: Continued: Standard uncertainty contributions,  $u(x_i)$ , calculated for the PtSi photodiode detector calibration against the UV-enhanced Si photodiode detector in the wavelength region of 200 nm to 400 nm as described in Section 8.4.1.

Wavelength [nm]	Inter-reflections between detector aperture and output of the monochromator										
	Effect of resolution of the multimeter on the output signal of the standard detector $u_{res}$ [%]	Source stability $u_{ss}$ [%]	Polarisation and non-uniform beam profile $u_{pnb}$ [%]	Beam divergence and vignetting $u_{bdv}$ [%]	Internal stray light $u_{isl}$ [%]	Effect of external stray light on the standard detector $u_{sesl}$ [%]	Spectral wavelength calibration $u_{\lambda}$ [%]	Repeatability of the standard detector $u_{sr}$ [%]	Bandwidth effects on the test detector $u_{tb}$ [%]		
260	5,45E-08	2,17E-01	4,10E-02	5,00E-03	1,53E-03	1,79E+00	1,71E-01	5,47E-01	5,20E-03		
270	3,33E-08	2,17E-01	4,10E-02	5,00E-03	1,53E-03	1,09E+00	5,76E-02	5,38E-01	8,66E-03		
280	2,26E-07	2,17E-01	4,10E-02	5,00E-03	1,53E-03	7,41E-01	2,36E-01	1,08E+00	8,08E-03		
290	1,55E-07	2,17E-01	4,10E-02	5,00E-03	1,53E-03	5,09E-01	2,91E-01	1,00E+00	1,21E-02		
300	1,13E-07	2,17E-01	4,10E-02	5,00E-03	1,53E-03	3,71E-01	1,60E-01	9,95E-01	1,15E-03		
310	9,20E-08	2,17E-01	4,10E-02	5,00E-03	1,53E-03	3,02E-01	5,66E-02	1,22E+00	5,77E-04		
320	8,00E-08	2,17E-01	4,10E-02	5,00E-03	1,53E-03	2,62E-01	3,12E-02	1,02E+00	5,77E-04		
330	7,16E-08	2,17E-01	4,10E-02	5,00E-03	1,53E-03	2,35E-01	3,52E-02	1,03E+00	5,77E-04		
340	6,53E-08	2,17E-01	4,10E-02	5,00E-03	1,53E-03	2,14E-01	3,73E-02	1,01E+00	1,15E-03		
350	6,15E-08	2,17E-01	4,10E-02	5,00E-03	1,53E-03	2,02E-01	1,62E-02	1,04E+00	2,89E-03		
360	6,04E-08	2,17E-01	4,10E-02	5,00E-03	1,53E-03	1,98E-01	9,04E-02	1,05E+00	7,51E-03		
370	5,84E-08	2,17E-01	4,10E-02	5,00E-03	1,53E-03	1,91E-01	4,66E-01	1,07E+00	7,51E-03		
380	5,27E-08	2,17E-01	4,10E-02	5,00E-03	1,53E-03	1,73E-01	5,29E-01	1,04E+00	2,31E-03		
390	4,78E-08	2,17E-01	4,10E-02	5,00E-03	1,53E-03	1,57E-01	3,21E-01	1,13E+00	1,15E-03		
400	4,36E-08	2,17E-01	4,10E-02	5,00E-03	1,53E-03	1,43E-01	2,22E-01	1,07E+00	5,77E-04		

*Uncertainty of measurement for the calibration of the PtSi photodiode detector against the UV-enhanced Si photodiode detector in the wavelength region of 200 nm to 400 nm*

Table I.3: Continued: Standard uncertainty contributions,  $u(x_i)$ , calculated for the PtSi photodiode detector calibration against the UV-enhanced Si photodiode detector in the wavelength region of 200 nm to 400 nm as described in Section 8.4.1.

Wavelength [nm]	Spatial uniformity of the test detector	Linearity of the test detector	Temperature coefficient of the test detector	Temperature dependence of the test detector	Effect of the multimeter on the test detector's output signal	Effect of resolution of the multimeter on the output signal of the test detector	Repeatability of the test detector
	$U_{Tsu}$ [%]	$U_{Tlin}$ [%]	$U_{Ttempc}$ [%]	$U_{Ttempd}$ [%]	$U_{Tmc}$ [%]	$U_{Tma}$ [%]	$U_{Tr}$ [%]
260	1,24E-01	2,00E-02	1,45E-01	8,08E-03	5,60E-04	3,59E-06	4,07E-01
270	1,24E-01	2,00E-02	1,36E-01	6,93E-03	3,39E-04	4,80E-06	3,58E-01
280	1,24E-01	2,00E-02	1,87E-01	1,10E-02	2,20E-04	6,45E-06	5,50E-01
290	1,24E-01	2,00E-02	2,21E-01	1,27E-02	1,39E-04	9,21E-06	3,56E-01
300	1,24E-01	2,00E-02	2,21E-01	1,21E-02	4,91E-04	1,05E-05	3,26E-01
310	1,24E-01	2,00E-02	1,87E-01	1,04E-02	3,96E-04	1,22E-05	4,26E-01
320	1,24E-01	2,00E-02	1,70E-01	9,24E-03	3,47E-04	1,35E-05	3,42E-01
330	1,24E-01	2,00E-02	1,53E-01	8,66E-03	3,11E-04	1,46E-05	3,74E-01
340	1,24E-01	2,00E-02	1,53E-01	8,66E-03	2,81E-04	1,58E-05	5,77E-01
350	1,24E-01	2,00E-02	1,36E-01	7,51E-03	2,61E-04	1,68E-05	5,22E-01
360	1,24E-01	2,00E-02	1,11E-01	5,77E-03	2,50E-04	1,73E-05	4,92E-01
370	1,24E-01	2,00E-02	2,55E-01	1,39E-02	2,08E-04	2,01E-05	6,34E-01
380	1,24E-01	2,00E-02	3,40E-01	1,85E-02	1,39E-04	2,83E-05	1,35E-07
390	1,24E-01	2,00E-02	2,55E-01	1,44E-02	1,03E-04	3,70E-05	6,80E-01
400	1,24E-01	2,00E-02	1,96E-01	1,10E-02	8,42E-05	4,46E-05	4,49E-01
							4,82E-01

*Uncertainty of measurement for the calibration of the PtSi photodiode detector against the UV-enhanced Si photodiode detector in the wavelength region of 200 nm to 400 nm*

---

Table I.4: Combined standard uncertainty,  $u_c(y)$ , and expanded uncertainty,  $U$ , calculated for the PtSi photodiode detector calibration against the UV-enhanced Si photodiode detector in the wavelength region of 200 nm to 400 nm.

Wavelength [nm]	Combined standard uncertainty $u_c(y)$ [%]	Expanded uncertainty ( $k=2$ ) $U$ [%]
260	2,1	4,3
270	1,5	3,1
280	1,7	3,4
290	1,5	3,1
300	1,4	2,9
310	1,6	3,2
320	1,4	2,9
330	1,4	2,9
340	1,5	3,0
350	1,5	3,0
360	1,5	3,0
370	1,6	3,2
380	1,5	3,0
390	1,4	2,8
400	1,3	2,6

## **Appendix J**

**Uncertainty of measurement for the calibration of the Si photodiode detector against UV-enhanced Si photodiode detector in the wavelength region of 600 nm to 1 100 nm**

*Uncertainty of measurement for the calibration of the Si photodiode detector against UV-enhanced Si photodiode detector in the wavelength region of 600 nm to 1 100 nm*

Table J.1: Standard uncertainty contributions,  $u(x_i)$ , calculated for the Si photodiode detector calibration against the UV-enhanced Si photodiode detector in the wavelength region of 600 nm to 1 100 nm as described in Section 8.4.1.

Wavelength [nm]	Absolute spectral power responsivity of the standard detector $U_s$ [%]	Drift in the standard detector $U_{sd}$ [%]	Spatial uniformity of the standard detector $U_{su}$ [%]	Linearity of the standard detector $U_{lin}$ [%]	Temperature coefficient of the standard detector $U_{tempc}$ [%]	Temperature dependence of the standard detector $U_{tempd}$ [%]	Effect of the amplifier $U_a$ [%]
600	1,60E-01	1,37E-02	1,00E-01	1,00E-01	1,00E-01	1,10E+00	2,00E-01
610	1,60E-01	1,25E-02	1,00E-01	1,00E-01	1,00E-01	1,10E+00	2,00E-01
620	1,60E-01	1,15E-02	1,00E-01	1,00E-01	1,00E-01	1,10E+00	2,00E-01
630	1,60E-01	1,05E-02	1,00E-01	1,00E-01	1,00E-01	1,10E+00	2,00E-01
640	1,60E-01	9,66E-03	1,00E-01	1,00E-01	1,00E-01	1,10E+00	2,00E-01
650	1,60E-01	8,91E-03	1,00E-01	1,00E-01	1,00E-01	1,10E+00	2,00E-01
660	1,60E-01	8,25E-03	1,00E-01	1,00E-01	1,00E-01	1,10E+00	2,00E-01
670	1,60E-01	7,66E-03	1,00E-01	1,00E-01	1,00E-01	1,10E+00	2,00E-01
680	1,60E-01	7,15E-03	1,00E-01	1,00E-01	1,00E-01	1,10E+00	2,00E-01
690	1,60E-01	6,71E-03	1,00E-01	1,00E-01	1,00E-01	1,10E+00	2,00E-01
700	1,60E-01	6,34E-03	1,00E-01	1,00E-01	1,00E-01	1,10E+00	2,00E-01
710	1,60E-01	6,03E-03	1,00E-01	1,00E-01	1,00E-01	1,10E+00	2,00E-01
720	1,60E-01	5,79E-03	1,00E-01	1,00E-01	1,00E-01	1,10E+00	2,00E-01
730	1,60E-01	5,57E-03	1,00E-01	1,00E-01	1,00E-01	1,10E+00	2,00E-01
740	1,60E-01	5,37E-03	1,00E-01	1,00E-01	1,00E-01	1,10E+00	2,00E-01
750	1,60E-01	5,19E-03	1,00E-01	1,00E-01	1,00E-01	1,10E+00	2,00E-01
760	1,60E-01	5,03E-03	1,00E-01	1,00E-01	1,00E-01	1,10E+00	2,00E-01
770	1,60E-01	4,88E-03	1,00E-01	1,00E-01	1,00E-01	1,10E+00	2,00E-01
780	1,60E-01	4,75E-03	1,00E-01	1,00E-01	1,00E-01	1,10E+00	2,00E-01
790	1,60E-01	4,62E-03	1,00E-01	1,00E-01	1,00E-01	1,10E+00	2,00E-01
800	1,60E-01	4,51E-03	1,00E-01	1,00E-01	1,00E-01	1,10E+00	2,00E-01
810	1,60E-01	4,41E-03	1,00E-01	1,00E-01	1,00E-01	1,10E+00	2,00E-01
820	1,60E-01	4,32E-03	1,00E-01	1,00E-01	1,00E-01	1,10E+00	2,00E-01
830	1,60E-01	4,23E-03	1,00E-01	1,00E-01	1,00E-01	1,10E+00	2,00E-01
840	1,60E-01	4,15E-03	1,00E-01	1,00E-01	1,00E-01	1,10E+00	2,00E-01
850	1,60E-01	4,08E-03	1,00E-01	1,00E-01	1,00E-01	1,10E+00	2,00E-01
860	1,60E-01	4,01E-03	1,00E-01	1,00E-01	1,00E-01	1,10E+00	2,00E-01
870	1,60E-01	3,95E-03	1,00E-01	1,00E-01	1,00E-01	1,10E+00	2,00E-01
880	1,60E-01	3,89E-03	1,00E-01	1,00E-01	1,00E-01	1,10E+00	2,00E-01
890	1,60E-01	3,84E-03	1,00E-01	1,00E-01	1,00E-01	1,10E+00	2,00E-01
900	1,60E-01	3,80E-03	1,00E-01	1,00E-01	1,00E-01	1,10E+00	2,00E-01
910	1,70E-01	3,75E-03	1,00E-01	1,00E-01	1,00E-01	1,10E+00	2,00E-01
920	2,00E-01	3,71E-03	1,00E-01	1,00E-01	1,00E-01	1,10E+00	2,00E-01
930	3,80E-01	3,67E-03	1,00E-01	1,00E-01	1,00E-01	1,10E+00	2,00E-01
940	3,80E-01	3,64E-03	1,00E-01	1,00E-01	1,00E-01	1,10E+00	2,00E-01
950	3,80E-01	3,61E-03	1,00E-01	1,00E-01	1,00E-01	1,10E+00	2,00E-01
960	3,75E-01	3,58E-03	1,00E-01	1,00E-01	1,00E-01	1,10E+00	2,00E-01
970	3,75E-01	3,55E-03	1,00E-01	1,00E-01	1,00E-01	1,10E+00	2,00E-01
980	3,80E-01	3,52E-03	1,00E-01	1,00E-01	1,00E-01	1,10E+00	2,00E-01
990	3,80E-01	3,50E-03	1,00E-01	1,00E-01	1,00E-01	1,10E+00	2,00E-01
1 000	3,80E-01	3,48E-03	1,00E-01	1,00E-01	1,00E-01	1,10E+00	2,00E-01
1 010	3,80E-01	3,46E-03	1,00E-01	1,00E-01	1,00E-01	1,10E+00	2,00E-01
1 020	3,80E-01	3,44E-03	1,00E-01	1,00E-01	1,00E-01	1,10E+00	2,00E-01
1 030	3,85E-01	3,42E-03	1,00E-01	1,00E-01	1,00E-01	1,10E+00	2,00E-01
1 040	3,85E-01	3,40E-03	1,00E-01	1,00E-01	1,00E-01	1,10E+00	2,00E-01
1 050	3,90E-01	3,39E-03	1,00E-01	1,00E-01	1,00E-01	1,10E+00	2,00E-01
1 060	3,95E-01	3,37E-03	1,00E-01	1,00E-01	1,00E-01	1,10E+00	2,00E-01
1 070	3,95E-01	3,36E-03	1,00E-01	1,00E-01	1,00E-01	1,10E+00	2,00E-01
1 080	3,95E-01	3,35E-03	1,00E-01	1,00E-01	1,00E-01	1,10E+00	2,00E-01
1 090	4,00E-01	3,34E-03	1,00E-01	1,00E-01	1,00E-01	1,10E+00	2,00E-01
1 100	4,05E-01	3,32E-03	1,00E-01	1,00E-01	1,00E-01	1,10E+00	2,00E-01

*Uncertainty of measurement for the calibration of the Si photodiode detector against UV-enhanced Si photodiode detector in the wavelength region of 600 nm to 1 100 nm*

Table J.2: Continued: Standard uncertainty contributions,  $u(x_i)$ , calculated for the Si photodiode detector calibration against the UV-enhanced Si photodiode detector in the wavelength region of 600 nm to 1 100 nm as described in Section 8.4.1.

Wavelength [nm]	Effect of the multimeter on the standard detector's output signal			Effect of resolution of the multimeter on the output signal of the standard detector	Source stability	Polarisation and non-uniform beam profile	Inter-reflections between detector and output aperture of the monochromator
	$u_{mc}$ [%]	$u_{ma}$ [%]	$u_{Sm}$ [%]	$u_{Sres}$ [%]	$u_{ss}$ [%]	$u_{pnb}$ [%]	$u_{reff}$ [%]
600	1,93E-04	2,14E-05	1,94E-04	1,85E-07	2,50E-01	1,00E-01	1,00E-02
610	1,76E-04	2,32E-05	1,77E-04	1,68E-07	2,50E-01	1,00E-01	1,00E-02
620	1,58E-04	2,54E-05	1,60E-04	1,51E-07	2,50E-01	1,00E-01	1,00E-02
630	1,42E-04	2,78E-05	1,45E-04	1,36E-07	2,50E-01	1,00E-01	1,00E-02
640	1,30E-04	3,01E-05	1,34E-04	1,25E-07	2,50E-01	1,00E-01	1,00E-02
650	1,21E-04	3,21E-05	1,25E-04	1,16E-07	2,50E-01	1,00E-01	1,00E-02
660	1,13E-04	3,41E-05	1,18E-04	1,09E-07	2,50E-01	1,00E-01	1,00E-02
670	1,08E-04	3,56E-05	1,13E-04	1,03E-07	2,50E-01	1,00E-01	1,00E-02
680	1,03E-04	3,72E-05	1,09E-04	9,84E-08	2,50E-01	1,00E-01	1,00E-02
690	9,88E-05	3,85E-05	1,06E-04	9,48E-08	2,50E-01	1,00E-01	1,00E-02
700	9,50E-05	3,99E-05	1,03E-04	9,12E-08	2,50E-01	1,00E-01	1,00E-02
710	9,34E-05	4,05E-05	1,02E-04	8,97E-08	2,50E-01	1,00E-01	1,00E-02
720	9,28E-05	4,08E-05	1,01E-04	8,90E-08	2,50E-01	1,00E-01	1,00E-02
730	9,28E-05	4,08E-05	1,01E-04	8,90E-08	2,50E-01	1,00E-01	1,00E-02
740	9,26E-05	4,09E-05	1,01E-04	8,89E-08	2,50E-01	1,00E-01	1,00E-02
750	9,43E-05	4,02E-05	1,03E-04	9,05E-08	2,50E-01	1,00E-01	1,00E-02
760	9,63E-05	3,94E-05	1,04E-04	9,24E-08	2,50E-01	1,00E-01	1,00E-02
770	9,99E-05	3,82E-05	1,07E-04	9,58E-08	2,50E-01	1,00E-01	1,00E-02
780	1,02E-04	3,73E-05	1,09E-04	9,83E-08	2,50E-01	1,00E-01	1,00E-02
790	1,05E-04	3,63E-05	1,11E-04	1,01E-07	2,50E-01	1,00E-01	1,00E-02
800	1,09E-04	3,52E-05	1,15E-04	1,05E-07	2,50E-01	1,00E-01	1,00E-02
810	1,11E-04	3,45E-05	1,17E-04	1,07E-07	2,50E-01	1,00E-01	1,00E-02
820	1,13E-04	3,42E-05	1,18E-04	1,08E-07	2,50E-01	1,00E-01	1,00E-02
830	1,12E-04	3,45E-05	1,17E-04	1,07E-07	2,50E-01	1,00E-01	1,00E-02
840	1,08E-04	3,55E-05	1,14E-04	1,04E-07	2,50E-01	1,00E-01	1,00E-02
850	1,00E-04	3,81E-05	1,07E-04	9,60E-08	2,50E-01	1,00E-01	1,00E-02
860	8,97E-05	4,21E-05	9,91E-05	8,61E-08	2,50E-01	1,00E-01	1,00E-02
870	8,07E-05	4,64E-05	9,31E-05	7,74E-08	2,50E-01	1,00E-01	1,00E-02
880	7,19E-05	5,16E-05	8,85E-05	6,90E-08	2,50E-01	1,00E-01	1,00E-02
890	6,45E-05	5,72E-05	8,62E-05	6,19E-08	2,50E-01	1,00E-01	1,00E-02
900	3,88E-04	9,42E-05	3,99E-04	5,59E-08	2,50E-01	1,00E-01	1,00E-02
910	3,52E-04	1,00E-04	3,66E-04	5,07E-08	2,50E-01	1,00E-01	1,00E-02
920	3,23E-04	1,06E-04	3,40E-04	4,66E-08	2,50E-01	1,00E-01	1,00E-02
930	3,04E-04	1,11E-04	3,24E-04	4,39E-08	2,50E-01	1,00E-01	1,00E-02
940	2,88E-04	1,15E-04	3,10E-04	4,15E-08	2,50E-01	1,00E-01	1,00E-02
950	2,73E-04	1,19E-04	2,98E-04	3,94E-08	2,50E-01	1,00E-01	1,00E-02
960	2,57E-04	1,25E-04	2,85E-04	3,70E-08	2,50E-01	1,00E-01	1,00E-02
970	2,47E-04	1,28E-04	2,78E-04	3,56E-08	2,50E-01	1,00E-01	1,00E-02
980	2,42E-04	1,30E-04	2,75E-04	3,49E-08	2,50E-01	1,00E-01	1,00E-02
990	2,41E-04	1,30E-04	2,74E-04	3,48E-08	2,50E-01	1,00E-01	1,00E-02
1 000	2,45E-04	1,29E-04	2,77E-04	3,54E-08	2,50E-01	1,00E-01	1,00E-02
1 010	2,45E-04	1,29E-04	2,77E-04	3,53E-08	2,50E-01	1,00E-01	1,00E-02
1 020	2,58E-04	1,24E-04	2,86E-04	3,72E-08	2,50E-01	1,00E-01	1,00E-02
1 030	2,78E-04	1,18E-04	3,02E-04	4,01E-08	2,50E-01	1,00E-01	1,00E-02
1 040	3,11E-04	1,09E-04	3,29E-04	4,48E-08	2,50E-01	1,00E-01	1,00E-02
1 050	3,59E-04	9,90E-05	3,72E-04	5,17E-08	2,50E-01	1,00E-01	1,00E-02
1 060	6,48E-05	5,69E-05	8,63E-05	6,22E-08	2,50E-01	1,00E-01	1,00E-02
1 070	7,87E-05	4,75E-05	9,19E-05	7,55E-08	2,50E-01	1,00E-01	1,00E-02
1 080	9,43E-05	4,02E-05	1,03E-04	9,05E-08	2,50E-01	1,00E-01	1,00E-02
1 090	1,15E-04	3,36E-05	1,20E-04	1,10E-07	2,50E-01	1,00E-01	1,00E-02
1 100	1,43E-04	2,77E-05	1,46E-04	1,37E-07	2,50E-01	1,00E-01	1,00E-02

*Uncertainty of measurement for the calibration of the Si photodiode detector against UV-enhanced Si photodiode detector in the wavelength region of 600 nm to 1 100 nm*

Table J.3: Continued: Standard uncertainty contributions,  $u(x_i)$ , calculated for the Si photodiode detector calibration against the UV-enhanced Si photodiode detector in the wavelength region of 600 nm to 1 100 nm as described in Section 8.4.1.

Wavelength [nm]	Beam divergence and vignetting	Internal stray light	Effect of external stray light on standard detector	Spectral wavelength calibration	Repeatability of the standard detector	Bandwidth effects on the test detector	Spatial uniformity of the test detector	Linearity of the test detector
	$u_{bdv}$ [%]	$u_{isl}$ [%]	$u_{sesl}$ [%]	$u_{\lambda}$ [%]	$u_{sr}$ [%]	$u_{tb}$ [%]	$u_{tsu}$ [%]	$u_{lin}$ [%]
600	0,00E+00	1,50E-03	6,09E-01	9,55E-03	5,44E-01	2,00E-02	1,00E-01	1,00E-01
610	0,00E+00	1,50E-03	5,55E-01	1,22E-02	1,08E-01	2,00E-02	1,00E-01	1,00E-01
620	0,00E+00	1,50E-03	4,97E-01	1,25E-02	4,42E-01	2,00E-02	1,00E-01	1,00E-01
630	0,00E+00	1,50E-03	4,49E-01	3,32E-02	1,05E-01	2,00E-02	1,00E-01	1,00E-01
640	0,00E+00	1,50E-03	4,11E-01	2,85E-02	1,04E-01	2,00E-02	1,00E-01	1,00E-01
650	0,00E+00	1,50E-03	3,82E-01	1,85E-02	1,02E-01	2,00E-02	1,00E-01	1,00E-01
660	0,00E+00	1,50E-03	3,57E-01	1,64E-02	1,13E-01	2,00E-02	1,00E-01	1,00E-01
670	0,00E+00	1,50E-03	3,40E-01	1,11E-02	9,83E-02	2,00E-02	1,00E-01	1,00E-01
680	0,00E+00	1,50E-03	3,24E-01	2,35E-02	9,98E-02	2,00E-02	1,00E-01	1,00E-01
690	0,00E+00	1,50E-03	3,12E-01	1,71E-02	9,28E-02	2,00E-02	1,00E-01	1,00E-01
700	0,00E+00	1,50E-03	3,01E-01	1,27E-02	9,41E-02	2,00E-02	1,00E-01	1,00E-01
710	0,00E+00	1,50E-03	2,95E-01	1,03E-02	8,92E-02	2,00E-02	1,00E-01	1,00E-01
720	0,00E+00	1,50E-03	2,93E-01	1,41E-02	8,73E-02	2,00E-02	1,00E-01	1,00E-01
730	0,00E+00	1,50E-03	2,93E-01	2,65E-02	3,93E-01	2,00E-02	1,00E-01	1,00E-01
740	0,00E+00	1,50E-03	2,93E-01	1,04E-02	9,17E-02	2,00E-02	1,00E-01	1,00E-01
750	0,00E+00	1,50E-03	2,98E-01	8,87E-03	4,24E-01	2,00E-02	1,00E-01	1,00E-01
760	0,00E+00	1,50E-03	3,04E-01	2,54E-02	8,60E-02	2,00E-02	1,00E-01	1,00E-01
770	0,00E+00	1,50E-03	3,15E-01	2,16E-02	1,00E-01	2,00E-02	1,00E-01	1,00E-01
780	0,00E+00	1,50E-03	3,23E-01	1,16E-02	9,20E-02	2,00E-02	1,00E-01	1,00E-01
790	0,00E+00	1,50E-03	3,33E-01	1,40E-02	2,49E-01	2,00E-02	1,00E-01	1,00E-01
800	0,00E+00	1,50E-03	3,47E-01	2,25E-02	5,75E-01	2,00E-02	1,00E-01	1,00E-01
810	0,00E+00	1,50E-03	3,53E-01	1,13E-02	1,20E+00	2,00E-02	1,00E-01	1,00E-01
820	0,00E+00	1,50E-03	3,56E-01	1,95E-02	1,20E+00	2,00E-02	1,00E-01	1,00E-01
830	0,00E+00	1,50E-03	3,53E-01	9,11E-03	1,12E+00	2,00E-02	1,00E-01	1,00E-01
840	0,00E+00	1,50E-03	3,42E-01	1,21E-02	1,23E+00	2,00E-02	1,00E-01	1,00E-01
850	0,00E+00	1,50E-03	3,16E-01	1,34E-02	1,27E+00	2,00E-02	1,00E-01	1,00E-01
860	0,00E+00	1,50E-03	2,84E-01	1,61E-02	1,22E+00	2,00E-02	1,00E-01	1,00E-01
870	0,00E+00	1,50E-03	2,55E-01	7,18E-03	1,21E+00	2,00E-02	1,00E-01	1,00E-01
880	0,00E+00	1,50E-03	2,27E-01	1,44E-02	1,19E+00	2,00E-02	1,00E-01	1,00E-01
890	0,00E+00	1,50E-03	2,04E-01	1,65E-02	1,12E+00	2,00E-02	1,00E-01	1,00E-01
900	0,00E+00	1,50E-03	1,86E-01	1,63E-02	1,19E+00	2,00E-02	1,00E-01	1,00E-01
910	0,00E+00	1,50E-03	1,68E-01	1,01E-02	1,21E+00	2,00E-02	1,00E-01	1,00E-01
920	0,00E+00	1,50E-03	1,54E-01	1,59E-02	1,18E+00	2,00E-02	1,00E-01	1,00E-01
930	0,00E+00	1,50E-03	1,45E-01	8,58E-03	9,28E-01	2,00E-02	1,00E-01	1,00E-01
940	0,00E+00	1,50E-03	1,37E-01	5,16E-03	1,17E+00	2,00E-02	1,00E-01	1,00E-01
950	0,00E+00	1,50E-03	1,30E-01	5,82E-03	1,21E+00	2,00E-02	1,00E-01	1,00E-01
960	0,00E+00	1,50E-03	1,22E-01	4,60E-03	1,17E+00	2,00E-02	1,00E-01	1,00E-01
970	0,00E+00	1,50E-03	1,18E-01	4,64E-03	1,14E+00	2,00E-02	1,00E-01	1,00E-01
980	0,00E+00	1,50E-03	1,15E-01	4,50E-03	1,01E+00	2,00E-02	1,00E-01	1,00E-01
990	0,00E+00	1,50E-03	1,15E-01	1,01E-02	1,07E+00	2,00E-02	1,00E-01	1,00E-01
1 000	0,00E+00	1,50E-03	1,17E-01	1,49E-02	1,05E+00	2,00E-02	1,00E-01	1,00E-01
1 010	0,00E+00	1,50E-03	1,17E-01	4,42E-02	1,07E+00	2,00E-02	1,00E-01	1,00E-01
1 020	0,00E+00	1,50E-03	1,23E-01	7,33E-02	1,08E+00	2,00E-02	1,00E-01	1,00E-01
1 030	0,00E+00	1,50E-03	1,33E-01	1,10E-01	1,06E+00	2,00E-02	1,00E-01	1,00E-01
1 040	0,00E+00	1,50E-03	1,48E-01	1,45E-01	1,01E+00	2,00E-02	1,00E-01	1,00E-01
1 050	0,00E+00	1,50E-03	1,71E-01	1,86E-01	1,02E+00	2,00E-02	1,00E-01	1,00E-01
1 060	0,00E+00	1,50E-03	2,05E-01	2,19E-01	1,00E+00	2,00E-02	1,00E-01	1,00E-01
1 070	0,00E+00	1,50E-03	2,49E-01	1,95E-01	9,87E-01	2,00E-02	1,00E-01	1,00E-01
1 080	0,00E+00	1,50E-03	2,98E-01	1,93E-01	9,82E-01	2,00E-02	1,00E-01	1,00E-01
1 090	0,00E+00	1,50E-03	3,63E-01	1,99E-01	9,72E-01	2,00E-02	1,00E-01	1,00E-01
1 100	0,00E+00	1,50E-03	4,51E-01	2,31E-01	9,62E-01	2,00E-02	1,00E-01	1,00E-01

*Uncertainty of measurement for the calibration of the Si photodiode detector against UV-enhanced Si photodiode detector in the wavelength region of 600 nm to 1 100 nm*

Table J.4: Continued: Standard uncertainty contributions,  $u(x_i)$ , calculated for the Si photodiode detector calibration against the UV-enhanced Si photodiode detector in the wavelength region of 600 nm to 1 100 nm as described in Section 8.4.1.

Wavelength [nm]	Temperature dependence of the test detector	Effect of the multimeter on the test detector's output signal			Effect of resolution of the multimeter on the output signal of the test detector	Effect of external stray light on test detector	Repeatability of the test detector
	$u_{Tempd}$ [%]	$u_{Tmc}$ [%]	$u_{Tma}$ [%]	$u_{Tm}$ [%]	$u_{Tres}$ [%]	$u_{Tesl}$ [%]	$u_{Tr}$ [%]
600	1,10E+00	1,81E-04	2,26E-05	1,82E-04	1,75E-07	5,75E-01	5,67E-01
610	1,10E+00	1,66E-04	2,43E-05	1,68E-04	1,61E-07	5,28E-01	9,97E-01
620	1,10E+00	1,51E-04	2,65E-05	1,53E-04	1,46E-07	4,79E-01	1,05E-01
630	1,10E+00	1,35E-04	2,91E-05	1,38E-04	1,31E-07	4,29E-01	1,09E-01
640	1,10E+00	1,21E-04	3,20E-05	1,26E-04	1,17E-07	3,86E-01	1,16E-01
650	1,10E+00	1,13E-04	3,42E-05	1,18E-04	1,09E-07	3,58E-01	1,88E-01
660	1,10E+00	1,05E-04	3,65E-05	1,11E-04	1,01E-07	3,33E-01	1,60E-01
670	1,10E+00	1,00E-04	3,81E-05	1,07E-04	9,66E-08	3,18E-01	1,96E-01
680	1,10E+00	9,53E-05	3,98E-05	1,03E-04	9,20E-08	3,03E-01	2,68E-01
690	1,10E+00	9,16E-05	4,13E-05	1,00E-04	8,84E-08	2,91E-01	8,79E-02
700	1,10E+00	9,06E-05	4,17E-05	9,97E-05	8,74E-08	2,87E-01	3,70E-01
710	1,10E+00	8,87E-05	4,25E-05	9,83E-05	8,55E-08	2,81E-01	6,15E-01
720	1,10E+00	8,93E-05	4,23E-05	9,88E-05	8,62E-08	2,83E-01	1,13E-01
730	1,10E+00	8,79E-05	4,29E-05	9,78E-05	8,48E-08	2,79E-01	2,42E-01
740	1,10E+00	8,80E-05	4,28E-05	9,79E-05	8,49E-08	2,79E-01	2,14E-01
750	1,10E+00	9,03E-05	4,18E-05	9,96E-05	8,72E-08	2,87E-01	9,25E-03
760	1,10E+00	9,20E-05	4,11E-05	1,01E-04	8,88E-08	2,92E-01	4,19E-01
770	1,10E+00	9,41E-05	4,03E-05	1,02E-04	9,08E-08	2,99E-01	8,83E-02
780	1,10E+00	9,68E-05	3,92E-05	1,04E-04	9,35E-08	3,08E-01	9,58E-02
790	1,10E+00	1,00E-04	3,79E-05	1,07E-04	9,70E-08	3,19E-01	3,43E-01
800	1,10E+00	1,03E-04	3,70E-05	1,10E-04	9,97E-08	3,25E-01	9,48E-01
810	1,10E+00	1,05E-04	3,65E-05	1,11E-04	1,01E-07	3,32E-01	7,07E-01
820	1,10E+00	1,06E-04	3,61E-05	1,12E-04	1,02E-07	3,35E-01	7,40E-01
830	1,10E+00	1,04E-04	3,66E-05	1,11E-04	1,01E-07	3,31E-01	6,91E-01
840	1,10E+00	1,02E-04	3,74E-05	1,09E-04	9,85E-08	3,23E-01	1,91E-01
850	1,10E+00	9,36E-05	4,05E-05	1,02E-04	9,04E-08	2,97E-01	8,02E-01
860	1,10E+00	8,49E-05	4,42E-05	9,58E-05	8,19E-08	2,69E-01	7,12E-01
870	1,10E+00	7,72E-05	4,83E-05	9,11E-05	7,45E-08	2,45E-01	7,22E-01
880	1,10E+00	6,88E-05	5,38E-05	8,73E-05	6,64E-08	2,18E-01	6,85E-01
890	1,10E+00	6,15E-05	5,98E-05	8,58E-05	5,93E-08	1,95E-01	7,05E-01
900	1,10E+00	3,68E-04	9,74E-05	3,80E-04	5,32E-08	1,72E-01	7,59E-01
910	1,10E+00	3,33E-04	1,04E-04	3,49E-04	4,81E-08	1,56E-01	1,20E+00
920	1,10E+00	3,06E-04	1,10E-04	3,25E-04	4,42E-08	1,44E-01	1,19E+00
930	1,10E+00	2,86E-04	1,15E-04	3,09E-04	4,14E-08	1,35E-01	1,18E+00
940	1,10E+00	2,73E-04	1,19E-04	2,98E-04	3,95E-08	1,29E-01	1,17E+00
950	1,10E+00	2,59E-04	1,24E-04	2,87E-04	3,74E-08	1,22E-01	1,17E+00
960	1,10E+00	2,45E-04	1,29E-04	2,77E-04	3,54E-08	1,16E-01	1,16E+00
970	1,10E+00	2,35E-04	1,33E-04	2,70E-04	3,40E-08	1,11E-01	1,14E+00
980	1,10E+00	2,30E-04	1,35E-04	2,67E-04	3,32E-08	1,09E-01	1,14E+00
990	1,10E+00	2,27E-04	1,36E-04	2,65E-04	3,28E-08	1,08E-01	1,12E+00
1 000	1,10E+00	2,28E-04	1,36E-04	2,66E-04	3,30E-08	1,08E-01	1,11E+00
1 010	1,10E+00	2,25E-04	1,37E-04	2,64E-04	3,26E-08	1,07E-01	5,05E-01
1 020	1,10E+00	2,39E-04	1,31E-04	2,72E-04	3,45E-08	1,13E-01	1,06E+00
1 030	1,10E+00	2,59E-04	1,24E-04	2,87E-04	3,75E-08	1,23E-01	1,06E+00
1 040	1,10E+00	2,95E-04	1,13E-04	3,16E-04	4,27E-08	1,40E-01	1,13E+00
1 050	1,10E+00	3,46E-04	1,01E-04	3,61E-04	5,01E-08	1,64E-01	1,02E+00
1 060	1,10E+00	6,42E-05	5,74E-05	8,61E-05	6,19E-08	2,03E-01	9,83E-01
1 070	1,10E+00	8,00E-05	4,68E-05	9,27E-05	7,72E-08	2,54E-01	8,75E-01
1 080	1,10E+00	9,80E-05	3,88E-05	1,05E-04	9,46E-08	3,11E-01	9,96E-01
1 090	1,10E+00	1,20E-04	3,22E-05	1,25E-04	1,16E-07	3,82E-01	1,11E+00
1 100	1,10E+00	1,51E-04	2,64E-05	1,53E-04	1,46E-07	4,80E-01	9,64E-01



*Uncertainty of measurement for the calibration of the Si photodiode detector against UV-enhanced Si photodiode detector in the wavelength region of 600 nm to 1 100 nm*

---

Table J.5: Combined standard uncertainty,  $u_c(y)$ , and expanded uncertainty,  $U$ , calculated for the Si photodiode detector calibration against the UV-enhanced Si photodiode detector in the wavelength region of 600 nm to 1 100 nm.

Wavelength [nm]	Combined standard uncertainty $u_c(y)$ [%]	Expanded uncertainty (k = 2) $U$ [%]
600	1,2	2,5
610	1,3	2,7
620	0,93	1,9
630	0,77	1,6
640	0,73	1,5
650	0,71	1,5
660	0,68	1,4
670	0,67	1,4
680	0,68	1,4
690	0,62	1,3
700	0,71	1,5
710	0,86	1,8
720	0,61	1,3
730	0,75	1,6
740	0,64	1,3
750	0,73	1,5
760	0,74	1,5
770	0,63	1,3
780	0,64	1,3
790	0,76	1,6
800	1,3	2,6
810	1,5	3,1
820	1,6	3,2
830	1,5	3,0
840	1,4	2,9
850	1,6	3,3
860	1,5	3,1
870	1,5	3,1
880	1,5	3,0
890	1,4	2,9
900	1,5	3,1
910	1,8	3,6
920	1,8	3,6
930	1,6	3,3
940	1,8	3,6
950	1,8	3,6
960	1,8	3,6
970	1,7	3,5
980	1,6	3,3
990	1,7	3,4
1 000	1,6	3,3
1 010	1,3	2,7
1 020	1,6	3,3
1 030	1,6	3,3
1 040	1,6	3,3
1 050	1,6	3,2
1 060	1,6	3,2
1 070	1,5	3,0
1 080	1,6	3,2
1 090	1,7	3,4
1 100	1,6	3,3

## **Appendix K**

**Uncertainty of measurement for the calibration of the Si photodiode detector against the pyroelectric detector and Si-trap detector in the wavelength region of 600 nm to 1 100 nm**

*Uncertainty of measurement for the calibration of the Si photodiode detector against the pyroelectric detector and Si-trap detector in the wavelength region of 600 nm to 1 100 nm*

Table K.1: Uncertainty of measurement calculated for the Si photodiode detector calibration against the pyroelectric detector and Si-trap detector, as described in Section 8.4.2.

Calibration	No.	Input quantity $X_i$	Symbol	Estimated uncertainty		Probability distribution	Coverage factor $k$	Standard uncertainty		Sensitivity coefficient $c_i$	Uncertainty contribution	
				$u_e(x_i)$	unit			$u(x_i)$	unit		$u_i(y)$	unit
Absolute	1	Absolute spectral power responsivity of the standard detector	$u_s$	4,40E-01	%	Normal	2	2,20E-01	%	1,00E+00	2,20E-01	%
Absolute	2	Drift in the standard detector	$u_{sd}$	3,35E-02	%	Normal	1	3,35E-02	%	1,00E+00	3,35E-02	%
Absolute	3	Spatial uniformity of the standard detector	$u_{ssu}$	2,00E-02	%	Normal	1	2,00E-02	%	1,00E+00	2,00E-02	%
Absolute	4	Linearity of the standard detector	$u_{sin}$	1,00E-01	%	Normal	2	5,00E-02	%	1,00E+00	5,00E-02	%
Absolute	5	Effect of the amplifier	$u_a$	2,00E-01	%	Normal	2	1,00E-01	%	1,00E+00	1,00E-01	%
Absolute	6	Effect of the multimeter on the detectors' output signal	$u_{absM}$	2,00E-03	%	Normal	2	1,00E-03	%	1,00E+00	1,00E-03	%
Absolute	7	Source stability	$u_{absSS}$	1,00E-01	%	Normal	2	5,00E-02	%	1,00E+00	5,00E-02	%
Absolute	8	Stray light and standard detector noise	$u_{ssl}$	1,53E-01	%	Normal	1	1,53E-01	%	1,00E+00	1,53E-01	%
Absolute	9	Repeatability of the standard detector	$u_{sr}$	5,19E-03	%	Normal	1	5,19E-03	%	1,00E+00	5,19E-03	%
Absolute	10	Spatial uniformity of the test detector	$u_{tsu}$	1,00E-01	%	Normal	1	1,00E-01	%	1,00E+00	1,00E-01	%
Absolute	11	Temperature dependence	$u_{temp}$	1,00E-02	%	Normal	1	1,00E-02	%	1,00E+00	1,00E-02	%
Absolute	12	Repeatability of the test detector	$u_{tr}$	6,92E-03	%	Normal	1	6,92E-03	%	1,00E+00	6,92E-03	%
Spectral	13	Pyroelectric detector absorbance	$u_{pa}$	1,61E+00	%	Rectangular	$\sqrt{3}$	9,29E-01	%	1,00E+00	9,29E-01	%
Spectral	14	Effect of the multimeter on the detectors' output signal	$u_{specM}$	2,00E-03	%	Normal	2	1,00E-03	%	1,00E+00	1,00E-03	%
Spectral	15	Source stability	$u_{specSS}$	2,50E-01	%	Normal	2	1,25E-01	%	1,00E+00	1,25E-01	%
Spectral	16	Polarisation, diffraction, interference and angular effects	$u_{pdia}$	1,00E-01	%	Normal	1	1,00E-01	%	1,00E+00	1,00E-01	%
Spectral	17	Spectral wavelength calibration	$u_\lambda$	2,58E-01	%	Normal	2	1,29E-01	%	1,00E+00	1,29E-01	%
Spectral	18	Linearity of the test detector	$u_{Tlin}$	1,00E-01	%	Rectangular	$\sqrt{3}$	5,77E-02	%	1,00E+00	5,77E-02	%
Spectral	19	Stray light and test detector noise	$u_{Tsl}$	2,18E-01	%	Normal	1	2,18E-01	%	1,00E+00	2,18E-01	%
Spectral	20	Repeatability of the test detector	$u_{specTr}$	5,53E-01	%	Normal	1	5,53E-01	%	1,00E+00	5,53E-01	%
										$u_c(y)$	1,33E+00	%
										$U (k=2)$	2,7	%

## References

- Agilent. 2007 (February). *Agilent 34410a/11a 6 ½ digit multimeter service guide*. Fourth edn. Agilent Technologies, Inc., Agilent Technologies, Inc. 3501 Stevens Creek Blvd. Santa Clara, CA 95052 USA.
- BIPM. 2001 (February). *CCPR Key Comparison K2.b Spectral Responsivity 300 nm to 1 000 nm Technical Protocol*. Tech. rept. Bureau International des Poids et Mesures (BIPM).
- BIPM. 2019. *The International System of Units (SI)*.
- Botha, P.J. 2003 (June). *Calibration certificate of silicon photodiode for spectral response*. Tech. rept. OR\RA-2899. NMISA.
- CIE. 2021. *CIE S 017:2020 ILV: International Lighting Vocabulary*. [Online] Available at: <http://cie.co.at/e-ilv> [Accessed: 2021-04-16].
- Davis, A. 2000 (05). *Stray light in czerny turner monochromators*. Ph.D. thesis.
- DTI, Department of Trade & Industry. 2018. Measurement Units and Measurement Standards Act (18/2006). *Government Gazette of Republic of South Africa*, Vol. 640 (Number 41982), p. 216 – p. 223.
- Energetiq. 2011 (August). *Model eq-99 Idls™ laser-driven light source operation and maintenance manual*. Fourth edn. Energetiq Technology Inc., Energetiq Technology Inc. 7 Constitution Way, Woburn, MA 01801 USA.
- Gardner, J., Goodman, T., Kaplan, S., Ohno, Y., Palmer, J., Saito, T., Sauter, G., Sperling, A., Winter, S., & Zong, Y. 2011. *CIE 202:2011 Spectral Responsivity Measurement of Detectors, Radiometers and Photometers*. Tech. rept. International Commission on Illumination (CIE).
- Gardner, J., Woolliams, E., Baribeau, R., Bialek, A., Carter, E., Cox, M., Goodman, T., Krueger, U., Li, C., Nevas, S., Ohno, Y., Saito, T., Young, R., Zong, Y.,

- & Zwinkels, J. 2014. *CIE 214:2014 The Effect of Instrumental Bandpass Function and Measurement Interval on Spectral Quantities*. Tech. rept. International Commission on Illumination (CIE).
- Goebel, R, & Stock, M. 2004a. Report on the comparison CCPR-k2.b of spectral responsivity measurements in the range 300 nm to 1000 nm. *Metrologia*, **41**(1A), 02004–02004.
- Goebel, R, & Stock, M. 2004b (October). *Report on the key comparison CCPR-K2.b of spectral responsivity measurements in the wavelength range 300 nm to 1 000 nm*. Tech. rept. Bureau International des Poids et Mesures (BIPM).
- Gooch and Housego. 2013 (August). *Application Note (A11). Slit and Aperture Selection in Spectroradiometry. Revision C*. Tech. rept. Gooch & Housego. [Online] Available at: [https://gandh.com/wp-content/uploads/2014/01/A11\\_SLIT-AND-APERTURE-SELECTION-IN-SPECTRORADIOMETRY\\_8-13\\_GH.pdf](https://gandh.com/wp-content/uploads/2014/01/A11_SLIT-AND-APERTURE-SELECTION-IN-SPECTRORADIOMETRY_8-13_GH.pdf).
- Hamamatsu. 2015. *Si photodiodes*. Hamamatsu.
- Hengstberger, F. *et al.* 1984. *CIE 64:1984 Determination of the spectral responsivity of optical radiation detectors*. Tech. rept. International Commission on Illumination (CIE).
- Ientillucci, E.J. 2006 (December). *Diffraction Grating Equation with Example Problems*. Tech. rept. Digital Imaging and Remote Sensing Laboratory, Rochester Institute of Technology.
- ISO/CASCO, Committee on conformity assessment. 2010 (February). *ISO/IEC 17043 Conformity assessment — General requirements for proficiency testing*. Tech. rept. International Organization for Standardization.
- ISO/IEC. 2017. *ISO/IEC 17025: 2017. general requirements for the competence of testing and calibration laboratories*. BSI. OCLC: 1043856471.
- JCGM. 2008. *JCGM 100:2008 Evaluation of measurement data — Guide to the expression of uncertainty in measurement*. 1st edn. JCGM member organizations (BIPM, IEC, IFCC, ILAC, ISO, IUPAC, IUPAP and OIML).
- JCGM. 2012. *JCGM 200:2012 International vocabulary of metrology – Basic and general concepts and associated terms (VIM)*. 3rd edn. JCGM member organizations (BIPM, IEC, IFCC, ILAC, ISO, IUPAC, IUPAP and OIML).

- Kostkowski, H.J. 1997. *Reliable Spectroradiometry*. Spectroradiometry Consulting.
- Kruger, I., & Sieberhagen, R.H. 2015. Measuring the spectral irradiance of a high-powered focused light source. *Pages 1408–1417 of: 28th International Commission on Illumination Session*. Manchester, United Kingdom, no. CIE 216:2015. 28 June - 4 July.
- Larason, T., & Houston, J. 2008. *Spectroradiometric Detector Measurements: Ultraviolet, Visible, and Near Infrared Detectors for Spectral Power*. Special Publication (NIST SP 250-41), National Institute of Standards and Technology, Gaithersburg, MD.
- Lee, D, Park, S, Park, C, Shin, D, Kim, S, & Park, S. 2006 (October). Realization of the spectral responsivity scale in KRISS. *In: Simposio de Metrología 2006*.
- Lei, Fu, & Fischer, J. 1993. Characterization of photodiodes in the UV and visible spectral region based on cryogenic radiometry. *Metrologia*, **30**(4), 297–303.
- Lerner, J.M., & Thevenon, A. 1996. *The Optics of Spectroscopy. A Tutorial*. Tech. rept. HORIBA Scientific.
- Littler, I., Atkinson, E., & Manson, P. 2014. Predicting wavelength dependent responsivity-drift in silicon. *Chap. Detector-based Radiometry; Scale Realisation, page 167 of: Seongchong Park, KRISS, Petri Kärhä, Aalto University, & Erkki Ikonen, Aalto University/MIKES (eds), Proceedings of NEWRAD 2014 conference in Espoo, Finland*.
- McPherson. 2015 (November). *Model 2035 Scanning Monochromator Instruction Manual*. McPherson, 7A Stuart Road, Chelmsford, MA 01824.
- McPherson. 2017. *Diffraction grating datasheet*. McPherson. Diffraction Grating with 600g/mm blazed at 800 nm datasheet.
- Neumann, W. 2014. Optical spectroscopy with dispersive spectrometers basics - building blocks - systems - applications. *In: Fundamentals of dispersive optical spectroscopy systems*, vol. PM242. SPIE.
- Newport. 2021a. *Digital light intensity controller*. [Online] Available at: <https://www.newport.com/f/digital-light-intensity-controller> [Accessed: 2021-02-06].
- Newport. 2021b. *Information on spectral irradiance data*. [Online] Available at: <https://www.newport.com/n/>

- [information-on-spectral-irradiance-data](#) [Accessed: 2021-05-03].
- Newport. 2021c. *Light collection and optical system throughput*. [Online] Available at: <https://www.newport.com/t/light-collection-and-systems-throughput> [Accessed: 2021-05-03].
- Newport. 2021d. *Pyroelectric Sensor Physics*. [Online] Available at: <https://www.newport.com/n/pyroelectric-physics> [Accessed: 2021-07-09].
- Newport. 2021e. *Thermopile Sensor Physics*. [Online] Available at: <https://www.newport.com/n/thermopile-physics> [Accessed: 2021-08-30].
- NIST. 2004. *Engineering Metrology Toolbox*. [Online] Available at: <https://emtoolbox.nist.gov/Wavelength/Edlen.asp> [Accessed: 2021-02-12].
- NIST. 2019. *NIST Atomic Spectra Database Lines Form*. [Online] Available at: <https://www.nist.gov/pml/atomic-spectra-database> [Accessed: 2019-03-15].
- NMISA. 2003. *Empirical test RA-10: Uniformity of silicon detectors*.
- NMISA. 2014a (March). *Procedure for laboratory facilities and environmental maintenance of the photometry and radiometry laboratory*. Revision 7 edn. NMISA.
- NMISA. 2014b (November). *Procedure for the calibration of the spectral power response of a detector against a spectral response standard detector*. Revision 5 edn. NMISA.
- Parr, A. C., Datla, Raju Umapathi, & Gardner, James L. (eds). 2005. *Optical Radiometry*. Experimental methods in the physical sciences, no. v. 41. Amsterdam ; Boston: Academic Press. OCLC: ocm62124104.
- Richter, M, Kroth, U, Gottwald, A, Gerth, C, Tiedtke, K, Saito, T, Tassy, I, & Vogler, K. 2002. Metrology of pulsed radiation for 157-nm lithography. *Appl. opt.*, **41**(34), 7167–7172.
- SABS. 2018. *SANS 17025: 2018. General requirements for the competence of testing and calibration laboratories*. SABS.

- Sanders, C.L. et al. 1984. *CIE 63:1984 The Spectroradiometric Measurement of Light Sources*. Tech. rept. International Commission on Illumination (CIE).
- Schott. 2014. *Schott Filter GG395 Datasheet*. Schott. [Online] Available at: <https://shop.schott.com/medias/schott-longpass-gg395-jun-2017-en.pdf>.
- Shimadzu. 2020. *SHIMADZU Diffraction Gratings*. [Online] Available at: <https://www.shimadzu.com/opt/guide/diffraction/07.html> [Accessed: 2020-03-22].
- TC 2-43, CIE. 2011. *CIE198-SP1.2:2011 Determination of measurement uncertainties in Photometry. Supplement 1: Modules and examples for the determination of measurement uncertainties. Part 2: Examples for models with individual inputs*. Tech. rept. International Commission on Illumination (CIE).
- Theron, B, & Botha, PJ. 2003 (June). *Calibration certificate of silicon photodiode for spectral response*. Tech. rept. OR\RA-2905. NMISA.
- Werner, Dr L, & Vogel, K. 2018 (September). *Calibration certificate of an optical radiation detector with single PtSi/n-Si Schottky photodiode*. Tech. rept. 73328 18 PTB. Physikalisch-Technische Bundesanstalt (PTB).
- Werner, L. 2014 (May). *Report on the Key Comparison CCPR-K2.c-2003 Spectral Responsivity in the range of 200 nm to 400 nm*. Tech. rept. Physikalisch-Technische Bundesanstalt (PTB). [Online] Available at: <https://www.bipm.org/documents/20126/44556012/CCPR-K2.c.pdf/1e0427fd-aed3-c856-2e40-77b04f99fba0;,.>
- Werner, L, Fischer, J, Johannsen, U, & Hartmann, J. 2000. Accurate determination of the spectral responsivity of silicon trap detectors between 238 nm and 1015 nm using a laser-based cryogenic radiometer. *Metrologia*, **37**(4), 279–284.
- Winkler, R. 2018 (November). *Calibration certificate of silicon photodiode for spectral responsivity*. Tech. rept. 2017060356. National Physical Laboratory (NPL).
- Zhu, H, Hill, G, Besen, M, Smith, D, & Blackborow, P. 2006. *Ultra-high Brightness and Broadband Laser-Driven Light Source*. Tech. rept. Energetiq Technology, Inc., Woburn, MA 01801, USA.